Molecular Dynamics Simulations of Molecules under Confined Geometry: from Binary Mixture to Perfluorinated Polyphile

Dissertation

zur Erlangung des Doktorgrades der Naturwissenschaften
(Dr. rer. nat.)

der

Naturwissenschaftliche Fakultät II
Chemie, Physik und Mathematik

der Martin-Luther-Universität
Halle-Wittenberg

vorgelegt von

Frau Xiang Yang Guo

Defense: 16th September 2020 online

Reviewers

Prof. Dr. Daniel Sebastiani	Supervisor
Prof. Dr. Bettina Keller	2nd Reviewer

Contents

Declaration

I hereby declare that this thesis represents my own work and has been written without external help. The coworking and contribution from other researchers on the published works are acknowledged accordingly. The usages of other sources and scientific ideas from literature are indicated in the citations correctly.

Signature

Acknowledgments

I would like to take this opportunity to express my greatest thanks to all the people who have been helping me during my Ph.D. study.

Firstly, I would like to express my sincere appreciation and deepest gratitude to my advisor Prof. Dr. Daniel Sebastiani, for allowing me to join his group and for his patient guidance and continuous support of my Ph.D. study and research during these years. I value his efforts to create a multidisciplinary environment in his research group, which helped me to expand my horizons.

Many thanks are also due to other members of the Sebastiani research group, a very special thanks to Tobias Watermann, Dr. Christoph Allolio. I feel fortunate to have had them as my colleagues and coworker throughout my Ph.D. study. Since the very beginning, they have provided me constant help, guidance, and support. I will be forever grateful for all their attention and for the numerous things they've taught me. I would also like to thank Christopher Peschel and Guido von Rudorfffor for the collaboration on the published works and Dr. Hossam Elgabarty, Dr. Arne Scherrer for the useful advice and discussions.

Thank my parents for raising me and giving me the freedom to take my path and also to all the people who believed in me.

Finally, financial support from the China Scholarship Council is greatly acknowledged.

List of Publications

- Xiang-Yang Guo, Tobias Watermann, Shane Keane, Christoph Allolio and Daniel Sebastiani *'First Principles Calculations of NMR Chemical Shifts of Liquid Water at an Amorphous Silica Interface.'* Z. Phys. Chem., **2012**, 226, 1415-1424.

  For this publication, I analyzed the ab initio trajectories of the simulated molecular system. Furthermore, I analyzed the diffusion properties of the confined water molecules and I wrote the manuscript. Shane Keane, Christoph Allolio provided the ab initio trajectories and gave me advice on the manuscript. Tobias Watermann provided coworking throughout the analysis. Daniel Sebastiani supervised the project giving me valuable advice on writing the manuscript.

- Xiang-Yang Guo, Tobias Watermann and Daniel Sebastiani *'Local Microphase Separation of a Binary Liquid under Nanoscale Confinement.'* J. Phys. Chem. B, **2014**, 118, 10207−10213.

  For this publication, I set up the molecular system and carried out the MD simulations. Furthermore, I analyzed the MD trajectories. Tobias Watermann contributed to both the simulation setup and result analysis throughout the work. Daniel Sebastiani supervised the project giving me valuable advice on writing the manuscript.

- Guido F. von Rudorff, Tobias Watermann, Xiang-Yang Guo and Daniel Sebastiani *'Conformational Space of a Polyphilic Molecule with a Fluorophilic Side Chain Integrated in a DPPC Bilayer.'* Journal of Computational Chemistry, **2017**, 38, 576–583.

  For this publication, I performed the diffusion analysis of polyphilic molecule and provided coworking throughout the trajectories analysis.

- Xiang-Yang Guo, Christopher Peschel, Tobias Watermann, Guido Falk von Rudorff and Daniel Sebastiani *'Cluster Formation of Polyphilic Molecules Solvated in a DPPC Bilayer.'* Polymers, **2017**, 9, 488

  For this publication, I carried out the simulation setups and performed the MD simulations. Furthermore, I analyzed the MD trajectories. Guido Falk von Rudorff provided the initial structure and first set up of the simulated molecular system. Tobias Watermann provided coworking on both simulations set up and result analysis throughout the work. Daniel Sebastiani supervised the project and gave me valuable advice on writing the manuscript. Christopher Peschel contributed to data analysis and writing the manuscript.

Abstract

Two representative topics are examined in this dissertation: (I) properties of liquid molecules confined between mesoporous silica surfaces. (II) structural and dynamic actions of perfluorinated polyphilic molecules restricted to the lipid bilayer of dipalmitoylphosphatidylcholine (DPPC). The impact of nanoscale confinements on structural and dynamic properties of liquid water and ethanol-water mixture has been investigated for the first project within the scope of this doctoral research using molecular dynamics simulations based on density functional theory and atomic force field. The main focus here is on the structure's dependency and the hydrogen-bonding-network of the solvent near the confinement interface at atomistic resolution. In the case of a binary ethanol-water mixture, the results indicate that, due to the presence of the planar silanol interfaces, there is a major restructuring of the hydrogen bond network between water and ethanol, as well as adjustment in the water-water hydrogen bonds. A partial demixing of ethanol and water occurs in the vicinity of the silanols. Water is more likely to form stable clusters, while ethanol, on the other hand, is more flexible and has a greater possibility to form a hydrogen bond with a silanol group. Compared to the unconfined case, the hydrophobic environment created by a layer structure of ethanol alkyl groups further supports the stabilization of those water clusters.

Using classical molecular dynamics simulation, the behavior of perfluorinated polyphilic molecules (type B16/10) in a membrane environment is investigated in the second part of this doctoral study. The main focus here is to examine the initial stages of polyphilic additive molecules forming clusters when they are solved in a DPPC lipid bilayer. The polyphilic molecules contain a central aromatic (trans-bilayer) domain with (out-of-bilayer) glycerol terminations, complemented by a fluorophilic and an alkyl side chain, both contained within the bilayer's aliphatic segments. Large-scale molecular dynamics simulations of six such additive polyphilic molecules as a cluster reveal the initial steps towards supramolecular aggregation caused by the unique philicity properties of the molecules. The transient yet repeated development of a trimer is observed on a characteristic the time-scale of about 100 ns for our intermediate system size of six polyphiles. Thanks to their separate philicity, the alkane / perfluoroalkane side chains show a very distinct conformational distribution within the bilayer, given their similar anchoring in the polyphile transbilayer section. The polyphilic additives' diffusive mobility is about the same as that of the surrounding lipids, although it crosses all bilayer leaflets and appears to be self-associated. The findings provide important insight for understanding polyphilic molecules' intramembrane structure with specifically designed side chains of different philicity. These molecules are capable of allowing a controlled modification of membrane properties such as water and ion permeability.

Introduction

Molecules under confinement at the nanoscale are known to have properties noticeable different from those in the bulk. Computational modeling and simulation of those molecular assemblies can provide insight at the atomic level of the structural and dynamic aspects and predict the behavior of complex systems at a level of detail beyond the experimental limitation.

0.1 Liquids under Silica Confinement

Mesoporous silica has attached much attention due to its hierarchical structure, which is observed to be composed of orderly arranged pores with uniform size.[1,2] MCM-41, as one of the most studied type, is characterized by pores, less than 40 Å in diameter, within which liquids are restricted. Experimental studies regarding MCM-41 and the properties of liquids confined within it has been performed at length. Techniques such as quasi-elastic and deep elastic neutron scattering,[3–5] neutron diffraction with isotopic substitution ,[6] x-ray spectroscopy ,[7] sum frequency vibration spectroscopy ,[8] adsorption calorimetry ,[9] and NMR spectroscopy [10–12] have generated much experimental data which may be compared to simulation data.

The silanol groups on the silica surface play a special role in its ability to supplying hydrogen bonding sites for the confined solutions.[13] Concerning their density on the MCM-41 silica surface,[10,11,14] the consensus seems to be about 2 to 3 nm^{-2}, meaning these groups cannot form hydrogen bonds with each other as they are too far apart. Since the average distance between them is about 5.8 Å, one water molecule cannot be simultaneously hydrogen bonded to two silanol groups.[15] Up to three water molecules, however, may be hydrogen-bonded to a single silanol group.[13] The nature of water differed from bulk water when it's hydrogen-bonded to the hydroxyl groups on the silica surface. Recent neutron scattering evidence suggests that the hydrogen bond formed between a water molecule and a silanol in mesoporous silica is stronger than the hydrogen bonds between water molecules.[5] Understanding the properties of ethanol and water at interfaces on the molecular level is very important for many chemical and physical processes .[16,17] Water molecules can interact with the surface through hydrophobic or hydrophilic interactions and hydrogen-bonding. This leads to the partial ordering of water molecules in the vicinity of the confining surface.[18] To date, numerous studies focusing on water confined in porous frameworks have been carried out via simulations and experiments. B. Ratajska-Gadomska and W. Gadomski[19] reported the solvation of ethanol in water confined by gelatin gel studied by Raman spectroscopy. Their work indicates that when an ethanol-rich solution confined in gelatin gel, so-called ethanol sandwich clusters exist with a layer of water molecules inside. As mentioned before, the silanol groups on the silica surface have a hydrophilic character. This yields a certain competition of hydrogen bonds between silanol-solvent and solvent-solvent. Therefore, the conformation and the donor-acceptor preferences in the ethanol-water mixture are even more complicated than water/silica and ethanol-water bulk mixture.

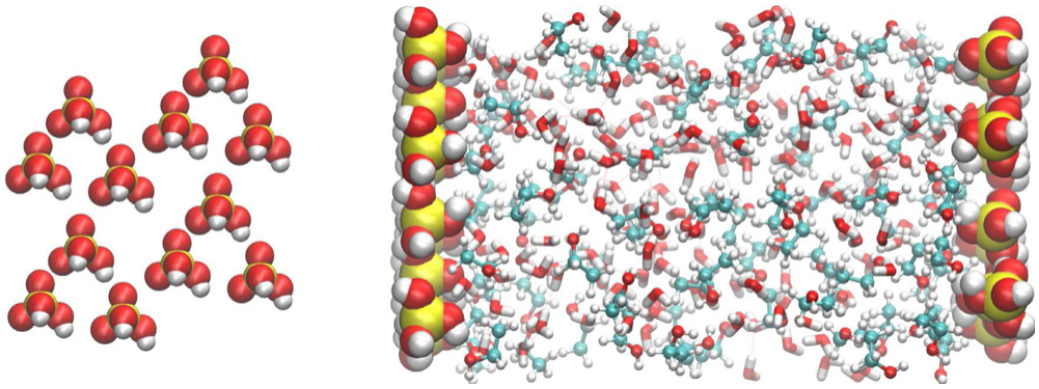

Figure 1: Picture of the silanol wall model normal to the wall surface (left) and a snapshot of an equilibrated ethanol−water/silanol system during a simulation at 338 K (right). Two silanol walls contain 24 Si(OH)4, with 87 ethanol molecules and 148 water molecules confined in between.

To provide further atomistic insight into these confined liquids, in the first part of this doctoral research, the impact of nanoscale silica confinements on structural and dynamical properties of liquid water and binary aqueous mixtures is investigated using molecular dynamics simulations. A simplified planar model that has the advantage of containing the same density of silanol groups as MCM-41 was constructed.

0.2 Polyphilic Molecules Incorporated into DPPC Bilayer

Molecules with the capability of self-assembling are of great interest for biochemical (lipid bilayers) and nanosized materials.[20] Understanding such behavior is essential for the logical design of the model and advanced (bio)molecule systems. In both experimental and simulation approaches, a variety of molecules have been inserted into lipid bilayers. It ranges from early attempts to inject alkanes into a lipid bilayer system to find out where they are situated inside the system,[21] up to the current investigations of fluorinated alkanes and alcohols.[22] Based on these studies, the second part of this thesis investigates a very complex compound that combines multiple philicities in one molecule. As the name suggests, these so-called polyphilic molecules are compounds composed of fragments of varying philicities. Polyphils containing a rigid rod-shaped aromatic center with opposing end-groups and lateral groups with specific philicities are given special attention here. Usually, the two end groups are highly polar, allowing the formation of multiple hydrogen bonds, which is possible only in the bilayer headgroup region and the aqueous phase, whereas the lateral groups are alkyl, partially fluorinated or perfluorinated chains.[23–25] In recent year, considerable attention has been paid to this novel class of molecules.[24–29] Polyphilic molecules can be used in a lipid bilayer to change the bilayer's phase transitions temperature.[30] Furthermore, as lately evinced, they induce effects like compression or stretching of bilayer systems.[31–35] Fluorocarbon compounds are also studied to affect the metabolism of rats[36,37] and for *in vitro* synthesis of lipid bilayer proteins.[38] To allow a complete understanding of the reason why this type of molecules influences the bilayer

properties, the polyphilic molecules themselves must be studied on a molecular scale. In this thesis, the molecule (B16/10) being investigated has three philicities, namely fluorophilic, hydrophilic and lipophilic parts.[25–29] The rigid aromatic phenylene – ethynylene-backbone forms its frame structure, and this backbone chain is terminated by two hydrophilic groups. Two side chains are connected in the center of the backbone, one of which is a perfluoro-*n*-alkane, and the other a regular n-alkane (see Figure 2). The length of the side chains may be derived from the name (16 carbon atoms for the alkyl chain and 10 carbon atoms for the perfluorinated alkyl groups). This molecular structure guarantees a trans-bilayer the orientation of the backbone, providing an anchor point at the middle of the bilayer for the alkyl/perfluoroalkyl chains. Mobile aliphatic side chains and polar end groups give several functionalization possibilities for tailoring the bilayer interactions. Phospholipid bilayers play a decisive role in many of their biological functions, as the fundamental building blocks of cellular membranes. The alteration of lipid bilayer functions by biomolecular interactions such as proteins or peptides has been extensively investigated.[39,40] Because of experimental investigations into the effect of purely synthetic molecules on the DPPC bilayers,[31,32] it serves well as a model system for a thorough investigation into the impact of our polyphilic molecules on the bilayer properties. Also recently, the idea of polyphilicity was used to alter the lipid bilayer itself directly by perfluorinating the lipid tail ends.[41]

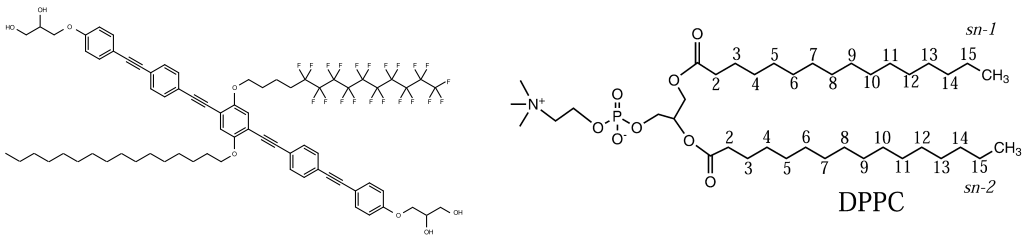

Figure 2: Molecular structure of the polyphilic molecule B16/10 and DPPC molecule studied in this thesis

The available experimental results show that the development of large bolapolyphile (BP) molecules domains within the bilayer and separation into different lamellar species can be observed[33,34] when BP molecules are introduced into the bilayer gel phase lipid (DPPC). The lipid bilayers' thermal behavior was drastically altered after incorporation of BP molecules and several endothermic transitions above T_m of pure DPPC bilayer occurred.[30] The BPs were distributed homogenously in the lipid bilayer plane during the liquid phase.[30,33]

Dipalmitoylphosphatidylcholine (DPPC) is a phospholipid compose of two palmitic acids bound to a phosphatidylcholine head-group and it is the main component of pulmonary surfactants.[42] DPPC lipid bilayer is well characterized and has been extensively studied as biological membrane modeling systems.[43,44] MD simulations of lipid bilayer have reached an exciting stage, where the time and length scales of simulations are approaching experimental resolutions and can be used to construe experiments on an increasingly complex model bilayers.[45] Within the MD of hybrid-bilayer systems, one can get an insight into the dynamical

behavior on a molecular scale. These simulations, therefore, provide additional information to experiments.[46–48] Besides, they can also provide a spatial resolution and time scale with molecular-level insight into the structure and dynamics of these structures which may not be experimentally feasible. These function, summarized, as rich sources of quantitative data on molecular versatility, lipid diffusion, ordering, and atomic interactions. To fully understand their important biophysical characteristics, a detailed understanding of the lipid bilayer properties is needed.

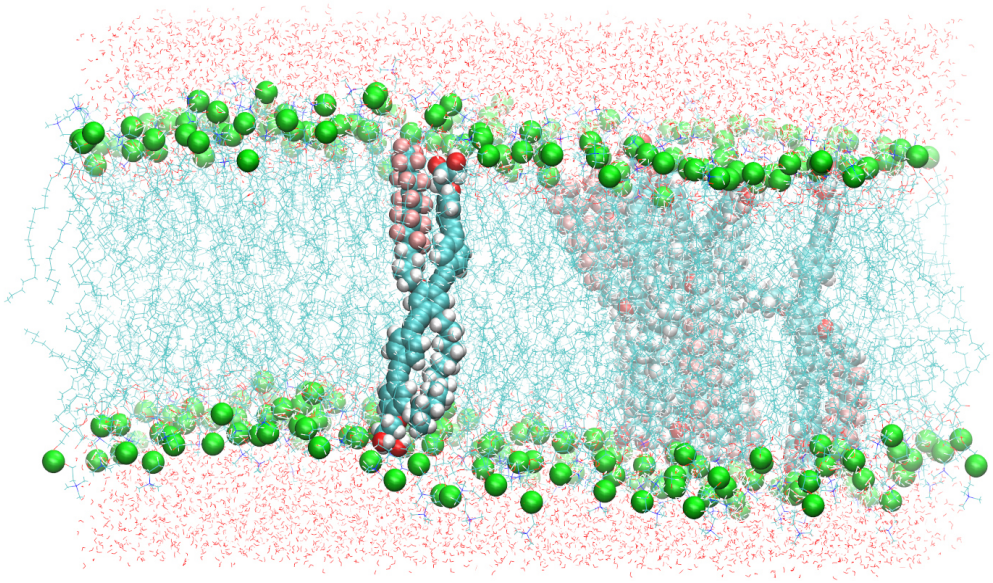

Figure 3: A snapshot of the simulated system containing six B16/10 molecules, 288 dipalmitoylphosphatidylcholines (DPPC) molecules, and 8756 water molecules. Periodic boundary conditions were used in all directions. Solid spheres are used to represent the atoms of B16/10 and phosphorus atoms of DPPC head groups. The green ones are phosphorus atoms, fluorine atoms of B16/10 side chains are pink, and carbon atoms are cyan. The DPPC lipid tails are illustrated by cyan lines.

This partial project aims to conduct the simulation and the computational characterization of B16/10 after solvated into a DPPC bilayer membrane (see Figure 3). The MD simulations help to gain an understanding of the structural driving forces that control the process of supramolecular self-organization in these systems, but also to elucidate how B16/10 (particularly the fluorinated segments) modifies the membrane's properties as such. On the one hand, this is related to the interaction of the fluorophilic components with the polar membrane-water interface and, on the other hand, it addresses the properties of the membrane as an individual, provided the mobility and diffusion properties of the lipid molecules and the permeability of the membrane concerning water molecules. The results of the MD simulations are compared with NMR and microscopy experimental data to check the performance of the simulations but also to interpret the experimental findings on a molecular level.

0.3 Thesis Content

This thesis is organized as follows: after this introduction, the first chapter is dedicated to a discussion of the theoretical background of the methods used in this work. A summary of the molecular dynamics theory is presented. The second chapter gives a full reproduction of the four published papers which represents the scientific content of this cumulative dissertation. The third chapter gives a summary of the conclusion derived from this doctoral research.

Chapter 1

Theory

This chapter aims to provide a brief introduction of the theoretical framework to carry out a molecular dynamics simulation. For further description, please refer to other literatur on this specific topic, for example, *Statistical Mechanics: Theory and Molecular Simulation* by Mark Tuckerman (PP:53-275).[49]

1.1 Fundamentals of Molecular Dynamics

Molecular dynamics (MD) simulation is an effective technique to compute the thermodynamic and dynamical properties of the molecules assemblies based on statistical mechanics. Nowadays, it has become one of the most important instruments for theoretical chemists and physicists to study the microscopic interactions of molecules in polymers, biomolecules, soft matters and other fluid systems at the atomic level.[50–55] In MD simulations, the positions and velocities of particles are propagated according to Newton's equation.[56–58] The output that describes the positions and velocities of the particles as they evolve with time is the so-called trajectory. It can capture the motion of particles and enable the calculation of the ensemble averages of physical quantities from the simulation results. This serves as a complement to conventional experiments and it plays a fundamental role in comprehending physical and dynamical quantities which are inaccessible to experiments. Fundamental to such simulations is the numerical integration the (classical) equations of motion and the representation of the system energy as a function of its atomic coordinates.

1.1.1 The Verlet Algorithm

In MD simulations, the interactions among particles are governed by the potential energy of the system U. Force acting the i-th particle is determined as the gradient of U with respect to the atomic displacements.

$$\vec{F_i} = -\nabla_{r_i} U(\vec{r}_1, ..., \vec{r}_N). \tag{1.1.1}$$

The interacting particles evolve with time step according to Newton's equations. The force and the position vectors of i-th particle are related via Eq. 1.1.2:

$$\vec{F_i} = m_i \frac{\cdot d^2 \vec{r}_i}{dt^2}, \tag{1.1.2}$$

where $\vec{F_i}$ is the force acting upon the particle i at time t, m_i and $r_i = (x_i, y_i, z_i)$ are the mass, and the position vector of the particle i, respectively.

Beginning with a Taylor expansion of the position in time $t + \Delta t$, one obtains :

$$\begin{aligned} \mathbf{r}_i(t + \Delta t) &\approx \mathbf{r}_i(t) + \Delta t \dot{\mathbf{r}}_i(t) + \frac{1}{2}\Delta t^2 \ddot{\mathbf{r}}_i(t) \\ &\approx \mathbf{r}_i(t) + \Delta t \mathbf{v}_i(t) + \frac{\Delta t^2}{2m_i}\mathbf{F}_i(t) \end{aligned} \tag{1.1.3}$$

One can eliminate the velocity term in Eq. 1.1.3 by writing a similar expansion for $\mathbf{r}_i(t-\Delta t)$:

$$\mathbf{r}_i(t - \Delta t) \approx \mathbf{r}_i(t) - \Delta t \mathbf{v}_i(t) + \frac{\Delta t^2}{2m_i}\mathbf{F}_i(t), \tag{1.1.4}$$

after combining Eq. 1.1.3 and Eq. 1.1.4:

$$\mathbf{r}_i(t + \Delta t) \approx 2\mathbf{r}_i(t) - \mathbf{r}_i(t - \Delta t) + \frac{\Delta t^2}{2m_i}\mathbf{F}_i(t) \tag{1.1.5}$$

The position vector is updated at a finite time interval. Eq. 1.1.5 is the classical *Verlet algorithm*.[59] Given a starting point in the phase space, one can use Eq. 1.1.3 to generate a set of coordinates at time Δt, which can then be propagated using Eq. 1.1.5 to a trajectory of arbitrary length. The velocities can be obtained as a centered difference:

$$\mathbf{v}_i(t) = \frac{\mathbf{r}_i(t + \Delta t) - \mathbf{r}_i(t - \Delta t)}{2\Delta t} \tag{1.1.6}$$

Repeating calculation of forces, positions and velocities, the motion of particle can be obtained and saved in MD trajectory. Interestingly, when adding Eq. 1.1.3 and Eq. 1.1.4, all the odd-order terms are eliminated, thus the *local* error in the Verlet algorithm is $\mathcal{O}(\Delta t^4)$, even though Eq. 1.1.5 contains no explicit third-order term.[59]

The Velocity Verlet Algorithm

The Verlet algorithm has been proved to have excellent stability for relatively large time steps.[59–61] However, it also has the disadvantage of *not generating* the complete phase space trajectory on the fly, as it does not propagate the velocities. The velocity Verlet algorithm[50] was then introduced. Swope, Andersen, Berens, and Wilson[50] proposed the velocity version of Verlet algorithm which takes the form

$$\vec{r}(t + \triangle t) = \vec{r}(t) + \triangle t \cdot \vec{v}(t) + \frac{1}{2}(\triangle t)^2 \frac{d^2\vec{r}(t)}{dt^2} \tag{1.1.7}$$

$$\vec{v}(t + \triangle t) = \vec{v}(t) + \frac{1}{2} \triangle t [\frac{d^2\vec{r}(t)}{dt^2} + \frac{d^2\vec{r}(t + \triangle t)}{d(t + \triangle t)^2}] \tag{1.1.8}$$

The velocity version of Verlet is simple, compact, stable and more commonly used compared to the original Verlet algorithm.

1.1.2 Shake and Rattle

Shake[51,52] and Rattle[62] are two methods that deal with Verlet integration and used for many body (polyatomic) system having internal constraints. Verlet formulation regarding position is done by Shake. The Rattle is based on the velocity version of Verlet algorithm,[62] it is like a new version of Shake. It computes the positions and velocities at the time (t + △t) from the positions and velocities at the time (t), without earlier information. Molecules can be described with the help of Cartesian coordinates, by describing each atom with internal constraints.

1.1.3 The Shake and Rattle Algorithms

One of the most crucial issues with all numerical integration algorithms is that the time step Δt must be smaller than the speediest modes in the given molecular system. Typically, such modes oscillate on the range of just a few femtoseconds e.g. bond stretches involving hydrogen atoms. However, this time step size is very short compared to many important reactions happening in large biological systems. For example, folding or conformational changes of proteins occur of the order of nanoseconds to microseconds. In order to reduce the computational effort of simulating such large scale molecular systems, it is necessary to use a time step as large as possible. The most common approach to increase the time step is to apply constraints (or fix) to the fastest degrees of freedom in the system and to solve the classical equations of motion for the slower degrees of freedom. The SHAKE and RATTLE algorithms are widely used constraint schemes in large scale molecular simulations.[51,52,62,63]

The SHAKE algorithm is mostly used together with the Verlet algorithm.
In reference to the Eqs. 1.1.4, 1.1.5 and 1.1.6, the Verlet algorithm within the presence of constraints is expressed as:

$$\vec{r}_i(t+\Delta t) \approx 2\vec{r}_i(t) - \vec{r}_i(t-\Delta t) + \frac{\Delta t^2}{2m_i}\vec{F}_i(t) + \frac{\Delta t^2}{2m_i} g_S[\vec{r}(t), \vec{v}(t)], \tag{1.1.9}$$

where g_S includes the forces associated with the constraints. The velocities are then recalculated based on the the coordinates, which are constrained throughout. On the other hand, the RATTLE algorithm is particular to the velocity Verlet algorithm. Again, referring to the Eqs. 1.1.7, 1.1.8:

$$\vec{r}_i(t) \approx \vec{r}_i(t+\Delta t) - \Delta t\vec{v}_i(t+\Delta t) + \frac{\Delta t^2}{2m_i}\vec{F}_i(t+\Delta t) + \frac{\Delta t^2}{2m_i} g_{RR}[\vec{r}(t)], \tag{1.1.10}$$

where g_{RR} again the force associated with the constraints. The velocities $\vec{v}_i(t+\Delta t)$ are then generated as

$$\vec{v}_i(t+\Delta t) \approx \vec{v}_i(t) + \frac{\Delta t}{2m_i}\left[\vec{F}_i + \vec{F}_i(t+\Delta t) + g_{RR}(t) + g_{VR}(t)\right], \tag{1.1.11}$$

where g_{VR} is the constrained forces.

1.2 MD Simulations in the Canonical Ensemble

Standard MD simulation can only produce a micro-canonical ensemble (NVE), in which the total number of particles (N), the volume (V) and energy (E) of the system are maintained, rather than a canonical ensemble (constant NVT) such as those often found in experiments, where temperature (T) instead of energy (E) is conserved. Extended MD algorithms have been proposed extensively for performing MD simulation in a canonical ensemble or at constant temperature. In the year 1984, a more rigorous NVT MD method is introduced by Nosé, and subsequently developed by Hoover (1985),[64] now kown as the standard Nosé-Hoover (NH) thermostat method.[65] A thermal reservoir represented by an additional, virtual variable s and effective mass Q is specified in this approach, which works on the physical system as an external one. It results in the development of an expanded Lagrangian particle system and the vector s. The heat exchange between the internal and external systems is capable of controlling system temperature. The successful mass controls these two systems ' coupling, thereby influencing the system temperature oscillation. In essence, the method allows fluctuation in the total energy of the physical system. However, the results made by the NH thermostat are not guaranteed to cover all of the available phase space. This shortage is resolved by Martyna et al. (1992),[66] who introduced a chain of Nosé-Hoover-type thermostat, alternatively called the NH chain (NHC) thermostat method. In addition, Tuckerman et al. (1999)[67] have provided a more rigorous statistical foundation for general non-Hamiltonian systems. With this foundation, the standard NH and NHC thermostat methods have been proved that through the use of a particular thermal reservoir, including potential and kinetic energies, the calculated partition function of these methods are equivalent to the partition function in a canonical ensemble, which means the calculated quantities are equal to those in a canonical ensemble.

The Nosé-Hoover Thermostat

Follwing the representation by Tuckerman.[49] The Hamiltonian for a system of N particles contains an additional degree of freedom s and its conjugate momentum p_s:

$$\mathcal{H}_{\text{Nose}} = \sum_{i=1}^{N} \frac{\mathbf{p}_i^2}{2m_i s^2} + U(\mathbf{r}_1, \ldots, \mathbf{r}_N) + \frac{p_s^2}{2Q} + gkT \ln s \tag{1.2.1}$$

where $U(\mathbf{r}_1, \ldots, \mathbf{r}_N)$ is the potential energy, k and T are the Boltzmann constant and the target temperature respectively, and g is equal to $3N + 1$. s acts as an "agent" that scales the velocities to shift the instantaneous kinetic energy towards the target level. Q is a parameter, with units of energy $\times$ time^2, that determines the time scale on which the "thermosta" acts, and also can be viewed as an *effective mass* for s. In the extended system described by 1.2.1, $\mathcal{H}_{\text{Nose}}$ is conserved, and therefore we have a microcanonical ensemble. However, the "*potential*" term for s, $gkT \ln s$, was chosen such that the microcanonical distribution of the total $6N + 2$-dimensional phase space of $\mathcal{H}_{\text{Nose}}$ gives a *canonical* distribution in the physical $6N$-dimensional phase space, which can indeed be shown to be the case by integrating the partition function of the $6N + 2$-dimensional phase space over s and p_s[pp.180-181].[49]

The equations of motion generated by $\mathcal{H}_{\text{Nose}}$ are:

$$\dot{\mathbf{r}}_i = \frac{\partial \mathcal{H}_{\text{Nose}}}{\partial \mathbf{p}_i} = \frac{\mathbf{p}_i}{m_i s^2} \tag{1.2.2}$$

$$\dot{\mathbf{p}}_i = -\frac{\partial \mathcal{H}_{\text{Nose}}}{\partial \mathbf{r}_i} = \mathbf{F}_i \tag{1.2.3}$$

$$\dot{s} = \frac{\partial \mathcal{H}_{\text{Nose}}}{\partial p_s} = \frac{p_s}{Q} \tag{1.2.4}$$

$$\dot{p}_s = -\frac{\partial \mathcal{H}_{\text{Nose}}}{\partial s} = \sum_{i=1}^{N} \frac{\mathbf{p}_i^2}{m_i s^3} - \frac{gkT}{s} = \frac{1}{s}\left[\sum_{i=1}^{N} \frac{\mathbf{p}_i^2}{m_i s^2} - gkT\right] \tag{1.2.5}$$

Following the reformulation by Hoover[64] (with slight modification from Martyna[66]), 1.2.2 can be put in a more convenient form by introducing the following change of variables:

$$\mathbf{p}_i' = \frac{\mathbf{p}_i}{s} \tag{1.2.6}$$

$$\mathrm{d}t' = \frac{\mathrm{d}t}{s} \tag{1.2.7}$$

$$\frac{1}{s}\frac{\mathrm{d}s}{\mathrm{d}t'} = \frac{\mathrm{d}\eta}{\mathrm{d}t'} \tag{1.2.8}$$

$$p_s = p_\eta \tag{1.2.9}$$

and redefining g in 1.2.1 to become $6N$, we end up with a new set of equations of motion:

$$\dot{\mathbf{r}}_i = \frac{\mathbf{p}_i}{m_i}\dot{\mathbf{p}}_i = \mathbf{F}_i - \frac{p_\eta}{Q}\mathbf{p}_i\dot{\eta} = \frac{p_\eta}{Q}\dot{p}_\eta = \sum_{i=1}^{N} \frac{\mathbf{p}_i^2}{m_i} - gkT \tag{1.2.10}$$

One can see that the equation for momentum has a friction term that depends on p_η, and that the evolution of this p_η is driven by the difference between the instantaneous kinetic energy and its canonical average gkt (the last equation). The friction term thus mimics the behavior of a heat bath by controlling the fluctuations in the kinetic energy.

The Nose-Hoover equations 1.2.10 have an associated conserved quantity:

$$\mathcal{H}'(\mathbf{r}, \eta, \mathbf{p}, p_\eta) = \mathcal{H}(\mathbf{r}, \mathbf{p}) + \frac{p_\eta^2}{2Q} + gkT\eta, \tag{1.2.11}$$

which can be used to monitor the numerical stability of the simulation.

1.3 MD Simulations with Force Field

Accurate determination of the energy of the molecules and forces acting on each particle highly relies on the quality of the potential energy functions used in the MD simulation. Potential energy functions are simplified mathematical functions that are utilized to describe the interactions between interacting particles. The collection of all the potential energy functions and their coefficients for different types of particles is called "Force Field" (FF).[55,68–70] They normally use the same or similar forms of potential energy functions to describe the bonded and

non-bonded interactions. In the framework of this dissertation, the CHARMM Force Field was chosen which is very widely used in simulations of biological systems (proteins, nucleic acids, biological membranes).[71,72] For information on other frequent applied FFs, please refer to literature, such as AMBER,[73] OPLS[74] etc. The potential energy function of CHARMM Force Field has the following mathematical form:

$$E = \sum_{bonds} K_b(b - b_0)^2 + \sum_{angles} K_\theta(\theta - \theta_0)^2 + \sum_{Urey-Bradley} K_{\mathrm{UB}}(r_{1,3} - r_{1,3;0})^2 \tag{1.3.1}$$

$$+ \sum_{dihedrals} K_\phi(1 + \cos n\phi - \delta) + \sum_{improper} K_\psi(\psi - \psi_0)^2 \tag{1.3.2}$$

$$+ \sum_{i,j>i} \frac{1}{4\pi\epsilon} \frac{q_i q_j}{|r_{ij}|} + 4\epsilon_{ij} \left[\left(\frac{\sigma_{ij}}{r_{ij}} \right)^{12} - \left(\frac{\sigma_{ij}}{r_{ij}} \right)^{6} \right] \tag{1.3.3}$$

The intramolecular component of the obove potential energy function includes terms account for "bonded" interactions, where b_0, θ_0, ψ_0, and $r_{1,3}$ respectively are the bond, angle, improper, and Urey-Bradley equilibrium values, the K's are the corresponding force constants, and n and δ are the dihedral (ϕ) multiplicity and phase. The last two terms are "non-bonded" interactions, represented by a Coulomb-type pairwise interaction between atoms based on their partial charges (q_i) (bonded atoms are excluded up to the third or fourth bonded neighbor), and a van der Waals term represented by the Lennard-Jones (LJ) 6-12 potential and the electrostatic energy, a mathematically simple model that apporximates the interaction between a pair of neutral atoms, where ϵ_{ij} is the depth of the potential wall and σ_{ij} is the finite distance at which the inter-particle potential is zero.[70,75,76] These parameters are normally derived from experimental data or *ab initio* QM alculation on small model molecules.[77–79]

Chapter 2

Results published within this thesis

2.1 First Principles Calculations of NMR Chemical Shifts of Liquid Water at an Amorphous Silica Interface

- Xiang-Yang Guo, Tobias Watermann, Shane Keane, Christoph Allolio and Daniel Sebastiani

  Z. Phys. Chem., **2012**, 226, 1415-1424.

  https://doi.org/10.1524/zpch.2012.0290

Z. Phys. Chem. **226** (2012) 1415–1424 / **DOI** 10.1524/zpch.2012.0290

First Principles Calculations of NMR Chemical Shifts of Liquid Water at an Amorphous Silica Interface

By Xiang Yang Guo[1], Tobias Watermann[1], Shane Keane[1], Christoph Allolio[1], and Daniel Sebastiani[1,2,*]

[1] Physics Department, Freie Universität Berlin, Arnimalle 14, 14195 Germany
[2] Institute of Chemistry, Martin-Luther-Universität Halle Wittenberg, Kurt-Mothes-Strasse 2, 06120 Halle, Germany

Dedicated to Professor Hans Wolfgang Spiess on the occasion of his 70th birthday

(Received June 4, 2012; accepted in revised form September 21, 2012)
(Published online October 29, 2012)

Car-Parrinello Molecular Dynamics Simulations / DFT / NMR Chemical Shift Calculations / MCM-41 / Liquid Water Structure / Confinement

We investigate the anomalous structure and hydrogen bond network of water molecules confined inside a silica nanopore (MCM-41 type). In addition to geometric data, we use proton NMR chemical shifts as a measure for the strength of the H-bonding network. We compute the ^{1}H NMR shifts of confined water based on a first principle approach in the framework of density functional perturbation theory under periodic boundary conditions. The hydrophilic character of the silica is well manifested in the water density profile. Our calculations illustrate both the modifications of the ^{1}H NMR chemical shifts of the water with respect to bulk water and a considerable slowing down of water diffusion. In the vicinity of silanols, weakly hydrogen bonded liquid water is observed, while at the center region of the pore, the hydrogen bonding network is enhanced with respect to bulk water.

1. Introduction

Periodically structured porous materials have evoked wide interest for various applications in recent years. Their micro-structure is observed to be composed of orderly arranged pores with uniform size [1]. MCM-41, as one of the most studied type, is characterized by pores less than 40 Å in diameter, within which liquids can be confined. Experimental studies regarding MCM-41 and the properties of liquids confined within it have been performed at length. Techniques such as quasi-elastic and deep elastic neutron scattering [2–4], neutron diffraction with isotopic substitution [5], x-ray spectroscopy [6], sum frequency vibration spectroscopy [7], adsorption calorimetry [8],

* Corresponding author. E-mail: daniel.sebastiani@fu-berlin.de

and NMR spectroscopy [9–11] have provided a lot of experimental data which may be compared to simulation data.

The silanol groups on the silica surface play a special role for its ability of supplying hydrogen bonding sites for the confined solvent [14]. With respect to their density on the MCM-41 silica surface [9,10,13], the consensus seems to be about 2 to 3 nm^{-2}, meaning these groups cannot form hydrogen bonds with each other as they are too far apart. Since the average distance between them is about 5.8 Å, one water molecule cannot be simultaneously hydrogen bonded to two silanol groups [1]. Up to three water molecules, however, may be hydrogen bonded to a single silanol group [14]. The nature of water differed from bulk water when it is hydrogen bonded to the hydroxyl groups on the silica surface. Recent neutron scattering evidence suggests that the hydrogen bond formed between a water molecule and a silanol in mesoporous silica is stronger than the hydrogen bonds between water molecules [4].

Many simulations have been conducted focusing on the water silica interface. Since the structure of MCM-41 is not fully known, many varying models have been proposed to simulate its surface. For example, Shirono *et al.* [15] and Kleestorfer *et al.* [16] used a block of alpha-quartz out of which they cut circular pores of various sizes. In cases where there remained oxygens attached to only one silicon atom, hydrogen atoms were added to create the silanol groups characteristic of the surface of MCM-41. Gallo *et al.* [12] used beta-cristobalite which was melted and equilibrated at 1000 K. It was then quenched and a cylindrical pore 15 Å in diameter was carved into it. Again, oxygens left attached to only one silicon atom were capped with hydrogen atoms. Sherendovich *et al.* [9] use different experimentally derived criteria to recommend a model of MCM-41 based on the structure of tridymite. The model they proposed was not in fact tridymite, but a fictitious structure created from pieces of it stuck together in different configurations. With respect to the silica-water interface, Sulpizi *et al.* [29] conducted *ab initio* Molecular Dynamics (AIMD) on the hydroxilated (0001) α-quartz surface system. Two types of silanol groups were addressed in their results, so called out-of-plane silanols with a strong acidic character and in-plane silanols with weaker acidity.

In this work, a simplified surface model is constructed which has the virtue of containing the same density of silanol groups as MCM-41. We obtain the density and translational mobility profiles of water confined in this model by applying first principle density functional theory based molecular dynamics (AIMD) simulation. Then we compute ensemble averages of Nuclear Magnetic Resonance (NMR) calculations on the confined water molecules and compare the results with bulk water. Furthermore we analyze the distribution of the water NMR shifts along the pore axis and the impact of the geometric confinement on the bound water NMR shifts so as to increase our understanding of the influence of spatial confinement on the structure and dynamics of water.

2. Computional details

The water-silica interface is represented by a simplified yet realistic surface model which demonstrates the experimentally known structure of the MCM-41 pore. Figure 1

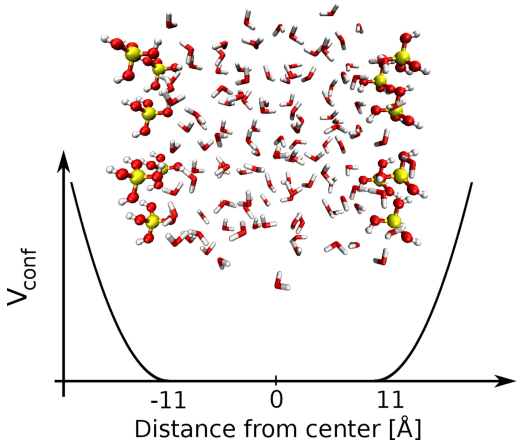

Fig. 1. Two silica-water unit cells from a snapshot of the MD simulation (*xz* side view). The three-dimensional periodic cell contains six silicic acid groups at the walls and 59 water molecules in between. Si, O and H atoms are represented in yellow, red and white respectively. The silica surface is represented by three isolated $Si(OH)_4$ tetrahedrons.

shows a snapshot of the model. Silicic acid $Si(OH)_4$ is used to model the silanol groups with the three outer hydroxy groups fixed.

Following the experimental results from the NMR spectroscopy [9,10] on the structure of MCM-41, the density of the silanol groups is taken to be $3\,nm^{-2}$. The possible hydrogen bonding between Si-O-Si bridge and water is missing in this model. We assume it is only of minor influence since the highly concentrated silanol groups on the surface hamper sterically the formation of this type of hydrogen bonds. In the next more sophisticated model, the actual amorphous pore will be considered.

The diffusion of water into the surface is prevented by a harmonic potential (Fig. 1). The potential only acts on the water molecules to allow free Si−OH vibrations. The simulation is carried out in a fully periodic box with a size of $28 \times 10 \times 10$ Å, two flat silanol walls are placed 22 Å apart, 6 Å space is left at either end of the potential to reduce periodic effects in the *x* direction. 59 water molecules are placed between the two walls. In order to employ a timestep of 1 fs, we choose heavy water instead of H_2O to double the calculation speed.

We run DFT based molecular dynamics simulations in the CP2K package [30]. The BLYP [31] exchange-correlation functional was used, as well as the TZVP basis sets and GTH pseudopotentials [32]. The DFT-D2 Grimme [33] dispersion correction was also used. In total, the simulation ran for over 45 ps.

The system was first equilibrated for 10 ps using the canonical ensemble, employing a Nosé–Hoover thermostat. The temperature was set to be 320 K. The simulation was then switched to the microcanonical ensemble for the remaining time.

The NMR chemical shifts are computed as ensemble averages from ab initio nuclear shielding calculations within the CP2K package [30]. A random set of 15 snapshots from the NVE trajectory was sampled, and chemical shifts of all atoms were calculated. For the referencing of the nuclear shielding tensors to chemical shifts, we utilized the method applied in Ref. [23] The NMR simulation used a Gaussian aug-

mented plane wave approach with GAPW plane wave cutoff 320 Ry, the BLYP-DFT exchange-correlation functional and the TZV2PX-MOLOPT-GTH basis set were employed [34].

It should be noted that we do not compute the quantum propagation of the nuclear spin state which occurs on a timescale of millisecond in a typical NMR experiment, but instead we compute directly the energy difference of the 2 states. Hence the simulation duration on a picosecond level is adequate to achieve the necessary sampling for the averaged instantaneous chemical shifts [35–40].

3. Results and discussion

3.1 Translational dynamical properties

One of the most salient properties of water confined in MCM-41, discovered by experiments and MD simulations [12,15,17,18] is a slower translational dynamics with respect to bulk water. The translational dynamics of our system were measured by calculating the diffusion coefficient of the system. The ratio of the diffusion coefficient of water confined in MCM-41 to that of bulk water

$$q = \frac{D_{D_2O}^{\text{Confined}}}{D_{D_2O}^{\text{Bulk}}}$$

has been ascertained experimentally and *via* simulation. Values of q range quite widely from 0.23 to 0.64 [15,17,18,24], with the consensus showing a much slower diffusion of water within MCM-41 pores. In this work, the reference self diffusion coefficient value for bulk heavy water is taken to be 0.187 Å^2/ps from Ref. [28]. In order to obtain the value of q for our system, we calculated the diffusion coefficient D for our confined water according to Einstein's relation

$$D = \frac{\text{MSD}}{2dt} = \left\langle \frac{(R_{D_2O}(t) - R_{D_2O}(0))^2}{2dt} \right\rangle_{D_2O}$$

with the numerator representing the mean-square displacement (MSD), t the time, and d the number of dimensions in which the quantity is measured. For the simulation of confined water, only diffusion in the two periodic directions (in our case the y and z dimensions) is taken into account in order to reduce possible distortion due to the presence of the walls [18].

The mean-square displacement (MSD) of water molecules over time in the confined cases is presented in Fig. 2. From this graph, the diffusion coefficient for confined water is calculated to be 0.05 Å^2/ps. As 0.187 Å^2/ps for bulk water, the resulting ratio q is about 0.27 which falls into the range we obtained from literature.

As pointed out in several studies [11,12], however, taking the diffusion coefficient of the whole system all at once fails to take adequate consideration of different effects of the confinement at different position within the pore.

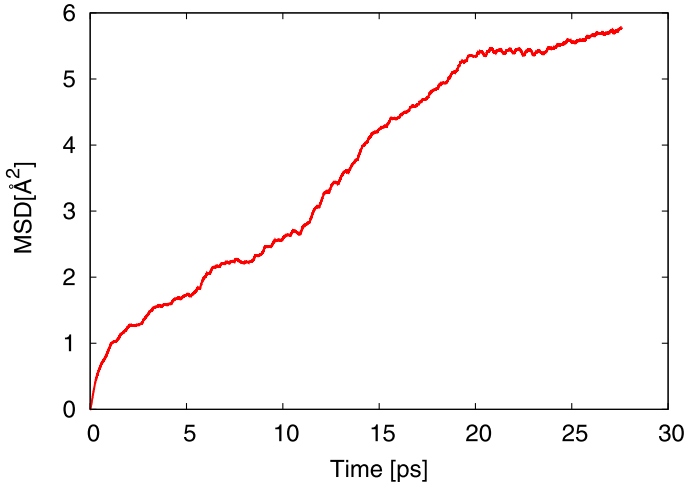

Fig. 2. Global MSD of the oxygen atoms of confined water at $T = 320$ K.

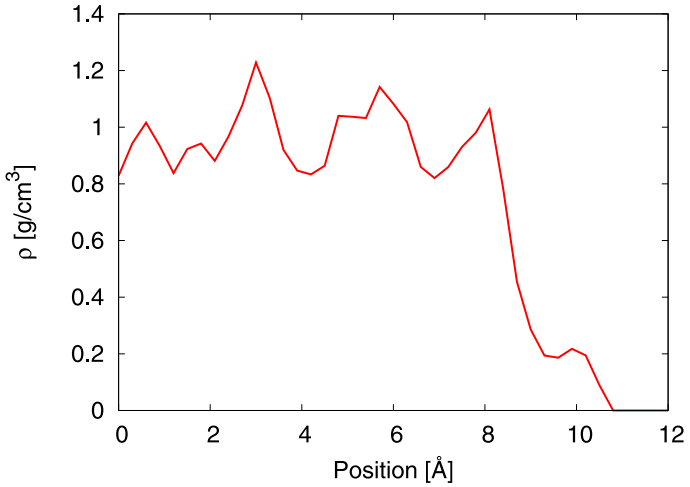

Fig. 3. Density Profile of Water confined between two silica slabs. The origin $x = 0$ Å corresponds to the center of the pore.

3.2 Density profile

The water density profile can demonstrate the configuration of confined water and the hydrophilic character of the silica surfaces. In the earlier empirical structure refinement simulations by R. Mancinelli *et al.* [5,27], the density of confined water in a MCM-41 pore is found to be higher in the vicinity of the silanol walls; at 300 K in the interfacial region the density was observed to be about 3 times as large as the density in the middle. This phenomenon stems from a so-called cohesive failure between water molecules. *I. e.* when water is confined between hydrophilic surfaces, voids occur in the middle of the water layer which leads to cohesive failure [26]. As to the present experimental results, Kocherbitov *et al.* [8] measured the apparent density of water in the MCM-41 pores at 298 K to be 0.88 g/cm^3 using H_2O and N_2 sorption method.

In our simulation, the density profile of water was constructed by creating a histogram of the spatial locations of all atoms across the pore with bins 0.3 Å wide and averaging over the entire NVE trajectory, as shown in Fig. 3. The position represents

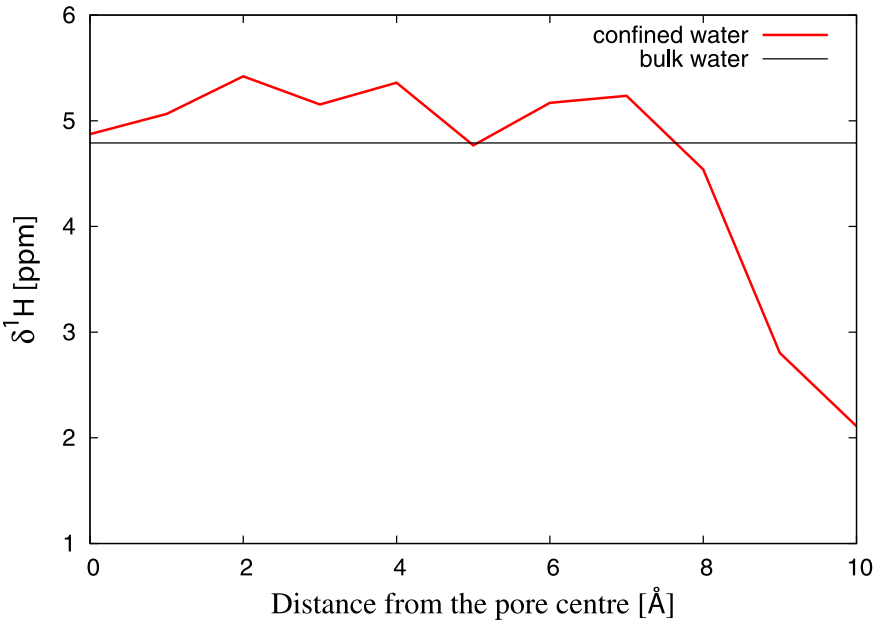

Fig. 4. Calculated ^{1}H NMR chemical shifts of water confined between silica slabs compared with bulk water, the distribution has been symmetrized with respect to the center ($x = 0$ Å), the value of ^{1}H NMR shifts are averaged in the x direction over the length of the model and the NVE trajectory of the system. The graph is drawn up to where the atoms in $Si(OH)_4$ start to appear.

the distance of the oxygen atoms from the center along the pore axis perpendicular to the silica surface. At the core region of the cell (0 Å to 2 Å) a lower density appears in our result, and at the outer edge (7 Å to 9 Å) as well, then it gradually decays to zero at the silica wall. Notable density oscillations are observed from Fig. 3, which reveals that the spatial layering occurred in confined water due to the hydrophilic character of the substrate [21]. For example, we see 2 density peaks near the silica substrate, which indicates that there are 2 separate layers of water in this region. However in several other simulations, the produced density profile showed either one [5,18] or two [12,24,25] peaks in the interfacial region and lower density in the core region. The small bump in the density profile near the very edge of the pore is also present in other results [12,18]. One possible reason for the minimum appearing here is the presence of the silanol groups oxygen atoms in that area taking up space.

3.3 ^{1}H NMR chemical shift calculations

Lately the *ab initio* calculation of nuclear chemical shifts has become one of the most powerful methods for structure determination on the molecular level. Not merely can the calculation interpret the spectra returned by the experiments [23], but also it can produce instantaneous results that are beyond experimental capability. Particularly the instantaneous ^{1}H NMR shifts can provide significant probe for the hydrogen bonding network of specific chemical environments [41,42].

The NMR shifts profile we obtained, as shown in Fig. 4, substantially indicates the configuration of water confined between the 2 silica slabs. The experimental ^{1}H NMR chemical shift $\delta = 4.79$ ppm for bulk water is taken from the value given in Ref. [22]. Figure 4 displays that in the major part of the cell, within 7.6 Å away from the center,

stronger H-bonded water appears with δ varying from 4.7 ppm to 5.4 ppm. The largest $\delta = 5.4$ ppm is reached at $x = 2$ Å. At the core of the pore ($x = 0$ Å), $\delta = 4.86$ ppm. Due to the confining effects of silica slabs, the NMR shifts are greater than those of bulk water. But at the core of the pore, the calculated shift approximates that of the bulk water, reflecting the hydrogen bonding in this region resembles bulk water H-bond network. While the shifts drop to upper-field as approaching the wall, in the vicinity of silanol walls (from $x = 7.6$ Å to $x = 10$ Å), water molecules are found to form weaker hydrogen bonds with each other or with silanols, the minimum value 2.1 ppm is found at $x = 10$ Å. As discussed before, the density profile shows layering effect took place in our cell. According to Gallo *et al.* [21], the interactions of the substrate atoms and thin water layers causes a strong distortion of the H-bond network. This explains why we see a decline of the shifts near the wall, even though it has been experimentally proven that the single silanol-water H-bond is stronger than the water-water H-bond [4].

We analogize the water filling process inside the pore by calculating the running average of ^{1}H chemical shifts up to a certain distance from the wall using equation

$$\delta_{\mathrm{Avg}}{}^1\mathrm{H}(x) = \frac{1}{N_{\mathrm{H}}} \sum_{x'=x_{\mathrm{wall}}}^{x} \delta^1\mathrm{H}(x)$$

$\delta_{\mathrm{Avg}}{}^1\mathrm{H}(x)$ represents the average δ value of a fictitious water film with thickness x. For each value of $\delta_{\mathrm{Avg}}{}^1\mathrm{H}(x)$, we sampled from the wall to the plane at corresponding distance and calculated all the shifts of water between the 2 planes. Taking the limitation of sampling into account, we leave out the first averaged value from $x = 0$ Å to 0.5 Å. The range of averaged NMR shifts along the x direction over the length of the cell covers from 2 to 4.9 ppm which is in good agreement with the experimental value from 1.74 to 4.7 ppm achieved in Buntkowsky's group [1]. Grünberg *et al.* obtained the chemical shift spectra of confined water at varying hydration level using ^{1}H solid-state NMR. In their results for the fully hydrated pore, one single signal appears at 4.7 ppm, and with very small water content ($\leq 2.7\%$), one dominating peak locates at 1.74 ppm which is ascribed to the shift of silanol groups.

Figure 5 shows that the behavior of water in our model resembles the water filling process described in Ref. [1]. Comparing our data with the experimental findings, we observe the same varying tendency in the chemical shifts. The minimum value of δ in Fig. 5 was obtained by computing the shifts of water locating within 0.5 Å to the silica substrate, so as to correspond the very low water filling factor in the experiments. In the interfacial region,the experimental NMR shift is an approximation to the shift of silanol groups. Therefore, it is believed that all water molecules at this region were hydrogen bonded to the silanols. With increased water content, additional water molecules start to form hydrogen bonds with each other which gives rise to ascending chemical shifts. This phenomenon is also reflected in Fig. 5, but increasing distance from the wall plays the role instead of increasing water filling factor. When the water content goes up to 3.2%, a notable peak at 2.5 ppm arises beside a weakened line at 1.74 ppm, which indicates the coexistence of 2 different types of hydrogen bonds. The NMR peak shifts consistently towards down-field upon further increasing hydration level. When there is 23% of water, the line at 2.5 ppm is broadened and shifts to 3.4 ppm. When the pore is completely filled, a single shift appears at 4.7 ppm.

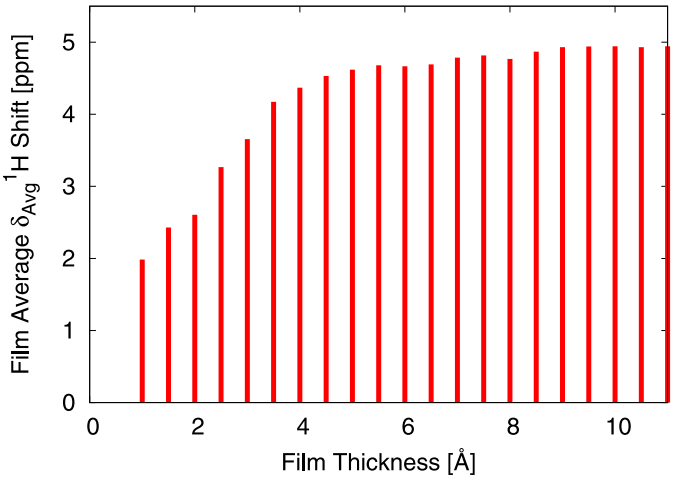

Fig. 5. Average of the ^{1}H NMR chemical shift values of those water molecules residing within a film of given thickness from the wall. The film thickness axis 0 Å and 11 Å are corresponding to the wall and the cell center respectively.

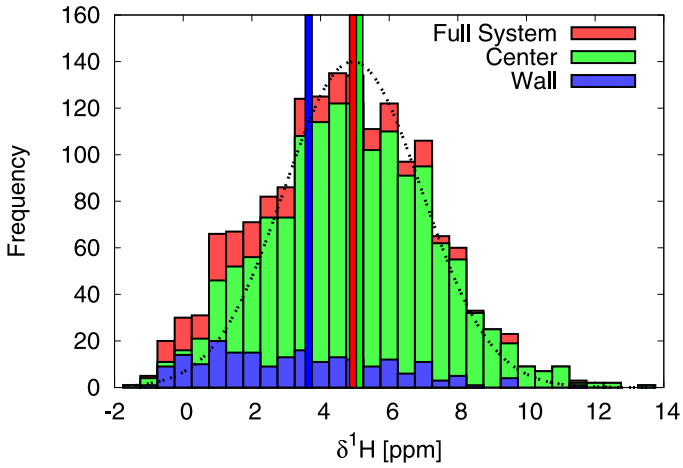

Fig. 6. Calculated ^{1}H NMR shift distribution of confined water. The ordinate is the occurence of the shifts for various δ values. $\delta = 3.65$ ppm is the averaged value for the water within 3 Å proximity to the walls (blue), $\delta = 4.94$ ppm is the global average of the whole system (red), and $\delta = 5.13$ ppm is the average shift of the water at the center of the pore (green). The dashed curve represents a gaussian centered at $\delta = 4.94$ ppm (black).

Our averaged NMR shifts imitate this process (as shown in Fig. 5) in such a way that the δ value continually goes up from 2 ppm to 5.5 ppm as increasing thickness of the film which starts from the wall (0 Å). This denotes that the bonding between water and the silanols becomes less and less dominating which leads to the the growing of the shifts until $x = 5.5$ Å. A plateau arises at 5.5 Å $< x <$ 11 Å reflecting the water molecules at the center region are mostly bounded to each other and not influenced by the walls.

Figure 6 illustrates the spacial distribution of the ^{1}H NMR shifts inside the cell. Those water molecules situated within 3 Å proximity to the silica wall are denoted as wall water, and the rest are considered to be center water. In this way, the confined water is divided into 3 layers, silanol-water interface (wall water), water-water (center

water) and water-silanol interface (wall water). The computed global average value of the ^{1}H chemical shift for all the water inside this cell is 4.94 ppm, the averaged water shift in the close region of walls is 3.65 ppm, and that for the water in the core area is 5.13 ppm. Comparing the whole distribution with a Gaussian centered at the global average δ value 4.94 ppm, we can easily see that more water molecules fall into the up field in the proximity of silanols. Most wall water resides at the left half of the graph with $\delta \leq 4.94$ ppm. The overall average shift of the system moves towards lower δ (upper field) under the effects of silica walls. This gives further evidence that the silanol groups play a twisting role for the water-water hydrogen bonding network in the interfacial region [21].

4. Conclusion

In this paper, DFT based molecular dynamics simulations and first principles NMR chemical shift calculations are applied on a simplified surface model based on the structural properties of the MCM-41 pore. Our calculations demonstrate the strong influence of spatial confinement on the structure and dynamical properties of water.

On the structural level, we see a strong influence on the ^{1}H chemical shifts of the confined water. While at the center of the pore a 0.5 ppm increased chemical shift compared to bulk water is found, the chemical shift gradually decreases when approaching the wall, until it reaches a value 3 ppm below bulk water reference. This implies an enhanced hydrogen bonding network for the water at the center, and a strongly weakened network close to the silica-water interface. In the density profile, distinctive peaks appear next to the wall, indicating a structuring of the water by the wall geometry. By calculating average chemical shifts for fictitious water films at the wall, we can see a change from low chemical shifts for thin films towards bulk water like chemical shifts for a film thickness above 4 Å. This is in good agreement with a previous experimental model on the gradual filling of nanopores.

With respect to the dynamical behavior, we see a decrease in the diffusion rate by a factor of 4 when comparing to bulk water values.

Acknowledgement

This work has been supported by the German Research Foundation (DFG) under grants SE 1008/5 and 1008/8. Computing infrastructure was provided by the Northern German Supercomputing Alliance (HLRN) under grant HLRN/bec00073 and ZEDAT high-performance cluster in Freie Universität Berlin. We thank the German academic exchange service (DAAD) for a RISE internship.

References

1. B. Grünberg, T. Emmler, E. Gedat, I. Shenderovich, G. H. Findenegg, H. H. Limbach, and G. Buntkowsky, Chem. Eur. J. **10** (2004) 5689.
2. A. Faraone, L. Liu, C. Mou, P. Shih, J. Copley, and S. Chen, J. Chem. Phys. **7** (2003) 3963.
3. F. Mansour, R. M. Dimeo, and H. Peemoeller, Phys. Rev. E **66** (2002) 041307.

4. C. Pantalei, R. Senesi, C. Andreani, P. Sozzani, A. Comotti, S. Bracco, M. Beretta, Mario, P. Sokol, and G. Reiter, Phys. Chem. Chem. Phys. **13** (2011) 6022.
5. R. Mancinelli, S. Imberti, A. K. Soper, K. H. Liu, C. Y. Mou, F. Bruni, and M. A. Ricci, J. Phys. Chem. B **113** (2009) 16169.
6. P. Smirnov, T. Yamaguchi, S. Kittaka, S. Takahara, and Y. Kuroda, J. Phys. Chem. B **104** (2000) 5498.
7. V. Ostroverkhov, G. A. Waychunas, and Y. R. Shen, Phys. Rev. Lett. **94** (2005) 046102.
8. V. Kocherbitov and V. Alfredsson, J. Phys. Chem. B **112** (2007) 12906.
9. I. G. Shenderovich, D. Mauder, D. Akcakayiran, G. Buntkowsky, H. H. Limbach, and G. Findenegg, J. Chem. Phys. B **111** (2007) 12088.
10. X. S. Zhao, G. Q. Lu, A. K. Whittaker, G. J. Millar, H. Y. Zhu, J. Chem. Phys. B **101** (1997) 6525.
11. D. W. Hwang, A. K. Sinha, C. Y. Cheng, T. Y. Yu, and L. P. Hwang, J. Phys. Chem. B **105** (2001) 5713.
12. P. Gallo, M. Rovere, and S. H. Chen, J. Phys.: Condens. Matter **24** (2012) 064109.
13. S. Pizzanelli, S. Kababya, V. Frydman, M. Landau, and S. Vega, J. Phys. Chem. B **109** (2005) 8029.
14. E. P. Ng and S. Mintova, Micropor. Mesopor. Mat. **14** (2008) 1.
15. K. Shirono and H. Daiguji, J. Phys. Chem. B **111** (2007) 7938.
16. K. Kleestorfer, H. Vinek, and A. Jentys, J. Mol. Catal. A: Chem. **166** (2001) 53.
17. S. Takahara, N. Sumiyama, S. Kittaka, T. Yamaguchi, B. Funel, and M. Claire, Adsorption **109** (2005) 5814.
18. A. Lerbret, G. Lelong, P. Mason, M. L. Saboungi, and J. Brady, Food Biophys. **6** (2011) 233.
19. M. E. Tuckerman, *Statistical Mechanics: Theory and Molecular Simulation*, Oxford Graduate Texts, Oxford University Press Inc., New York (2010).
20. A. R. Bizzarriand and S. Cannistraro, J. Phys. Chem. B **106** (2002) 6617.
21. P. Gallo, M. Rapinesi, and M. Rovere, J. Chem. Phys. **117** (2002) 7.
22. H. E. Gottlieb, V. Kotlyar, and N. Abraham, J. Org. Chem. **62** (1997) 7512.
23. D. R. Banyai, T. Murakhtina, and D. Sebastiani, Magn. Reson. Chem. **48** (2010) S56.
24. P. A. Bonnaud, B. Coasne, and R. J-M. Pellenq, J. Phys.-Condens. Mat. **22** (2010) 284110.
25. A. A. Milischuk and B. M. Ladanyi, J. Chem. Phys. **135** (2011) 174709.
26. T. G. Lombardo, N. Giovambattista, and P. G. Debenedetti, Faraday Discuss. **141** (2009) 359.
27. R. Mancinelli, F. Bruni, and M. A. Ricci, J. Phys. Chem. Lett. **1** (2010) 1277.
28. R. Mills, J. Phys. Chem. **77** (1973) 685.
29. M. Sulpizi, M. Gaigeot, and M. Sprik, J. Chem. Theory **8** (2012) 1037.
30. Computer code CP2K, available from www: www.cp2k.org/.
31. A. D. Becke, Phys. Rev. A **38** (1988) 3098.
32. S. Goedecker, M. Teter, and J. Hutter, Phys. Rev. B **54** (1996) 1703.
33. S. Grimme, J. Comput. Chem. **27** (2006) 1787.
34. J. VandeVondele and J. Hutter, J. Chem. Phys. **127** (2007) 114105.
35. D. Sebastiani and M. Parrinello, Chem. Phys. Chem. **3** (2002) 675
36. J. Schmidt, J. VandeVondele, I. F. Kuo, D. Sebastiani, J. I. Siepmann, J. Hutter, and C. J. Mundy, J. Phys. Chem. B **113** (2009) 11959.
37. J. Schmidt, A. Hoffmann, H. W. Spiess, and D. Sebastiani, J. Phys. Chem. B **110** (2006) 23204.
38. T. Murakhtina, J. Heuft, J. E. Meijer, and D. Sebastiani, Chem. Phys. Chem. **7** (2006) 2578.
39. Y. J. Lee, T. Murakhtina, D. Sebastiani, and H. W. Spiess, J. Am. Chem. Soc. **129** (2007) 12406.
40. A. Hoffmann, D. Sebastiani, E. Sugiono, K. S. Kim, H. W. Spiess, and I. Schnell, Chin. Phys. Lett. **388** (2004) 164.
41. K. Münnemann and H. W. Spiess, Nature Phys. **7** (2011) 522.
42. T. Metzroth, A. Hoffmann, R. Martín-Rapún, M. M. J. Smulders, K. Pieterse, A. R. A. Palmans, J. A. J. M. Vekemans, E. W. Meijer, H. W. Spiess, and J. Gauss, Chem. Sci. **2** (2011) 69.

2.2 Local Microphase Separation of a Binary Liquid under Nanoscale Confinement

- Xiang-Yang Guo, Tobias Watermann and Daniel Sebastiani

  J. Phys. Chem. B, **2014**, 118, 10207−10213.

  https://doi.org/10.1021/jp505203t

THE JOURNAL OF PHYSICAL CHEMISTRY B

Article

pubs.acs.org/JPCB

Local Microphase Separation of a Binary Liquid under Nanoscale Confinement

Xiang-Yang Guo, Tobias Watermann, and Daniel Sebastiani*

Institut für Chemie, Martin-Luther-Universität Halle-Wittenberg, 06120 Halle (Saale), Germany

ABSTRACT: The structural and diffusive properties of an ethanol−water mixture under hydrophilic nanoscale confinement are investigated by means of molecular dynamics simulations based on the CHARMM force field. The resulting density profiles illustrate that demixing of solvents occurs at the pore wall region, which is composed of silanol molecules in our case. Ethanol molecules are more likely to attach to the wall via hydrogen bonds than water molecules. A noticeable O−H bond orientation is observed for the ethanol molecules in this region, which can be explained by the formation of two specific hydrogen bonds between ethanol and silanol. Water, in contrast, resides mostly outside the interfacial region and is in favor of forming small hydrogen bonded strings and clusters with other water molecules. This phenomenon is corroborated by both the orientation of ethanol hydroxyl groups and the radial distribution functions of the solvent oxygen atom to the silanol hydrogen atom. Ethanol selectively attaches to the wall and forms a layer close to the wall. The hydrophobic headgroups of these ethanol molecules lead to an internal hydrophobic interface layer, which in turn yields cluster structures in the adjacent water. The self-diffusion of water in the confined ethanol−water mixture at the center of the pore is faster than that of water in the bulk ethanol−water mixture; ethanol, on the other hand, diffuses slower when it is confined.

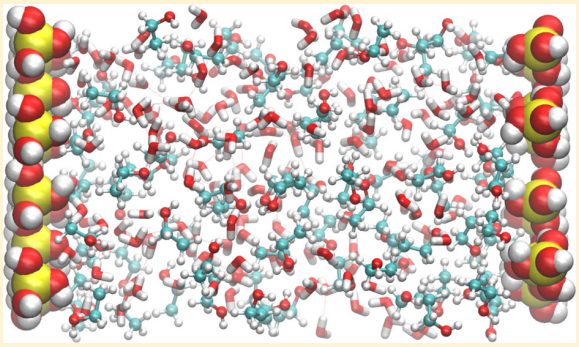

INTRODUCTION

Ethanol (EtOH) as one of the simplest alcohols has a lot of applications in laboratories and industrial processes. Considerable research into the nature of ethanol−water solutions at the molecular level gives us some insight into their properties. Already in the bulk phase, an ethanol−water mixture as a highly polar hydrogen-bonding liquid offers a great richness of structural diversity and physical−chemical phenomena.[1−3] Also, it has been discovered that, when ethanol is mixed with water, the entropy of the solution increases far less than expected. Experimental evidence indicates that the hydrophobic part of alcohol molecules gives rise to the existence of heterogeneous structure at the molecular level in aqueous solutions.[4−10]

Understanding the properties of ethanol−water at interfaces on the molecular level is very important for many chemical and physical processes.[11−14] It has been proved by many studies that surface-directed phase separation appears in confined binary mixtures while one component is preferentially attracted to the walls.[15−18] However, with regard to the interaction of ethanol−water mixtures with silica surfaces, our atomistic understanding is far from satisfactory. Water molecules can interact with the surface through hydrophobic or hydrophilic interactions and hydrogen bonding. This leads to the partial ordering of water molecules in the vicinity of the confining surface.[19] To date, numerous studies focusing on water confined in porous frameworks have been carried out via simulations and experiments.[20−27]

Previously, we have reported an ab initio study of pure water under silica confinement by using a surface model that resembles the pore structural feature of MCM-41.[28] We concluded that the presence of the silica walls has a strong effect on the structure and dynamical properties of pure water. At the center of the pore, the calculated ^{1}H chemical shifts of the confined water are found to be higher than bulk water, which implies an enhanced hydrogen bonding network in this region. In the vicinity of the wall, a strongly weakened hydrogen bonding and distinctive layering of the water density appeared. Furthermore, a decrease in the diffusion coefficient of the confined water rate by a factor of 4 was observed when comparing to bulk water values. The recognition of the confinement effect stimulated us to carry on the investigation to a new aspect, namely, the simulations of liquid mixtures under silica confinement.

Rodriguez et al.[29] studied equimolar mixtures of water and acetonitrile confined between two silica walls using MD simulations. Their result on the hydrophilic confinement shows a net increment of water in the interplate region with a highly inhomogeneous local distribution. This stable water layer is found to be fully coordinated to the silanol groups due to the optimal geometrical arrangement of the wall surfaces. B. Ratajska-Gadomska and W. Gadomski[30] reported the solvation of ethanol in water confined by gelatin gel studied by Raman

Received: May 27, 2014
Revised: August 7, 2014
Published: August 8, 2014

   dx.doi.org/10.1021/jp505203t | J. Phys. Chem. B 2014, 118, 10207−10213

spectroscopy. Their work indicates that, when an ethanol-rich solution is confined in gelatin gel, so-called ethanol sandwich clusters exist with a layer of water molecules inside. In order to provide further atomistic insight into alcohol solutions under confinement, we present here a study of ethanol−water mixtures confined within silica surfaces. The silanol groups on the silica surface have a hydrophilic character. This yields a certain competition of hydrogen bonds between silanol−solvent and solvent−solvent. Therefore, the conformation and the donor−acceptor preferences in the ethanol−water mixture are even more complicated than water−silica and ethanol−water bulk mixtures. In this work, we perform classical MD simulations on ethanol−water mixtures at the presence of two silanol walls. We compute the density profiles and self-diffusion coefficients for both ethanol and water, and the results are compared with bulk solvents. The radial distribution functions and orientations of ethanol molecules are calculated as well. Furthermore, we analyze the hydrogen bonding in the ethanol + water/silanol system so as to increase our understanding of the influence of spatial confinement on the structure and dynamics of alcohol mixtures.

COMPUTATIONAL DETAILS

The NAMD software package[31] was used throughout this work to perform the molecular dynamic simulations. The CHARMM force field parameter files[32−34] were applied for both solvent molecules and silanol groups. The TIP3P water model was used. The particle-mesh Ewald (PME) algorithm was used for long-range electrostatics interactions, and a switching function with a cutoff of 12 Å and a switchdist of 10 Å was employed for the Lennard-Jones interactions. Diffusion simulations were carried out at six different temperatures from 298 to 348 K. A microcanonical (NVT) ensemble and canonical (NVE) ensemble were used, and the Langevin dynamics has been employed to keep the system at the desired temperature during NVT simulations. The simulation outcomes were analyzed through our own programs and VMD plugins.[35−37]

A snapshot of the unit cell during one simulation is presented in Figure 1. Two flat silanol walls consisting of 24 $Si(OH)_4$ are

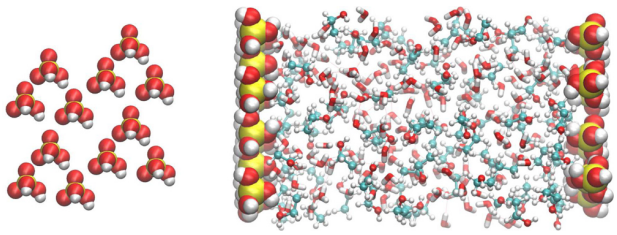

Figure 1. Picture of the silanol wall model normal to the wall surface (left) and a snapshot of an equilibrated ethanol−water/silanol system during a simulation at 338 K (right). Two silanol walls contain 24 $Si(OH)_4$, with 87 ethanol molecules and 148 water molecules confined in between.

placed along the x direction on both sides of an ethanol−water solution box with a size of 30 × 20 × 20 Å^3. The unit cell contains 148 water, 87 ethanol, and 24 silicic acids. The total number of atoms is 1443. This corresponds to a molar composition of x_{H_2O} = 0.63 and x_{EtOH} = 0.37. Three hydroxyl groups facing outside the unit cell are fixed in space. In case molecules enter the vacuum region between the periodic boxes, a force is applied on both sides of the wall to keep them in the solvent region.

To permit full electrostatic calculations via PME summation, the systems were made periodic in all directions with the elementary cell extended to accommodate a vacuum outside the silica surfaces along the x direction. The introduction of a vacuum gap between the unit cells is sufficiently large that adjacent images of the surface do not interact across the vacuum, which enables a surface to be modeled within the constraints of 3-D periodic boundary conditions. The resulting dimension of a simulation cell is 65 × 20 × 20 Å^3. In order to better manifest the effect of confinement, simulations of bulk water, bulk ethanol, and bulk ethanol−water mixture under the same conditions were carried out to enable comparisons with a confined system. The periodic unit cell of the bulk ethanol−water mixture is the same as the solution box between the slabs, also with a size of 30 × 20 × 20 Å^3.

RESULTS AND DISCUSSION

Diffusion. Self-diffusion is the simplest yet most fundamental form of transport at the molecular level which describes the translational motion of the individual component in a mixture.[38] The self-diffusion motion of molecules is characterized by a self-diffusion coefficient D_s. At 298.15 K, the D_s of bulk water and bulk ethanol has been experimentally determined to be 2.299 × 10^{9} [39] and 1.09 × 10^{9} m^2 s^{-1}, respectively.[40] The mobility of pure water in silica confinement is known to be slower than that in the pure bulk state due to the interactions with the hydrophilic pore walls. Experimental and computational reports indicate that D_s of confined water ranges from 23 to 64% of the value of bulk water.[22,28,41−43] Nevertheless, in our system, water interacts not only with the silanol wall but also with ethanol, and the mutual diffusion of the two components leads to altering of individual self-diffusion. Figure 2 displays the values of D_s for water and

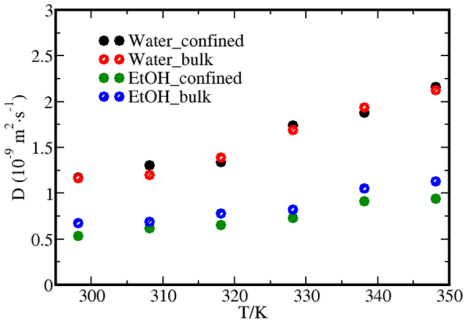

Figure 2. Self-diffusion coefficients of water and ethanol in confined alcohol solution at different temperatures compared with the corresponding bulk mixture.

ethanol confined in our hydrophilic slabs, along with the values of the corresponding unconfined (bulk) mixture under the same conditions. The temperature of the simulations varies from 298 to 348 K. All the diffusion coefficients D_s are determined from the time dependence of the mean squared displacement (MSD) via the Einstein relationship

$$D_s = \frac{\mathrm{MSD}}{2dt} = \left\langle \frac{(R(t) - R(0))^2}{2dt} \right\rangle \quad (1)$$

dx.doi.org/10.1021/jp505203t | J. Phys. Chem. B 2014, 118, 10207−10213

with t representing the time and d the number of dimensions in which the diffusion is measured. For the simulations of confined water and ethanol, only diffusion in the two directions parallel to the surface is taken into account.[42]

Our simulations show (Figure 2) that ethanol has a slower diffusion under confinement than in the bulk mixture at all temperatures. At 298 K, ethanol in the confined and bulk mixture exhibits diffusion constants of $D_s^{\text{EtOH mix}} = 0.53 \times 10^9$ and 0.67×10^9 m^2 s^{-1}, respectively. In both cases, the self-diffusion of ethanol is slower than that in pure liquid, which corresponds to $D_s^{\text{EtOH pure}} = 1.08 \times 10^9$ m^2 s^{-1} obtained by our simulation. Water in the confined mixture, on the other hand, behaves differently. Surprisingly, the self-diffusion of confined water in the alcohol water mixture has almost the same rate as in the bulk mixture. At some temperatures, we see a slightly accelerated diffusion for water in the confined state. This anomalous dynamics of water under confinement is closely related to the solvent structure between slabs, as described in the following sections.

Intraliquid Layer Formation. The mixture density (Figure 3a) illustrates the overall spatial distribution of the water−ethanol solution inside the cell, which is similar to that in other hydrophilic confinement reported in the literature.[20,24,44] The average density of the confined mixture is about $\rho_{\text{mix}} = 0.84$ g/cm^3. Inspection of Figure 3a reveals the presence of a well-defined adsorption layer from $x = 12.5$ Å to the wall. The highest density of the mixture is reached right next to the wall with an amplitude of around 1.30 g/cm^3. The intermediate layer (8−12.5 Å) represents the boundary between the structured interfacial liquid and the ordinary bulk liquid, since no further structuring is evident beyond this layer. The density reaches a constant value around 0.92 g/cm^3 at the center ($x \leq$ 6.0 Å).

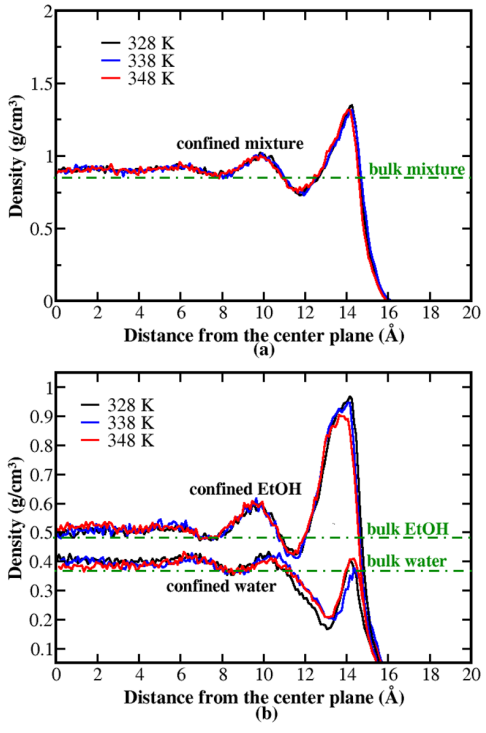

Figure 3. Density of the water/ethanol mixture (a) and partial densities of ethanol and water (b), all between silanol slabs at various T as a function of the perpendicular distance to the center (yz) plane at $x = 0$; the silica wall starts from 15 Å. All densities are averaged over the NVT trajectory and symmetrized to the center plane. The densities are compared to the corresponding densities for the bulk mixture, which is 0.48 g/cm^3 for EtOH, 0.37 g/cm^3 for water, and 0.85 g/cm^3 for the mixture.

The partial densities (Figure 3b) illustrate, in more detail, the contributions of the individual solvents to the total density profile. In the interfacial region, a surge in EtOH density is observed starting from 12.0 Å, which also reaches its maximum in close vicinity to the wall at 14.0 Å. The amplitude for the highest peak at 328 K is $\rho_{\text{EtOH}} = 0.96$ g/cm^3, which is around twice as high as the EtOH density at the center region. The high density at the first peak indicates strong hydrogen bonding between ethanol molecules and silanol groups. Then, a diffuse layer from 7.7 to 10.7 Å follows with amplitude around 0.6 g/cm^3. For $0 \leq x \leq 7.0$ Å, the density approaches a plateau with a value of the cell average of 0.5 g/cm^3. In contrast to ethanol, the water density is found to exhibit a rapid decrease in the proximity of the wall. After a narrow adsorption layer at 14.0 Å, the water density falls rapidly under the bulk value and reaches a minimum at 13.0 Å. Another layer of water is found located at 8−11 Å. At the center of the cell ($0 \leq x \leq 7$), the water density is distinctively higher than in the interfacial region with a value around 0.4 g/cm^3, which is also higher than the water density in the bulk mixture. Comparing the two graphs, we note that, in the proximity of the wall, we observe a surprisingly pronounced demixing: ethanol is concentrated at the wall, while water disseminates to the cell center.

The increased partial density of ethanol at the confinement silanol groups gives rise to the formation of a hydrophobic layer inside the liquid. This very interesting phenomenon results in an apparent competition of the hydrophilicity of the pore walls from the point of view of the water phase. Hence, the water which is located toward the center of the pore effectively sees a hydrophobic interface.

Regarding the temperature dependence of the density profile, we observe only a small variation in position and amplitude of the peaks. The highest EtOH density is obtained at the lowest temperature 328 K where the lowest water density is reached. This indicates that the demixing of ethanol and water tends to increase upon lowering the temperature, illustrating the reduction of entropic effects in favor of enthalpic aspects.

Internal Liquid Structure. The radial distribution functions (RDFs) between silanol hydrogen atoms and solvent oxygen atoms are presented in Figure 4 for water and ethanol confined in the silica slabs. The RDF in Figure 4 gives the probability of finding a solvent oxygen atom at distance r from a hydrogen atom of the silanols. Only those hydrogen atoms from the silanol hydroxyl group facing toward the center are included. The position of the first peak on both graphs is located at 1.97 Å, which is very close to the value of a typical H−O hydrogen bond length.[45] This means that both water and ethanol molecules are acting as hydrogen bond acceptors for the silanols. On the other hand, the area under the first peak in both graphs (Figure 4) shows that the probability of finding an ethanol oxygen is much higher than finding a water oxygen. Besides, most of the curve for ethanol is above 1, which corresponds to the partial demixing phenomenon observed in the vicinity of the wall. The oxygen atoms of the ethanol are much more likely to form hydrogen bonds with silanol. Integrating the RDF over r, we find that, at the wall region, the numbers of water and ethanol are almost the same, despite the

dx.doi.org/10.1021/jp505203t | J. Phys. Chem. B 2014, 118, 10207−10213

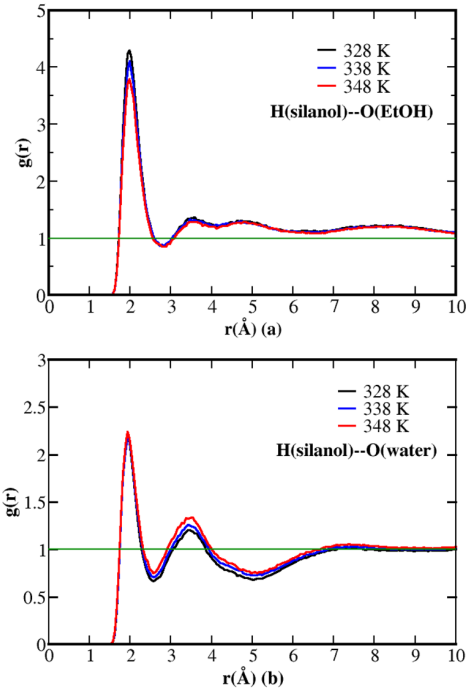

Figure 4. RDFs of silanol hydrogen atoms to solvent oxygen atoms: (a) H(si)−O(EtOH) and (b) H(si)−O(water) at three different temperatures.

fact that in the system there are many more water molecules. However, the numbers of two components start to differ from each other with increasing r from the wall; the number of water molecules goes up much faster when $r \geq 6$ Å.

As mentioned before, the solution becomes more structured as T decreases, and the change in temperature only affects the amplitudes of the peaks, not the positions. By comparing graphs in Figure 4a and b, the different impact of temperature on ethanol and water is demonstrated. In graph a, the growth of the height of the first peak with decreasing temperature corresponds to the fact that more ethanols are hydrogen bonded by the silanols at lower temperature. In comparison, the first peak in graph b for water does not vary much with temperature, but the height of the second peak goes up with the rising of temperature, whereas the second peak for $g(r)$ of H−O (EtOH) is not influenced by T. These results indicate the number of ethanol molecules at the wall region increases as the temperature decreases, but this influence becomes weaker with increasing distance from the wall. The number of water molecules at the adsorption layer, on the other hand, is not affected by the temperature, when the distance to the silanol oxygen is larger than 3.5 Å, the number of water molecules grows when temperature increases.

It is worth mentioning that, even without the presence of silanol walls, molecular segregation can still be observed in the bulk ethanol−water mixture. From the O−O RDF obtained form our simulation on bulk liquids at 298 K (Figure 5), the intrawater (Ow−Ow) RDF in pure water is compared with the Ow−Ow RDF in the bulk ethanol−water mixture. The first peak amplitude of the Ow−Ow RDF for the ethanol−water solution is obviously larger than that of the corresponding peak for pure water, but their shapes and positions are very similar. The second peaks of both Ow−Ow RDFs have close values in height and position. The Oe−Ow RDF has a different shape

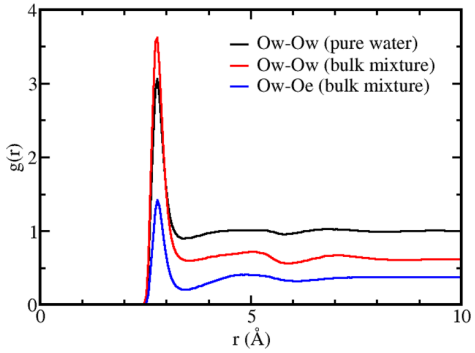

Figure 5. Oxygen−oxygen RDFs of bulk pure water compared with the bulk ethanol−water mixture. The RDFs are referenced to the molar fraction of water.

compared with the Ow−Ow RDF; especially its second peak at 5 Å is more apparent than that of the Ow−Ow RDFs. On the other hand, the first peak of the Oe−Oe RDF (Figure 6) for the

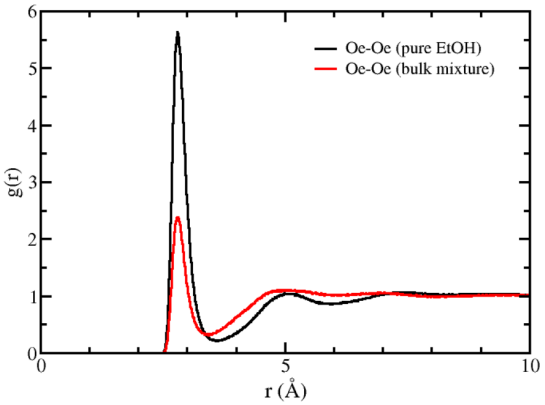

Figure 6. Oxygen−oxygen RDFs of bulk pure ethanol (black) compared with the bulk ethanol−water mixture (red).

mixture shrinks in size compared to pure ethanol and the second peak has a larger amplitude and radius. This is in very good agreement with the experimental results reported by Dixit et al.[4] on methanol−water solutions using the neutron diffraction method. Their research suggests that the methanol hydroxyl group enhances tetrahedral structure in the surrounding water; most water molecules form small clusters and serve as a bridge between hydroxyl groups of methanol molecules. Upon addition of water, the methanol hydroxyl groups were pushing apart while the methyl headgroups were getting closer. In conclusion, the partial microphase separation which is detectable already in unconfined water−alcohol mixtures is amplified under hydrophilic geometric confinement. In our system, ethanol as the less hydrophilic species has a higher possibility to form hydrogen bonds with silanol groups compared to water. Hence, the water clustering is significantly enhanced at the center of the cell when the ethanol hydroxyl group attaches to the wall and the hydrophobic alkyl parts face toward the center. Also, we notice that the decrease of temperature strengthens this demixing behavior of confined solvents.

Angular Distribution of Ethanol Molecules. The results discussed above suggest that the ethanol molecules form a layer in the wall region. It is also interesting to probe the orientation

dx.doi.org/10.1021/jp505203t | J. Phys. Chem. B 2014, 118, 10207−10213

of these ethanol molecules and the influence of the wall on this orientation. Conversely, the arrangement of ethanol at the interface also reflects the dynamically fluctuating H-bonding network between ethanol and silanol. We define α, γ, and θ as the angles between the normal vector of the wall surface pointing toward the cell center, i.e., surface vector (**1**, **0**, **0**) and O−H, CH_3−CH_2, and CH_2−OH bonds of the ethanol molecule.

We computed the occurrence of all possible angles over the whole trajectory. The ethanol angular distribution recorded in the simulation at 328 K is illustrated by Figures 7 and 8. The

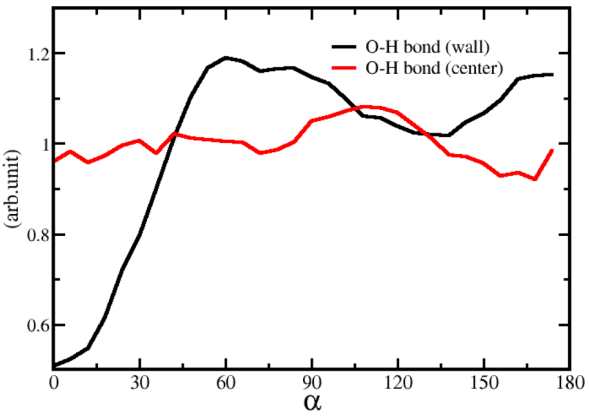

Figure 7. Angular distribution of the ethanol O−H bonds relative to the wall surface normal at the wall region (black) and at the cell center (red).

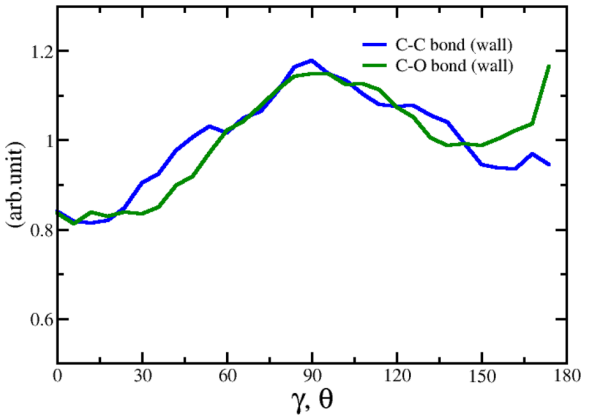

Figure 8. Angular distribution of ethanol CH_3−CH_2 bonds (blue) and CH_2−OH bonds (green) at the wall region.

"wall" and "center" denote the ethanol located within 5 Å to the silica wall or 5 Å cell center, respectively. The angle α is normalized by $1/\sin(\alpha)$; the same normalization was applied to γ and θ.

Figure 7 shows that the occurrence of ethanol at the wall region is generally much higher than that at the center region. Notably, there is no apparent orientation for the ethanol at the cell center and the OH bonds are evenly distributed in all possible angles from 0 to 180°. In contrast, at the interfacial region, the ethanol O−H bond is more likely to be found pointing to the wall with α ranging from 60 to 180°. Two maximal values are visible at around 60 and 180°, respectively, which suggests two forms of hydrogen bonding between silanol and ethanol, namely, O(EtOH)−H(Si) and O(Si)−H(EtOH). The CH_3−CH_2 and CH_2−OH bonds of the ethanol molecule at the wall region tend to have a broad distribution over all possible angles (Figure 8). A peak at 90° is observed, which corresponds to an orientation of the bonds parallel to the silica surfaces. This information confirms the qualitative observations from the simulation that more ethanol can be found hydrogen bonded to silanol groups.

Hydrogen Bonding Network. There are in total five possible hydrogen bond (H-bond) species inside the system, namely, ethanol−ethanol (e−e), ethanol−water (w−e), water−water (w−w), silanol−ethanol (e−si), and silanol−water (w-si) hydrogen bonds. The competitive interplay between those hydrogen bonds and the combination of hydrogen bonds with van der Waals interactions between the ethanol alkyl chains with silanol groups are responsible for the peculiar behavior of the confined solution.

We calculated the average hydrogen bond numbers of ethanol and water confined between the slabs for the trajectory at 328 and 338 K (Table 1). In a H-bond, an electropositive

Table 1. Average Numbers of Hydrogen Bonds in Our Geometrically Confined Water−Ethanol Mixtures

	Solvent−Silanol	
	w-si	e-si
328 K	9.5	9.2
338 K	9.2	8.9
	Solvent−Solvent at 328 K	
	w-w	w-e	e-e
total number[a]	110	92.4	18.1
wall region[b]	14.7	17.5	4.5
intermediate[b]	36.2	27.8	5.1
center region[b]	36.0	27.0	4.4
	Solvent−Solvent at 338 K		
	w-w	w-e	e-e
total number[a]	106	89.2	18.5
wall region[b]	14.3	16.6	4.8
intermediate[b]	34.4	26.6	5.2
center region[b]	35.9	26.5	4.4

[a]"Total number" denotes the average overall number of H-bonds inside the unit cell. [b]The solvent molecules located within 5 Å to the silanol walls and the center of the confinement are denoted as "wall region" and "center region", respectively, while the remaining solvent molecules are denoted by "intermediate".

hydrogen atom is shared between two electronegative atoms, e.g., the oxygens in ethanol, water, and silanol molecules. A H-bond is announced when the distance between a donor and an acceptor is less than 3.5 Å and when the angle between the bond vector and the O−O vector is less than a threshold angle 30°.

First, we notice that the number of water−silanol H-bonds is close to that of ethanol−silanol H-bonds. This reflects the fact that the number of ethanol and water molecules at the wall region is similar even though there are many more water molecules in the mixture. We can also see that the walls have a significant effect on the spatial distribution of all three solvent hydrogen bond species in the mixture. Solvent molecules are more structured in the intermediate region. At the wall region, the solvent−solvent H-bond number reaches the smallest value due to the hydrogen bonding capability of silanols. The number

dx.doi.org/10.1021/jp505203t | J. Phys. Chem. B 2014, 118, 10207−10213

of e−e hydrogen bonds is significantly smaller compared with w−w and w−e hydrogen bonds. This indicates that ethanol molecules were not clustering together like water; hence, their conformation can be distorted easier by silanol groups. This in turn is directly responsible for the high ethanol density at the wall region. We also note that this tendency does not change with temperature.

CONCLUSION

In this work, a binary mixture (water−ethanol) confined between silanol slabs was investigated by MD simulations based on the CHARMM force field. Our analysis of the trajectories revealed that, in the vicinity of silanols, a partial demixing of ethanol and water occurs. Water is more likely to form stable clusters, while ethanol is in contrast more flexible and therefore has a higher possibility to hydrogen bond with a silanol group. This, in return, enhances the water clustering structure; thus, demixing is most pronounced at the wall region. The molecular separation occurs due to the phenomenon of adsorption preference of silanol between water and ethanol. The results could also be important for better understanding the behavior of fluids in subsurface environments. Moreover, the self-diffusion coefficients of water and ethanol with and without confinement were calculated; the enhancement of the self-diffusion coefficients of water and the reduction of that of ethanol and the cause of this phenomenon are well manifested.

Special attention is paid to hydrogen bonding network and its influence on the anomalous diffusion behavior and molecular structure. Our simulations indicate that a significant restructuring of the hydrogen bond network between water and ethanol occurs as well as changes in the water−water hydrogen bonds due to the presence of the silanol walls. The hydrophobic environment generated by a layer structure of the ethanol alkyl groups further supports the stabilization of these water clusters as compared to the unconfined case.

AUTHOR INFORMATION

Corresponding Author

*E-mail: daniel.sebastiani@chemie.uni-halle.de.

Notes

The authors declare no competing financial interest.

ACKNOWLEDGMENTS

This work has been supported by the German Research Foundation (DFG) within the DFG-Forschergruppe 1583 (TP8). The computing infrastructure was provided by the ZEDAT high-performance cluster in Freie Universität Berlin. The authors thank the China Scholarship Council (CSC) for providing a scholarship.

REFERENCES

(1) Onori, G. Adiabatic Compressibility and Structure of Aqueous Solutions of Ethyl Alcohol. *J. Chem. Phys.* **1988**, *89*, 4325−4332.
(2) Wakisaka, A.; Matsuura, K.; Uranaga, M.; Sekimoto, T.; Takahashi, M. Azeotropy of Alcohol−water Mixtures from the Viewpoint of Cluster-level Structures. *J. Mol. Liq.* **2011**, *160*, 103−108.
(3) Wakisaka, A.; Komatsu, S.; Usui, Y. Solute-solvent and Solvent-solvent Interactions Evaluated through Clusters Isolated from Solutions: Preferential Solvation in Water-Alcohol Mixtures. *J. Mol. Liq.* **2001**, *90*, 175−184.
(4) Dixit, S.; Crain, J.; Poon, W. C. K.; Finney, J. L.; Soper, A. K. Molecular Segregation Observed in a Concentrated Alcohol-water Solution. *Nature* **2002**, *416*, 829−832.
(5) Harris, K. R.; Newitt, P. J.; Derlacki, Z. J. Alcohol Tracer Diffusion, Density, NMR and FTIR Studies of Aqueous Ethanol and 2,2,2-trifluoroethanol Solutions. *J. Chem. Soc., Faraday Trans.* **1998**, *94*, 1963−1970.
(6) Price, W. S.; Ide, H.; Arata, Y. Solution Dynamics in Aqueous Monohydric Alcohol Systems. *J. Phys. Chem. A* **2003**, *107*, 4784−4789.
(7) Guo, J. H.; Luo, Y.; Augustsson, A.; Kashtanov, S.; Rubensson, J. E.; Shuh, D. K.; Ågren, H.; Nordgren, J. Molecular Structure of Alcohol-Water Mixtures. *Phys. Rev. Lett.* **2003**, *91*, 157401−157402.
(8) Lin, K.; Hu, N.; Zhou, X.; Liu, S.; Luo, Y. Reorientation Dynamics in Liquid Alcohols from Raman Spectroscopy. *J. Raman Spectrosc.* **2012**, *43*, 82−88.
(9) Asenbaum, A.; Pruner, C.; Wilhelm, E.; Mijakovic, M.; Zoranic, L.; Sokolic, F.; Kezic, B.; Perera, A. Structural Changes in Ethanol−water Mixtures: Ultrasonics, Brillouin Scattering and Molecular Dynamics Studies. *Vib. Spectrosc.* **2012**, *60*, 102−106.
(10) Corsaro, C.; Maisano, R.; Mallamace, D.; Dugo, G. 1H NMR Study of Water/methanol Solutions as a Function of Temperature and Concentration. *Physica A* **2013**, *392*, 596−601.
(11) Sung, J.; Waychunas, G. A.; Shen, Y. R. Surface-Induced Anisotropic Orientations of Interfacial Ethanol Molecules at Air/Sapphire(1102) and Ethanol/Sapphire(1102) Interfaces. *J. Phys. Chem. Lett.* **2011**, *2*, 1831−1835.
(12) Tereshchuk, P.; Da Silva, J. L. F. Ethanol and Water Adsorption on Close-Packed 3d, 4d, and 5d Transition-Metal Surfaces: A Density Functional Theory Investigation with van der Waals Correction. *J. Phys. Chem. C* **2012**, *116*, 24695−24705.
(13) Cooke, D. J.; Gray, R. J.; Sand, K. K.; Stipp, S. L. S.; Elliott, J. A. Interaction of Ethanol and Water with the {1014} Surface of Calcite. *Langmuir* **2010**, *26*, 14520−14529.
(14) Andoh, Y.; Kurahashi, K.; Sakuma, H.; Yasuoka, K.; Kurihara, K. Anisotropic Molecular Clustering in Liquid Ethanol Induced by a Charged Fully Hydroxylated Silicon Dioxide (SiO 2) Surface. *Chem. Phys. Lett.* **2007**, *448*, 253−257.
(15) Yabunaka, S.; Okamoto, R.; Onuki, A. Phase Separation in a Binary Mixture Confined between Symmetric Parallel Plates: Capillary Condensation Transition near the Bulk Critical Point. *Phys. Rev. E* **2013**, *87*, 32405.
(16) Tanaka, H.; Araki, T. Surface Effects on Spinodal Decomposition of Incompressible Binary Fluid Mixtures. *Europhys. Lett.* **2000**, *51*, 154−160.
(17) Chen, W. Phase Separation of Binary Nonadditive Hard Sphere Fluid Mixture Confined in Random Porous Media. *J. Chem. Phys.* **2013**, *139*, 154712.
(18) Sharma, B. R.; Singh, R. N. Separation of Species of a Binary Fluid Mixture Confined between two Concentric Rotating Circular Cylinders in Presence of a Strong Radial Magnetic Field. *Heat Mass Transfer* **2010**, *46*, 769−777.
(19) Grünberg, B.; Emmler, T.; Gedat, E.; Shenderovich, I.; Findenegg, G. H.; Limbach, H.; Buntkowsky, G. Hydrogen Bonding of Water Confined in Mesoporous Silica MCM-41 and SBA-15 Studied by 1H Solid-state NMR. *Chem.—Eur. J.* **2004**, *10*, 5689−5696.
(20) Hwang, D. W.; Sinha, A. K.; Cheng, C. Y.; Yu, T. Y.; Hwang, L. P. Water Dynamics on the Surface of MCM-41 via 2H Double Quantum Filtered NMR and Relaxation Measurements. *J. Phys. Chem. B* **2001**, *105*, 5713−5720.
(21) Faraone, A.; Liu, L.; Mou, C. Y.; Shih, P. C.; Copley, J. R. D.; Chen, S. H. Translational and Rotational Dynamics of Water in Mesoporous Silica Materials: MCM-41-S and MCM-48-S. *J. Chem. Phys.* **2003**, *119*, 3963−3971.
(22) Shirono, K.; Daiguji, H. Molecular Simulation of the Phase Behavior of Water Confined in Silica Nanopores. *J. Phys. Chem. C* **2007**, *111*, 7938−7946.
(23) Kleestorfer, K.; Vinek, H.; Jentys, A. Structure Simulation of MCM-41 Type Materials. *J. Mol. Catal. A: Chem.* **2001**, *166*, 53−57.
(24) Gallo, P.; Rovere, M.; Chen, S. H. Water Confined in MCM-41: a Mode Coupling Theory Analysis. *J. Phys.: Condens. Matter* **2012**, *24*, 064109.

(25) Shenderovich, I. G.; Mauder, D.; Akcakayiran, D.; Buntkowsky, G.; Limbach, H. H.; Findenegg, G. H. NMR Provides Checklist of Generic Properties for Atomic-scale Models of Periodic Mesoporous Silicas. *J. Phys. Chem. B* **2007**, *111*, 12088−12096.
(26) Sulpizi, M.; Gaigeot, M.; Sprik, M. The Silica−Water Interface: How the Silanols Determine the Surface Acidity and Modulate the Water Properties. *J. Chem. Theory Comput.* **2012**, *8*, 1037−1047.
(27) Thompson, H.; Soper, A. K.; Ricci, M. A.; Bruni, F.; Skipper, N. T. The Three-dimensional Structure of Water Confined in Nanoporous Vycor Glass. *J. Phys. Chem. B* **2007**, *111*, 5610−5620.
(28) Guo, X. Y.; Watermann, T.; Keane, S.; Allolio, C.; Sebastiani, D. First Principles Calculations of NMR Chemical Shifts of Liquid Water at an Amorphous Silica Interface. *Z. Phys. Chem.* **2012**, *226*, 1415−1424.
(29) Rodriguez, J.; Elola, M. D.; Laria, D. Polar Mixtures under Nanoconfinement. *J. Phys. Chem. B* **2009**, *113*, 12744−12749.
(30) Ratajska-Gadomska, B.; Gadomski, W. Influence of Confinement on Solvation of Ethanol in Water Studied by Raman Spectroscopy. *J. Chem. Phys.* **2010**, *133*, 2345051−2345057.
(31) Phillips, J. C.; Braun, R.; Wang, W.; Gumbart, J.; Tajkhorshid, E.; Villa, E.; Chipot, C.; Skeel, R. D.; Kalé, L.; Schulten, K. Scalable Molecular Dynamics with NAMD. *J. Comput. Chem.* **2005**, *26*, 1781.
(32) Klauda, J. B.; Venable, R. M.; Freites, J. A.; O'Connor, J. W.; Tobias, D. J.; Mondragon-Ramirez, C.; Vorobyov, I.; MacKerell, A. D.; Pastor, R. W. Update of the CHARMM All-atom Additive Force Field for Lipids: Validation on Six Lipid Types. *J. Phys. Chem. B* **2010**, *114*, 7830−7843.
(33) Cruz-Chu, E. R.; Aksimentiev, A.; Schulten, K. Water-silica Force Field for Simulating Nanodevices. *J. Phys. Chem. B* **2006**, *110*, 21497−21508.
(34) Lopes, P. E. M.; Murashov, V.; Tazi, M.; Demchuk, E.; Mackerell, A. D. Development of an Empirical Force Field for Silica. Application to the Quartz-water Interface. *J. Phys. Chem. B* **2006**, *110*, 2782−2792.
(35) Humphrey, W.; Dalke, A.; Schulten, K. VMD: Visual molecular dynamics. *J. Mol. Graphics* **1996**, *14*, 33.
(36) Giorgino, T. Computing 1-D Atomic Densities in Macromolecular Simulations: The Density Profile Tool for VMD. *Comput. Phys. Commun.* **2014**, *185*, 317−322.
(37) Levine, B. G.; Stone, J. E.; Kohlmeyer, A. Fast Analysis of Molecular Dynamics Trajectories with Graphics Processing Units-Radial Distribution Function Histogramming. *J. Comput. Phys.* **2011**, *230*, 3556−3569.
(38) Vergeles, M.; Szamel, G. A Theory for Dynamic Friction on a Molecular Bond. *J. Chem. Phys.* **1999**, *110*, 6827−6835.
(39) Holz, M.; Heil, S. R.; Sacco, A. Temperature-dependent Self-diffusion Coefficients of Water and Six Selected Molecular Liquids for Calibration in Accurate 1H NMR PFG Measurements. *Phys. Chem. Chem. Phys.* **2000**, *2*, 4740−4742.
(40) Meckl, S.; Zeidler, M. D. Self-diffusion Measurements of Ethanol and Propanol. *Mol. Phys.* **1988**, *63*, 85−95.
(41) Takahara, S.; Nakano, M.; Kittaka, S. Neutron Scattering Study on Dynamics of Water Molecules Confined in MCM-41. *J. Phys. Chem. B* **1999**, *103*, 5814−5819.
(42) Lerbret, A.; Lelong, G.; Mason, P. E.; Saboungi, M. L.; Brady, J. W. Water Confined in Cylindrical Pores: A Molecular Dynamics Study. *Food Biophys.* **2011**, *6*, 233−240.
(43) Bonnaud, P. A.; Coasne, B.; Pellenq, R. J. M. Molecular Simulation of Water Confined in Nanoporous Silica. *J. Phys.: Condens. Matter* **2010**, *22*, 284110.
(44) Ng, E. P.; Mintova, S. Nanoporous Materials with Enhanced Hydrophilicity and High Water Sorption Capacity. *Microporous Mesoporous Mater.* **2008**, *114*, 1.
(45) Dougherty, R. C. Temperature and Pressure Dependence of Hydrogen Bond Strength: A Perturbation Molecular Orbital Approach. *J. Chem. Phys.* **1998**, *109*, 7372−7378.

2.3 Conformational Space of a Polyphilic Molecule with a Fluorophilic Side Chain Integrated in a DPPC Bilayer

- Guido F. von Rudorff, Tobias Watermann, Xiang-Yang Guo and Daniel Sebastiani
  Journal of Computational Chemistry, **2017**, 38, 576–583.
  https://doi.org/10.1002/jcc.24711

Conformational Space of a Polyphilic Molecule with a Fluorophilic Side Chain Integrated in a DPPC Bilayer

Guido F. von Rudorff,[a,b] Tobias Watermann,[b] Xiang-Yang Guo,[b] and Daniel Sebastiani*[b]

We investigate the conformational space of a polyphilic molecule with hydrophilic, lipophilic and fluorophilic parts inserted as a transmembrane agent into a dipalmitoylphosphatidylcholine bilayer by means of all-atom molecular dynamics simulations. Special focus is put on the competing structural driving forces arising from the hydrophilic, lipophilic and fluorophilic side chains and the aromatic backbone of the polyphile. We observe a significant difference between the lipophilic and the fluorophilic side chains regarding their intramembrane distribution. While the lipophilic groups remain membrane-centered, the fluorophilic parts tend to orient toward the phosphate headgroups. This trend is important for understanding the influence of polyphile agents on the properties of phospholipid membranes. From a fundamental point of view, our computed distribution functions of the side chains are related to the interplay of sterical, enthalpic and entropic driving forces. Our findings illustrate the potential of rationally designed membrane additives which can be exploited to tune the properties of phospholipid membranes. © 2017 Wiley Periodicals, Inc.

DOI: 10.1002/jcc.24711

Introduction

Modifying the behavior of membranes formed from lipid bilayers is of utmost importance for the development of medical applications. These modifications can range from small changes affecting membrane flexibility to larger modifications modifying the transport through membranes up to the formation of channels in the membrane. One way of modification is the introduction of trans-membrane molecules into the lipid bilayer. In our case, we use a special type of recently synthesized polyphilic trans-membrane molecules.[1–3]

Polyphilic molecules[4–9] are compounds that consist of fragments of different philicity. The molecules used here feature many possibilities of functionalization to tailor the interactions with the membranes toward different goals. The molecule we use has a phenylene ring backbone which is terminated with a glycerol group at either ends (see Fig. 1). In the middle of the backbone, two side chains are attached—one of which is a perfluoro-*n*-alkane, while the other one is a regular *n*-alkane. This molecular structure ensures a transmembrane orientation of the backbone, yielding an anchor point for the alkane/perfluoroalkane chains at the center of the membrane (Fig. 2).

The use of perfluoroalkanes is particularly interesting, as they are of interest in a wide range of applications in biological systems. Studies on fluorocarbons and fluorinated amphiphiles[10] included the use for *in vitro* protein synthesis and protein suluabilization,[11] pulminary drug delivery,[12] and also induced changes in vesicle properties such as permeability and interaction in biological systems.[13,14]

Several variations of the hydrophilic end groups and side chains of the polyphile have been synthesized and inserted into phospholipid bilayers, to tune aggregation behavior and order parameters of these additives.[1,2,5,15] In our work, we focus on a simple yet representative molecule (see Fig. 1) to reduce the computational cost of our simulations, and in turn allow for an adequate equilibration of the system. The used molecule features small hydrophilic end groups and two side chains of similar length.

In our simulations, we want to elucidate the structural driving forces which arise from the molecular interactions between a single polyphilic molecule (see Fig. 1) and a phospholipid membrane. This includes the orientation of the polyphile within the membrane and the conformational preferences of its side chains of different philicities.

Experimentally, polyphilic molecules are known to integrate inbetween a lipid bilayer membrane, even though perfluoro-*n*-alkanes are not miscible with *n*-alkanes.[16–19] As the model membrane environment is particularly well-understood, and offers a controlled separation of lipophilic and hydrophilic phases while consisting of only two simple kinds of molecules, we consider them to be an ideal candidate family for our set-up. As dipalmitoylphosphatidylcholine (DPPC) is used in our collaborating experimental groups[3] and well-covered in force-field support, we decided to use DPPC as a first membrane system. Parameters for the fluorophilic parts of the polyphiles have been developed and tested in a previous paper[20] and will be extended to cover the full polyphilic molecule.

[a] *G. F. von Rudorff*
Department of Physics and Astronomy, University College London, Gower Street, London, United Kingdom
[b] *G. F. von Rudorff, T. Watermann, Xiang-Yang Guo, D. Sebastiani*
Institute of Chemistry, Martin-Luther-Universität Halle-Wittenberg, von-Danckelmann-Platz 4, Halle 06120, Germany
E-mail: daniel.sebastiani@chemie.uni-halle.de
Contract grant sponsor: German Research Foundation (DFG) within the Forschergruppe FOR1145; Contract grant number: Se 1008/9-1

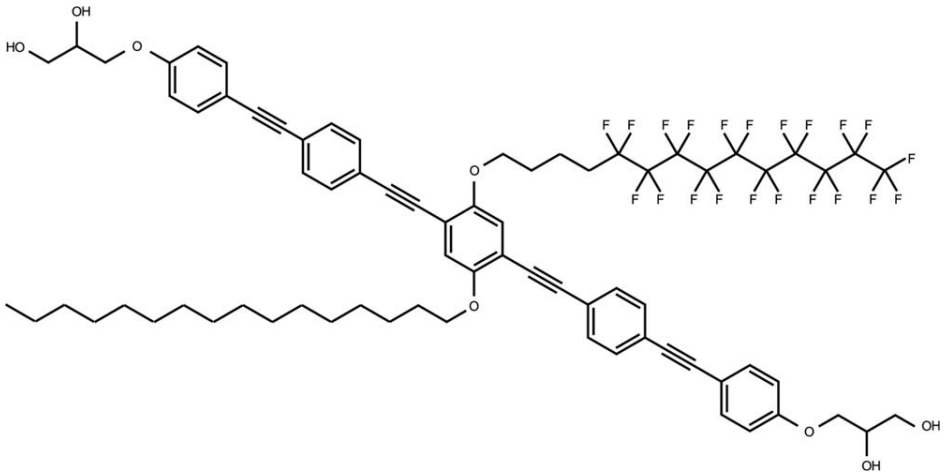

Figure 1. Chemical structure of the polyphilic molecule considered in this work.

Methodology

System

In our simulations, we use the molecule shown in Figure 1, a triphilic molecule in a DPPC bilayer environment. This molecule has been used in recent investigations within and outside of membranes. It offers a phenyl backbone with a length that allows for a transmembrane arrangement of the hydrophilic headgroups. In this transmembrane orientation, the two side chains, one alkyle and one perfluoroalkyle are fixed in the membrane center by their connection to the central phenyl ring. We perform simulations starting from two different starting conformations in two different orientations. We chose the two low energy conformations of the side chains that offer a strong change in the overall conformation of the molecule: all-trans (x-shaped) and all-trans with the first dihedral at the central phenyl ring turned by 180 degree (cross). Additionally, we started from two different orientations of the phenyl backbone: either directly perpendicular to the membrane plane or tilted by an angle of about 15 degrees. This is a typical angle found in experiments. As the polyphilic molecule is slightly longer than the membrane thickness, this angle also allows for the hydrophilic headgroups to arrange next to the DPPC headgroups. A more detailed description of the four starting points of our simulations can be found in the Supporting Information.

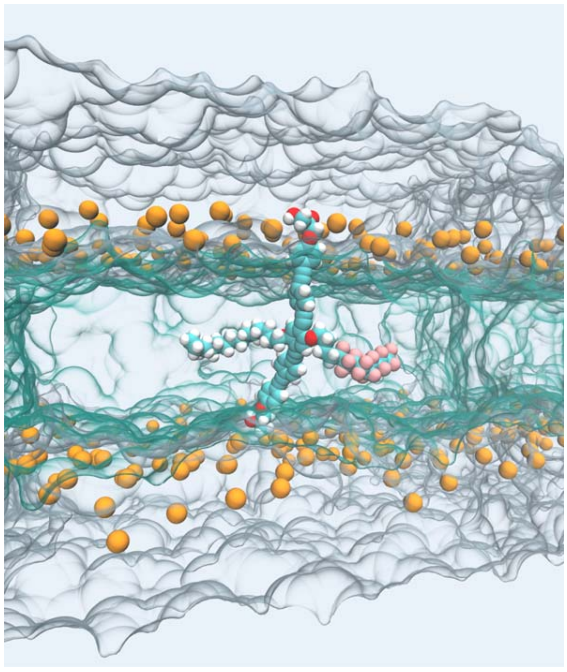

Figure 2. Single polyphile (all-atom representation) in a DPPC environment. The phosphorus atoms of the lipid head groups are denoted by orange spheres, the green layer is the volume occupied by the hydrocarbon tails of the lipids and the gray blocks show the volume occupied by the water layer. In simulations, the system was treated with periodic boundary conditions, effectively representing an infinite stack of infinite layers. [Color figure can be viewed at wileyonlinelibrary.com]

Computational details

All calculations are performed at atmospheric pressure, while the temperature has been set to 330 K. This temperature is just above the transition temperature of the membrane lipids from the gel state to the liquid state,[21,22] which is reproduced by the classical force field.[23] Simulations below this transition temperature are expected to be less insightful, as the mobility of the lipids is highly reduced, which means that very little to no movement is to be seen on the timescales accessible with our setup. With 330 K, we have chosen a temperature that is as near to room temperature as possible, that is also still in the experimentally relevant temperature range for pattern formation of the polyphilic molecules within the membranes.

We perform NPT calculations with a timestep of 1 fs in all cases, the trajectories have been equilibrated for 5 ns and run for a total of 50 ns each or 200 ns total. Additionally, one simulation with rigid bonds and a timestep of 2 fs for 400 ns is performed to assess the diffusion. Mean square displacements show a diffusion in good agreement with experimental

values[24] for the DPPC molecules. The diffusion constant of the polyphile slower than the DPPC molecules by roughly a factor of 2. The vdW cutoff follows the force field specifications[23] for lipid membranes, the electrostatics are treated with PME. The simulation setup consists of a pre-equilibrated[23] DPPC bilayer of 288 lipids enclosed by a water layer of roughly 10Å which sums up to a simulation box of $95\times95\times68$ Å^3. For our calculations, we chose the CHARMM force field,[25,26] which comes with both an extensively tested support[23] for a broad range of lipids and a clear parametrization procedure. For the glycerol end groups there are parameters available.[27,28] Recently, we have presented parameters for perfluoroalkanes.[20] As these parameters already cover the side chains of the polyphilic molecule in Figure 1, only some additional parameters were needed for proper coverage of the molecule. For them, we strictly followed the CHARMM parametrization procedure,[26] as discussed in the Supporting Information, where the resulting parameters as well as technical details[29–41] are listed. For all calculations, SHAKE constraints have been used for the water molecules only. While Lennard-Jones radii of 1.47 Å[42,43] and well above 3 Å[44] are common in literature, we have used the Lennard-Jones radius of 1.37 Å from our previous work. This value, along with the matching dihedral and angular potentials, has been shown to reproduce the helical structure of long perfluoro-*n*-alkanes as well as liquid densities over a wide pressure and temperature range.

The quantum chemical reference data (geometries, Hessians, charges) required for parametrization has been calculated by Gaussian 09.[45] All classical simulations were done by namd 2.9.[46] For analysis, we used VMD[47] and its Force Field Toolkit[34] together with MDAnalysis[48] and its RMSD alignment code.[49] For simulation preparation, a few tools from the GROMACS suite[50] have been used, as well.

Membrane insertion protocol

Simulating any molecules within membrane environments requires a "soft" procedure to embed the (smaller) molecules into these membrane snapshots. There are several established methods[51,52] to achieve a smooth insertion. A frequently applied protocol consists of shrinking the molecule drastically, then put it into the membrane at the desired location and scale it back to its original size. Simultaneously, energy minimizations are performed and all those molecules are removed which overlap with the inserted molecule. It turns out that in our context, the removal of lipids eventually leads to large holes in the membrane bilayer.

Therefore, we have somewhat modified this approach. Instead of removing any lipids, we create a repulsive force between them and the atomic centers of the molecule to be inserted. The size of the area where these forces are applied is slowly increased during a thermostatted molecular dynamics simulation, until the lipids have moved apart, creating sufficient space for the new molecule with the conventional force field interactions. Finally, the membrane and the new molecule can be added together without any clashs or collisions.

Results and Discussion

Intramolecular bending

The overlap of the intramolecular conformational space of the polyphile between the four independent trajectories represents an indicator of the convergence of our conformational sampling. To this end and also to characterize the conformational behavior of the polyphile in the membrane, we analyze two representative angles which characterize the orientation if the polyphile within the DPPC membrane.

The first angle is the smallest angle between the backbone of the polyphilic molecule and the normal vector of the membrane. This means that if the backbone is perpendicular to a single membrane layer, the angle α is zero, otherwise it is the minimum angle regardless of the rotation of the polyphilic molecule around the normal vector of the membrane layer. As there are two lipid layers in the bilayer membrane, we have two angles, α_1 and α_2 which are the angle α for the top and for the bottom layer of the membrane. Technically, this angle is calculated from the vector between the center of mass of the middle phenylene ring of the backbone and the center of mass of the last one and the membrane normal vector.

The second angle β is the bending angle of the phenylene ring backbone of the polyphilic molecule. A straight polyphile corresponds to an angle of $\beta=180°$. The specific angle definition is visualized in Figure 3 (top).

Figure 3 shows that the distribution of the angles α_i is quite similar for the trajectories and that the initial configurations have only little influence on the actual distribution. This means that the overlap between the conformations of the backbone is very high, hinting toward correct sampling of the system.

Figure 3 also shows that the reorganization of the lipid head groups on insertion of the polyphilic molecule into the membrane happens very fast. This can be deduced from the fact that none of the four trajectories has a hot spot around the angles the respective setup has been initialized with. As stated in the methods section, the initial conformations were perpendicular to the membrane plane ($\alpha_i = 0$) or tilted by 15 degrees ($\alpha_i = 15$). For no trajectory, there is a hot spot at that position. The highest density in the histogram is around $\alpha_1 = 35$ $\alpha_2 = 45$ which is considerably off the initial value. Figure 3 clearly shows that there is practically no probability of finding the polyphilic molecule somewhere near to the fifteen degrees. This means that the local ordering of the head group lipids should be observable within the timescale of 50 ns.

From the data in Figure 3, it is also clearly visible, that those orientations are preferred where the two angles α_i are not equal. This means that the backbone is bent most of the time. This bending can be further investigated by having a look at the angle β which is defined in Figure 3 and the distributions of which are shown in Figure 4.

Figure 4 shows the distribution functions of the backbone bending angle β of the polyphilic molecule for each of the four independent trajectories. The distribution maxima vary between 150° and 165°, the tails extend up to 130° and 145°. The variance observed for the different trajectories shows that full phase

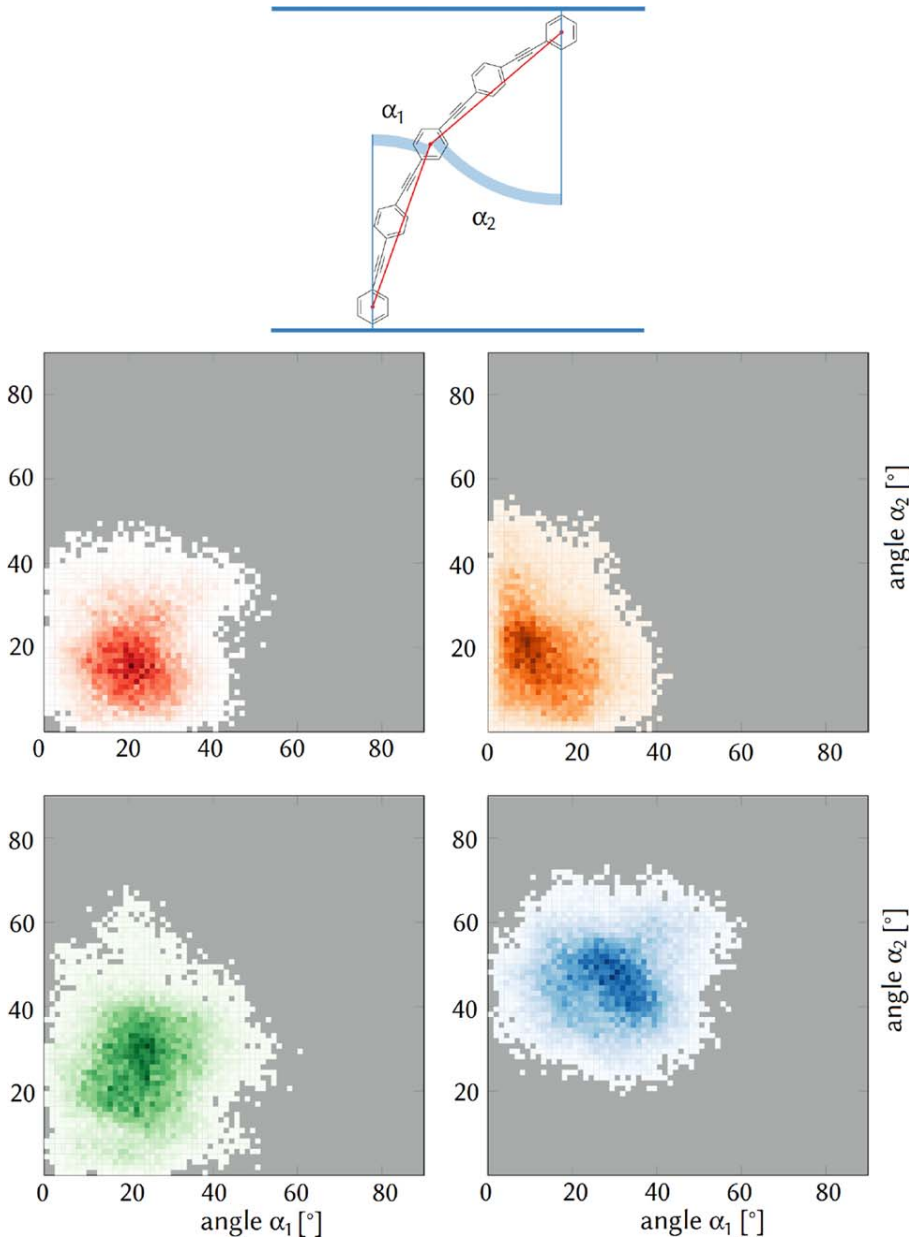

Figure 3. Top, centered: Definition of the membrane surface contact angles α_1, α_2 of the polyphile (only the phenylene ring backbone is shown). Red dots denote the center of mass of the carbons of the respective ring. Bottom: Twodimensional histograms of (α_1, α_2) for each independent trajectory. [Color figure can be viewed at wileyonlinelibrary.com]

space convergence has not yet been reached. Nevertheless, the similarity between the distribution functions indicates that the characteristics of the distribution functions are most probably realistic. A feature common to all trajectories is the absence of conformations with angles β close to 180° (despite the normalization with $1/\sin\beta$. This indicates that the polyphiles are always bent when inserted in the lipid membrane. This bending is indicative of a slight mismatch between the length of the lipophilic core of the polyphile and the thickness of the DPPC membrane. This result might have implications on experiments where the backbone is assumed to be straight in the analysis and interpretation of measurement results.[53]

Side chain localization within the membrane

The most important yet open question regarding the side chains of the polyphilic molecule is about their orientation within the membrane. As they are connected to the same phenylene ring in the middle of the backbone of the polyphilic molecule which happens to be in the middle of the membrane layer at all times in the simulation setup, the position of the terminal CH_3 or CF_3 groups of the side chains is a simple yet effective measure for describing the alignment of the side chains. If these terminal groups are near to the middle of the membrane, the side chains are located between the two lipid layers, making use of the low density at that part of

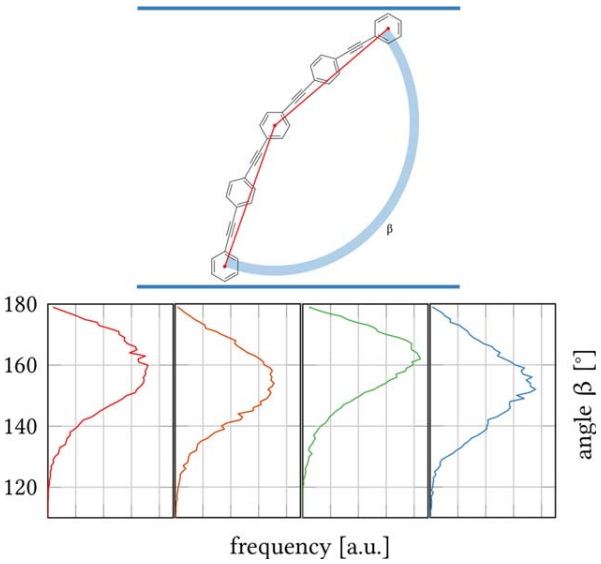

Figure 4. Top: Definition of the backbone bending angle β. Bottom: Distribution functions (histogram renormalized with $1/sin\beta$ for each of the four trajectories. [Color figure can be viewed at wileyonlinelibrary.com]

the system. If the terminal groups are far away from the middle of the membrane, that is, near to the head group region of the lipids, then they have to be aligned parallel to the alkyl strands of the lipid molecules due to the geometric constraints. For the rest of the analysis, we have considered the middle 10 Å of the membrane layer to qualify for a orientation of the side chains in the middle of the membrane, that is the first case described above. Therefore, if the distance of the terminal group of each side chain from the middle of the lipid bilayer is more than 5 Å, then the side chain is considered to be aligned along the alkyl strands of the lipids. While we exspect the alkyle side chain to be very compatible with the lipid chains of the DPPC, the prevalent interaction of the perfluorinated parts can be influenced by both, the stiffness of the side chain and the low miscibility of alkane and perfluoroalkane chains.

Using namd2, we calculated the interaction energies for the following pairs along 550 equidistant snapshots over the whole trajectory.

- DPPC lipid—all other DPPC lipids
- polyphile—all other DPPC lipids
- DPPC headgroups—non-fluorinated side chain of the polyphile
- DPPC headgroups—fluorinated side chain of the polyphile

From the calculations, it is clearly visible that the single polyphile is well-stabilized in the membrane by the interaction with the other DPPC lipids, with the largest contribution coming from the van der Waals interactions. For the two side chains, we observe a stabilizing electrostatic interaction with the lipid headgroups only for the fluorinated side chain. This is not observed for the non-fluorinated side chain.

During the molecular dynamics simulation, the instantaneous interaction energy between the DPPC lipids and the polyphile varies both for the van der Waals and for the Coulomb contribution. Insight into the flip-flop dynamics could be gained in future work by evaluating this difference in the intermediate state, but is at this time unfeasable due to the limited sampling caused by both, the rarity and speed of the flip-flop events. Histograms and further analysis of the interaction energies can be found in the Supporting Information.

However, over the course of the trajectory, a distribution of energies is sampled. This distribution has a large variance for either components. During flip-flop events, one would expect the distribution to be different, as the intermediate states are not energetically stable. In theory, knowing the difference in distribution of the interaction energies for flip-flop events as compared to the stable side-chain orientation would allow to assess the energetics of the flip-flop process. However, this process is seen very rarely in the trajectory and—due to its unstable intermediate states—completes fast, which drastically affects sampling to an extend that the distribution of interaction energies does not seem to be converged even for the length of our trajectories. Obtaining the interaction energy during such flip-flop events would require even longer trajectories or biasing methods confining the system to consecutive snapshots along a reaction coordinate.

Figure 5 shows that both cases can be observed with comparable probability. Switching between these two states is fast and typically takes less than 1 ns. This feature makes this sample system even more interesting, because the energy barrier between the three possible metastable conformations of any side chain seems to be rather small. Still, is is more likely to observe the side chains parallel to the alkyl strands than in the middle of the membrane (see Table 1).

For the case where the side chains of the polyphilic molecule are oriented along the alkyl strands of the lipids, there are two sides of the membrane the side chains can point to. This side does not necessarily stay the same in our simulations, as in total, there are some 15 changes in total. Again, this whole side chain layer switch process happens very fast (typically, between 5 ns and 10 ns for the alkyl side chain and about 15 ns for the perfluorinated side chain). This flip flop, that is, a full transition from pointing to one lipid layer to pointing to the other lipid layer without any stable intermediate third state is very fast compared to the times expected for a flip flop of a complete molecule—for model membranes, fast flip flops happen within seconds and slow ones are to be observed within minutes.[54] Most likely, this is a result of the chemical compatibility between the fluorinated side chains and the fatty environment within the membrane. This assumption is supported by higher flip flop durations for the chemically less compatible semifluorinated side chain.

Figure 5 shows the temporal evolution and the time-averaged spatial distribution functions of the terminal CH_3/CF_3 groups of the side chains of the polyphile within the membrane. The four independent trajectories are shown separately. The characteristic shape of the temporal evolution varies considerably among the independent runs: The first and last

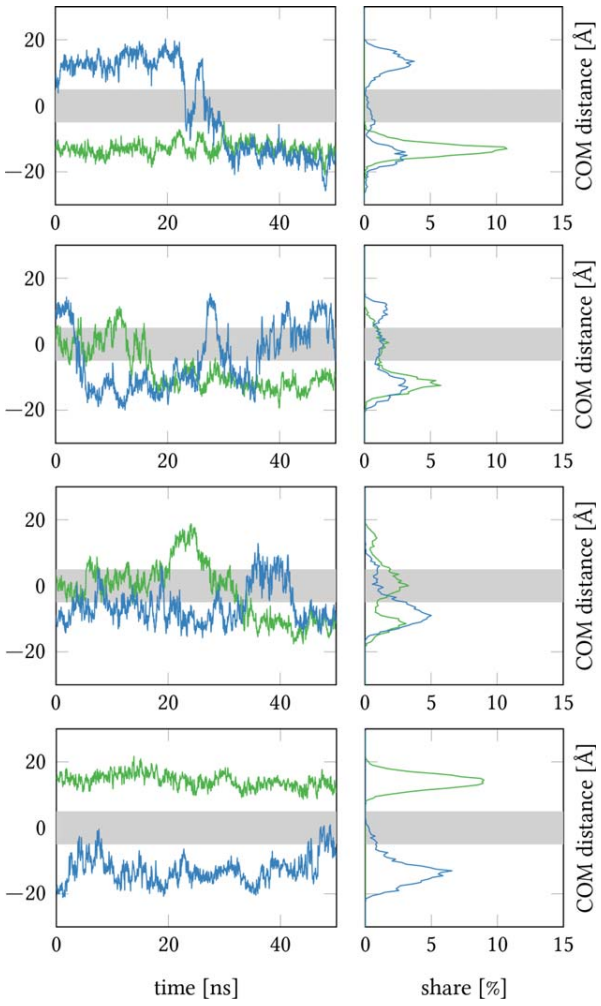

Figure 5. Trajectory (left) and distribution (right) of the terminal CF_3/CH_3 groups (green/blue) of the side chains of the side chains of the x-shaped polyphile relative to the membrane center. The shaded bar is considered as the center region. All four trajectories are shown independently. [Color figure can be viewed at wileyonlinelibrary.com]

trajectory show both CF_3 and CH_3 groups at stable localizations near the hydrophilic head groups (whose phosphorous atoms have an average coordinate of ± 20 Å), with a single crossover event from the "upper" to the "lower" head group region. In contrast to this, the second and third trajectory exhibits a less stable motional pattern of the CH_3/CF_3 endgroups, with a considerable probability in the center region of the bilayer (0 ± 5 Å, gray shaded area). This variability indicates that our phase space sampling cannot yet be considered as converged. Nevertheless, a clear trend is visible in

Table 1. Probability (%) of the side chain integration combinations where the perfluorinated side chain and the alkyl side chain are on the same side, the opposite lipid layer, or neither of these two options.

Trajectory	Same	Opposite	Undefined
Cross shaped initial geometries	38	36	27
x-shaped initial geometries	9	61	30
Overall average	23	48	28

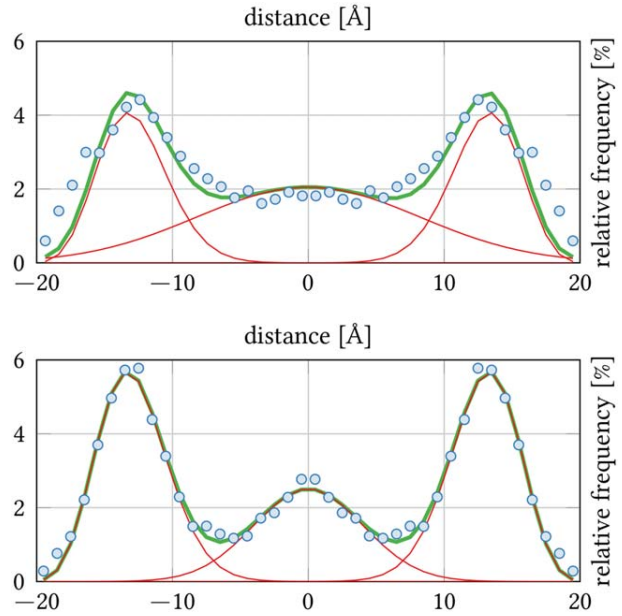

Figure 6. Histogram of the terminal group positions along the membrane normal vector and the alkyl side chain (top) and the perfluorinated side chain (bottom). The histogram from the simulation (circles) can be suitably explained by a Poisson-Gaussian fit (thick) which consists of three contributions (thin). The histogram from the simulation has been symmetrized. [Color figure can be viewed at wileyonlinelibrary.com]

the distribution functions toward a higher presence probability of the side chain endgroups in the vicinity of the lipid headgroup region, that is, around ± 15 Å. This trend is visualized even more concisely in Figure 6, where all four trajectories are shown in symmetrized and averaged form.

Figure 6 also shows that the tendency of localizing the CH_3/CF_3 endgroups toward the lipid headgroups is stronger for the perfluorinated chains than for the conventional alkane chains.

To formulate characteristic parameters for the distributions (Fig. 6) extracted from our simulations, we have fitted the distribution functions to a Poisson-type function:

$$P_\lambda(k) = \frac{\lambda^k}{k!} e^{-\lambda}$$

We see that this assumed probability distribution of the location of the side chains closely fits the simulation data for both side chain types. In the Supporting Information, we have shown that this Poisson-Gaussian fit works equally well for simulations at higher temperatures alongside a detailed description of the fitting process.

From the fit in Figure 6, we can obtain a relative weight for the terminal groups being at the center of the membrane (modeled by the Gaussian component of the fit) and for them being found in the outer part of which near the lipid head groups (modeled by the Poisson component). The components are shown in Figure 6, as well. According to them, the alkyl side chain is found in the center of the membrane 56% of the time, whereas the fluorinated side chain is found there 26% of the time. This clearly shows a tendency for the fluorinated side chain to avoid the center of the membrane.

Conclusions

We have determined the transmembrane orientation and intramolecular conformational distribution of a polyphilic molecule within a DPPC bilayer by means of all-atom molecular dynamics simulations of a total duration of 0.6 μs. The polyphile was structurally designed to introduce short perfluorinated and regular alkane chains into the center of the membrane, in view of modifying the membrane properties by its partially fluorophilic character.

Our simulations show that the polyphile is indeed commensurate with the membrane, albeit a certain intramolecular bending and an inclination with respect to the membrane plane is observed, which is assigned to a slight size mismatch between the membrane and the lipophilic backbone of the molecule. We find an interesting difference in the orientational preferences between the perfluorinated side chain and the conventional alkane chain. The perflourinated side chain orients along the lipophilic chains and toward the phosphate headgroups of the DPPC molecules, while the alkane side chain remains mostly in the center of the bilayer.

The self-diffusion for the lipids is in good agreement with experimental data. The diffusion constant of the polyphilic molecule is smaller by a factor of about 2. This illustrates that the polyphile is almost as mobile as a regular lipid, despite its twofold anchoring at both lipid-water interfaces and its additional side chains within the membrane.

Our simulations are a first step toward the understanding of intramembrane structure of polyphilic molecules with specifically designed side chains of different philicity. These molecules have the potential to enable a controlled modification of membrane properties such as water and ion permeability. In this context, the conformational space of the side chains is the key to the understanding of their structure–function relationships.

Keywords: polyphilic molecule · transmembrane · DPPC · perflourinated side chain · molecular dynamics

How to cite this article: G. F. von Rudorff, T. Watermann, X.-Y. Guo, D. Sebastiani. *J. Comput. Chem.* **2017**, *38*, 576–583. DOI: 10.1002/jcc.24711

Additional Supporting Information may be found in the online version of this article.

[1] C. Schwieger, A. Achilles, S. Scholz, J. Rüger, K. Bacia, K. Saalwaechter, J. Kressler, A. Blume, *Soft Matter* **2014**, *10*, 6147.
[2] X. Zeng, R. Kieffer, B. Glettner, C. Nürnberger, F. Liu, K. Pelz, M. Prehm, U. Baumeister, H. Hahn, H. Lang, G. A. Gehring, C. H. M. Weber, J. K. Hobbs, C. Tschierske, G. Ungar, *Science* **2011**, *331*, 1302.
[3] P. Scholtysek, A. Achilles, C.-V. Hoffmann, B.-D. Lechner, A. Meister, C. Tschierske, K. Saalwächter, K. Edwards, A. Blume, *J. Phys. Chem. B* **2012**, *116*, 4871.
[4] E. H. Hill, K. Stratton, D. G. Whitten, D. G. Evans, *Langmuir* **2012**, *28*, 14849.
[5] M. Schulz, A. Olubummo, W. H. Binder, *Soft Matter* **2012**, *8*, 4849.
[6] J. Hinks, Y. Wang, W. Han Poh, B. C. Donose, A. W. Thomas, S. Wuertz, S. C. Joachim Loo, G. C. Bazan, S. Kjelleberg, Y. Mu, T. Seviour, *Langmuir* **2014**, *30*, 2429.
[7] P. V. James, P. K. Sudeep, C. H. Suresh, K. George Thomas, *J. Phys. Chem. A* **2006**, *110*, 4329.
[8] E. H. Hill, D. G. Whitten, D. G. Evans, *J. Phys. Chem. B* **2014**, *118*, 9722.
[9] A. J. Crane, F. J. Martinez-Veracoechea, F. A. Escobedo, E. A. Muller, *Soft Matter* **2008**, *4*, 1820.
[10] M. P. Krafft, *Adv. Drug Deliv. Rev.* **2001**, *47*, 209.
[11] K. Park, C. Berrier, F. Lebaupain, B. Pucci, J. Popot, A. Ghazi, F. Zito, *Biochem. J.* **2007**, *403*, 183.
[12] J. C. Maurizis, M. Azim, M. Rapp, B. Pucci, A. Pavia, J. C. Madelmont, A. Veyre, *Xenobiotica* **1994**, *24*, 535.
[13] H. Permadi, B. Lundgren, K. Andersson, J. W. DePierre, *Biochem. Pharmacol.* **1992**, *44*, 1183.
[14] J. P. Vanden Heuvel, B. I. Kuslikis, M. J. Van Rafelghem, R. E. Peterson, *J. Biochem. Toxicol.* **1991**, *6*, 83.
[15] M. Schulz, S. Werner, K. Bacia, W. H. Binder, *Angew. Chem.* **2013**, *125*, 1877.
[16] H. Matsuda, A. Kitabatake, M. Kosuge, K. Kurihara, K. Tochigi, K. Ochi, *Fluid Phase Equilib.* **2010**, *297*, 187.
[17] Q. Chu, M. S. Yu, D. P. Curran, *Tetrahedron* **2007**, *63*, 9890.
[18] B. Cornils, *Angew. Chem. Int. Ed. (English)* **1997**, *36*, 2057.
[19] J.-P. Rolland, C. Santaella, B. Monasse, P. Vierling, *Chem. Phys. Lipids* **1997**, *85*, 135.
[20] G. F v. Rudorff, T. Watermann, D. Sebastiani, *J. Phys. Chem. B* **2014**, *118*, 12531.
[21] Z. V. Leonenko, E. Finot, H. Ma, T. E. S. Dahms, D. T. Cramb, *Biophys. J.* **2004**, *86*, 3783.
[22] K. Jacobson, D. Papahadjopoulos, *Biochemistry* **1975**, *14*, 152.
[23] J. B. Klauda, R. M. Venable, J. Alfredo Freites, J. W. O'Connor, D. J. Tobias, C. Mondragon-Ramirez, I. Vorobyov, A. D. MacKerell, R. W. Pastor, *J. Phys. Chem. B* **2010**, *114*, 7830.
[24] G. Lindblom, G. Orädd, A. Filippov, *Chem. Phys. Lipids* **2006**, *141*, 179.
[25] A. D. MacKerell, D. Bashford, D. Bellott, J. D. Evanseck, M. J. Field, S. Fischer, J. Gao, H. Guo, S. Ha, D. Joseph-McCarthy, L. Kuchnir, K. Kuczera, F. T. K. Lau, C. Mattos, S. Michnick, T. Ngo, D. T. Nguyen, B. Prodhom, W. E. Reiher, B. Roux, M. Schlenkrich, J. C. Smith, R. Stote, J. Straub, M. Watanabe, J. Wiórkiewicz-Kuczera, D. Yin, M. Karplus, *J. Phys. Chem. B* **1998**, *102*, 3586.
[26] K. Vanommeslaeghe, E. Hatcher, C. Acharya, S. Kundu, S. Zhong, J. Shim, E. Darian, O. Guvench, P. Lopes, I. Vorobyov, A. D. MacKerell, *J. Comput. Chem.* **2010**, *31*, 671.
[27] E. Hatcher, O. Guvench, A. D. MacKerell, *J. Chem. Theory Comput.* **2009**, *5*, 1315.
[28] A. D. MacKerell, *J. Comput. Chem.* **2004**, *25*, 1584.
[29] A. A. H. Pádua, *J. Phys. Chem. A* **2002**, *106*, 10116.
[30] W. Gordy, *J. Chem. Phys.* **1946**, *14*, 305.
[31] G. B. B. M. Sutherland, D. M. Dennison, *Proc. R. Soc. Lond. Ser. A* **1935**, *148*, 250.
[32] M. Thomas, M. Brehm, R. Fligg, P. Vöhringer, B. Kirchner, *Phys. Chem. Chem. Phys.* **2013**, *15*, 6608.
[33] P. Sinha, S. E. Boesch, C. Gu, R. A. Wheeler, A. K. Wilson, *J. Phys. Chem. A* **2004**, *108*, 9213.
[34] C. G. Mayne, J. Saam, K. Schulten, E. Tajkhorshid, J. C. Gumbart, *J. Comput. Chem.* **2013**, *34*, 2757.
[35] B. H. Besler, K. M. Merz, P. A. Kollman, *J. Comput. Chem.* **1990**, *11*, 431.
[36] U. Chandra Singh, P. A. Kollman, *J. Comput. Chem.* **1984**, *5*, 129.
[37] H. Bernhard Schlegel, *Theor. Chim. Acta* **1984**, *66*, 333.
[38] A. Amadei, M. D. Abramo, A. D. Nola, A. Arcadi, G. Cerichelli, M. Aschi, *Chem. Phys. Lett.* **2007**, *434*, 194.
[39] C. Møller, M. S. Plesset, *Phys. Rev.* **1934**, *46*, 618.
[40] B. Adisa, D. A. Bruce, *J. Phys. Chem. B* **2005**, *109*, 7548.
[41] B. Corry, D. Jayatilaka, B. Martinac, P. Rigby, *Biophys. J.* **2006**, *91*, 1032.
[42] E. Carosati, S. Sciabola, G. Cruciani, *J. Med. Chem.* **2004**, *47*, 5114.
[43] M. Pettersson, X. Hou, M. Kuhn, T. T. Wager, G. W. Kauffman, P. R. Verhoest, *J. Med. Chem.* **2016**, *59*, 5284.
[44] A. K. Rappe, C. J. Casewit, K. S. Colwell, W. A. Goddard, W. M. Skiff, *J. Am. Chem. Soc.* **1992**, *114*, 10024.

[45] M. J. Frisch, G. W. Trucks, H. B. Schlegel, G. E. Scuseria, M. A. Robb, J. R. Cheeseman, G. Scalmani, V. Barone, B. Mennucci, G. A. Petersson, H. Nakatsuji, M. Caricato, X. Li, H. P. Hratchian, A. F. Izmaylov, J. Bloino, G. Zheng, J. L. Sonnenberg, M. Hada, M. Ehara, K. Toyota, R. Fukuda, J. Hasegawa, M. Ishida, T. Nakajima, Y. Honda, O. Kitao, H. Nakai, T. Vreven, J. A. Montgomery, Jr., J. E. Peralta, F. Ogliaro, M. Bearpark, J. J. Heyd, E. Brothers, K. N. Kudin, V. N. Staroverov, R. Kobayashi, J. Normand, K. Raghavachari, A. Rendell, J. C. Burant, S. S. Iyengar, J. Tomasi, M. Cossi, N. Rega, J. M. Millam, M. Klene, J. E. Knox, J. B. Cross, V. Bakken, C. Adamo, J. Jaramillo, R. Gomperts, R. E. Stratmann, O. Yazyev, A. J. Austin, R. Cammi, C. Pomelli, J. W. Ochterski, R. L. Martin, K. Morokuma, V. G. Zakrzewski, G. A. Voth, P. Salvador, J. J. Dannenberg, S. Dapprich, A. D. Daniels, Ö. Farkas, J. B. Foresman, J. V. Ortiz, J. Cioslowski, D. J. Fox, Gaussian 09, Revision A.2; Gaussian Inc.: Wallingford, CT, **2009**.
[46] J. C. Phillips, R. Braun, W. Wang, J. Gumbart, E. Tajkhorshid, E. Villa, C. Chipot, R. D. Skeel, L. Kalé, K. Schulten, *J. Comput. Chem.* **2005**, *26*, 1781.
[47] W. Humphrey, A. Dalke, K. Schulten, *J. Mol. Graph.* **1996**, *14*, 33.
[48] N. Michaud-Agrawal, E. J. Denning, T. B. Woolf, O. Beckstein, *J. Comput. Chem.* **2011**, *32*, 2319.
[49] D. L. Theobald, *Acta Crystallogr. A* **2005**, *61(Pt 4)*, 478.
[50] S. Pronk, S. Páll, R. Schulz, P. Larsson, P. Bjelkmar, R. Apostolov, M. R. Shirts, J. C. Smith, P. M. Kasson, D. van der Spoel, B. Hess, E. Lindahl, *Bioinformatics* **2013**, *29*, 845.
[51] A. L. Lomize, I. D. Pogozheva, M. A. Lomize, H. I. Mosberg, *Protein Sci.* **2006**, *15*, 1318.
[52] M. G. Wolf, M. Hoefling, C. Aponte-Santamaría, H. Grubmüller, G. Groenhof, *J. Comput. Chem.* **2010**, *31*, 2169.
[53] L. K. Tamm, S. A. Tatulian, *Q. Rev. Biophys.* **1997**, *30*, 365.
[54] F. Kamp, J. A. Hamilton, *Proc. Natl. Acad. Sci. USA* **1992**, *89*, 11367.

Received: 11 May 2016
Revised: 20 August 2016; 17 November 2016
Accepted: 18 November 2016
Published online in Wiley Online Library

2.4 Cluster Formation of Polyphilic Molecules Solvated in a DPPC Bilayer

- Xiang-Yang Guo, Christopher Peschel, Tobias Watermann, Guido Falk von Rudorff and Daniel Sebastiani

  Polymers, **2017**, 9, 488

  https://doi.org/10.3390/polym9100488

polymers

MDPI

Article

Cluster Formation of Polyphilic Molecules Solvated in a DPPC Bilayer

Xiang-Yang Guo, Christopher Peschel, Tobias Watermann, Guido Falk von Rudorff and Daniel Sebastiani *

Institute of Chemistry, MLU Halle-Wittenberg, von-Danckelmann-Platz 4, 06120 Halle, Germany; xiang.guo@chemie.uni-halle.de (X.-Y.G.); christopher.peschel@chemie.uni-halle.de (C.P.); tobias.watermann@chemie.uni-halle.de (T.W.); guido@vonrudorff.de (G.F.v.R.)

* Correspondence: daniel.sebastiani@chemie.uni-halle.de; Tel.: +49-(0)345-55-25-836

Received: 15 September 2017; Accepted: 29 September 2017; Published: 6 October 2017

Abstract: We analyse the initial stages of cluster formation of polyphilic additive molecules which are solvated in a dipalmitoylphosphatidylcholine (DPPC) lipid bilayer. Our polyphilic molecules comprise an aromatic (trans-bilayer) core domain with (out-of-bilayer) glycerol terminations, complemented with a fluorophilic and an alkyl side chain, both of which are confined within the aliphatic segment of the bilayer. Large-scale molecular dynamics simulations (1 µs total duration) of a set of six of such polyphilic additives reveal the initial steps towards supramolecular aggregation induced by the specific philicity properties of the molecules. For our intermediate system size of six polyphiles, the transient but recurrent formation of a trimer is observed on a characteristic timescale of about 100 ns. The alkane/perfluoroalkane side chains show a very distinct conformational distribution inside the bilayer thanks to their different philicity, despite their identical anchoring in the trans-bilayer segment of the polyphile. The diffusive mobility of the polyphilic additives is about the same as that of the surrounding lipids, although it crosses both bilayer leaflets and tends to self-associate.

Keywords: lipid bilayer; DPPC; bolapolyphile; diffusion coefficient; perfluorinated; molecular dynamics (MD)

1. Introduction

Molecules which have the ability of self-assembling are of huge interest for biochemical (lipid bilayers), and nanosized materials [1]. To understand such behavior is crucial for the rational design of model and advanced systems. Many molecule types have been inserted into lipid bilayers in experiment and in simulations to understand their behavior. This ranges from early attempts by inserting alkanes into a lipid bilayer system to see where they are located inside the system [2], up to the latest investigations of fluorinated alkanes and alcohols [3]. In extend to those publications we investigated a very complex compound combining many philicities in one molecule. These so called polyphilic molecules, as the name suggests, are compounds consisting of fragments with different philicities. Special attention is paid here to polyphiles that contain a rigid rod-shaped aromatic core with opposing end groups and lateral groups with different philicities. The two end groups are typically highly polar, allowing the formation of multiple hydrogen bonds, which is only possible in the headgroup region of the bilayer and in the aqueous phase, whilst the lateral groups are alkyl, partially fluorinated or perfluorinated chains [4]. This novel class of molecules have received significant attention in recent years [5–10]. Polyphilic molecules can be used to modify the phase transitions temperature of a lipid bilayer [11] and also serve as a drug delivery agent [12,13]. Furthermore, they cause effects like compression or stretching of bilayer systems which was recently shown [11,14–18].

Fluorocarbon compounds are also studied for influencing the metabolism of rats [19,20] and for in vitro synthesis of lipid bilayer proteins [21].

To fully understand why this type of molecules influences the bilayer properties, the polyphilic molecules themselves have to be studied on a molecular scale. The molecule (B16/10) being investigated in this work possesses three philicities, namely fluorophilic, hydrophilic and lipophilic parts [6–10,22]. The rigid aromatic phenylene–ethynylene-backbone forms its frame structure, and two hydrophilic groups are terminating this backbone chain. In the middle of the backbone, two side chains are attached, one of which is a perfluoro-*n*-alkane, the other is a regular *n*-alkane (see Figure 1). The length of the side chains can be derived from the name (16 carbon atoms for the alkyl chain and 10 carbon atoms for the perfluorinated alkyl groups). This molecular structure ensures a trans-bilayer orientation of the backbone, yielding an anchor point for the alkyl/perfluoroalkyl chains at the center of the bilayer. Mobile aliphatic side chains and polar end groups offer many possibilities of functionalization to tailor the interactions with the bilayers. As the fundamental building blocks of cellular membranes, phospholipid bilayers play a decisive role in many of their biological functions. The modification of lipid bilayer functions via interactions with biomolecules such as proteins or peptides has been widely investigated [23–26]. Due to experimental investigations of the influence of purely synthetic molecules on DPPC bilayers [14,15,27], it serves perfectly as a model system for thorough investigation of the influence of our polyphilic molecules on the bilayer properties. The concept of polyphilicity was even recently used for directly modifying the lipid bilayer itself by perfluorinating the end of the lipid tails [28].

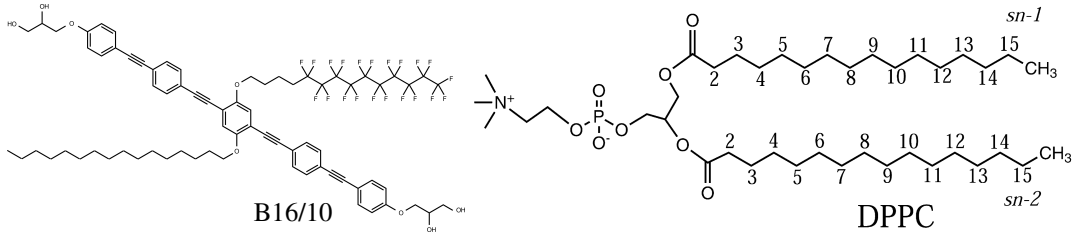

Figure 1. Molecular structure of the polyphilic molecule B16/10 and dipalmitoylphosphatidylcholine (DPPC) molecule studied in this report.

The available experimental results show that, when bolapolyphile molecules (BP) are incorporated into gel phase lipid (DPPC) bilayers, the formation of large BP domains within the bilayer and a separation into different lamellar species can be observed [16,17]. The thermal behavior of the lipid bilayers was drastically altered upon BP incorporation and several endothermic transitions above T_m of pure DPPC bilayer occurred [11]. In the liquid phase, the BPs were homogeneously distributed in the lipid bilayer plane [11,16].

Lipid bilayer simulations have reached an exciting point, where the time and length scales of simulations are approaching experimental resolutions and can be used to interpret experiments on increasingly complex model bilayers. Within molecular dynamics (MD) of hybrid-bilayer systems, one is able to get an insight into the dynamical behavior on a molecular scale. Therefore, these simulations provide complementary information to experiments [25,29–34]. Furthermore, they can yield molecular-level insight into the structure and dynamics of these systems with a spatial resolution and time-scale that may not be feasible experimentally. Summarized, they serve as rich sources of quantitative data on molecular flexibility, lipid diffusion, ordering and atomic interactions. A detailed understanding of lipid bilayer properties is necessary to fully understand their important biophysical characteristics.

Previously, we have reported a MD study of one single B16/10 molecule inserted as a trans-bilayer agent into a dipalmitoylphosphatidylcholine (DPPC) bilayer [35]. The results showed that B16/10 is commensurate with the bilayer, and at the same time, a certain intramolecular bending and an inclination with respect to the bilayer plane is observed. While the lipophilic groups remain

bilayer-centered, the fluorophilic parts tend to orient towards the phosphate headgroups, which is due to a slight size mismatch between the bilayer and the lipophilic backbone of the molecule.

In the present work, MD simulations with full atomic detail were carried out for a small trans-bilayer cluster containing six B16/10 molecules embedded into a DPPC bilayer on a large time scale. The difference of the dynamical and structural properties of the DPPC bilayer between pure bilayer system and the mixture of the lipid bilayer with B16/10 molecules is illustrated. The configurations and dynamics of incorporated B16/10 are studied. The results are compared with available experimental and literature data.

2. System Setup and Computational Details

A small cluster of six B16/10 molecules was embedded into a DPPC bilayer consisting 288 lipid molecules (144 per leaflet). The mixed molecular system was hydrated using 8756 TIP3 water molecules. The resulting periodic box has a dimension of $98 \times 98 \times 68$ Å^3. A snapshot of the system is shown in Figure 2.

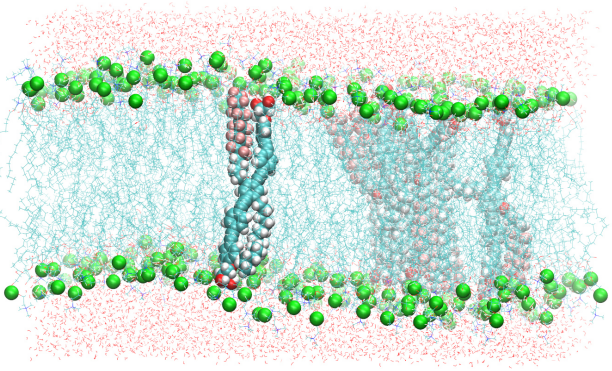

Figure 2. A snapshot of the simulated system containing six B16/10 molecules, 288 DPPC molecules and 8756 water molecules. Periodic boundary conditions were used in all directions. Atoms of B16/10 molecules and Phosphorus atoms of DPPC headgroups are represented by solid spheres. Phosphorus atoms are green, Fluorine atom of B16/10 side chains are pink, carbon atoms are cyan. All the lipid tails of DPPC are represented by cyan lines. One can see, that the backbone of the polyphile (cyan spheres) is bent and not straight.

The initial configurations of B16/10 molecules was selected based on the experimentally observed phase formation of similar structured molecules. According to the experimental results, similar structured B12 molecules spontaneously self-organize in lipid bilayers (DPPC), forming ordered snowflake like structures with 6-fold symmetry in giant unilamellar vesicles [16,17]. Furthermore, the initial structure completely vanished after an equilibration time of 20 ns. The first 20 ns have been omitted in all analyses. The structure after the equilibration is shown in Figure 3 as a top view onto the system.

All MD simulations in this work were performed by software package namd 2.9 using the CHARMM force field [32,36,37]. The detailed parameters for B16/10 are presented in a previous work of our group [38]. Three dimensional periodic boundary conditions were used. The system is kept at a constant pressure of 1 bar and a constant specified temperature (isobaric-isothermal NpT ensemble) using a modified Nose–Hoover method in which Langevin dynamics is used to control fluctuations in the barostat. The semi-isotropic pressure coupling was applied separately for the bilayer plane and bilayer normal with a coupling constant of 1 bar. Experimentally measured phase transition temperature of a DPPC bilayer is between 313 and 315 K [16,17]. It is experimentally observed that the presence of polyphile molecules increases this phase transition temperature. In order to avoid a simulation in a gel phase, we set the simulation temperature to 335 K in this work.

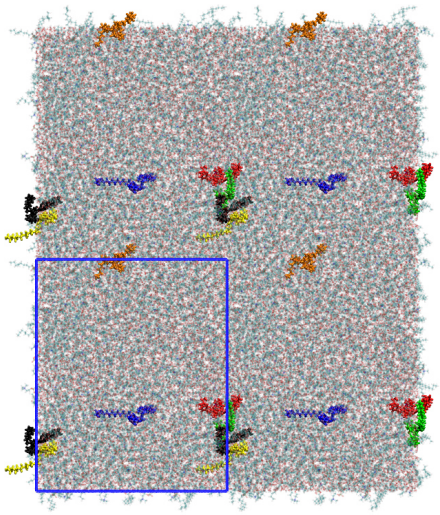

Figure 3. A snapshot of the simulated system as a top view after an equilibration time of 20 ns. The polyphiles are colored and a clustering can be observed for some of the molecules. The simulation cell dimensions are shown as blue rectangle.

The system was simulated for 1 µs with a time step of 2 fs. The bond lengths were constrained using the SHAKE algorithm. The vdW cutoff follows the force field specifications for lipid bilayers. A particle mesh Ewald summation was used to calculate the electrostatic interactions. Cutoff radius for van der Waals interactions was set to 1.0 nm. Particle mesh Ewald (PME) summations were applied for long-range electrostatic interactions with a grid spacing of 0.12 nm and a cutoff radius of 1.0 nm was employed for real space summation. For the purpose of comparison, simulations of a pure DPPC bilayer was carried out under same conditions. The TIP3P water model was used to solvate the system. Data analysis of the trajectories were done by using VMD plugins [39], the python module MDAnalysis [40], the freeware program package TRAVIS [41] and our own codes.

3. Results and Discussion

Statistical analysis was carried out to characterize the dynamical and structural properties of B16/10 trans-bilayer molecules inside a DPPC bilayer. In particular, we (i) calculated the lateral diffusion coefficients of DPPC and B16/10 molecules and (ii) investigated the axial location and orientation of B16/10 molecules and internal structure of B16/10 cluster. The results are compared with a pure DPPC bilayer system, available experimental data and former results of our group.

3.1. Lateral Diffusion

Investigation of DPPC and B16/10 molecules lateral mobility in a planar lipid bilayer are carried out and the results are compared with the pure bilayer system. The averaged self-diffusion coefficients of B16/10 and DPPC molecules are calculated from the mean squared displacement (MSD) $\langle r^2(t)\rangle$ using the Einstein relation:

$$MSD(t) = \langle \boldsymbol{r}^2(t)\rangle = \langle [\boldsymbol{r}(t) - \boldsymbol{r}(0)]^2\rangle \quad (1)$$

$$D = \frac{1}{2d}\lim_{t\to\infty}\frac{d}{dt}\langle [\boldsymbol{r}(t) - \boldsymbol{r}(0)]^2\rangle, \quad (2)$$

where d is the number of dimension which is 2 for our calculation. The MSD is calculated with respect to the center of mass (COM) of all lipid molecules to avoid artifacts from water layer movement. The averaged MSD for DPPC and B16/10 molecules are shown in Figure 4.

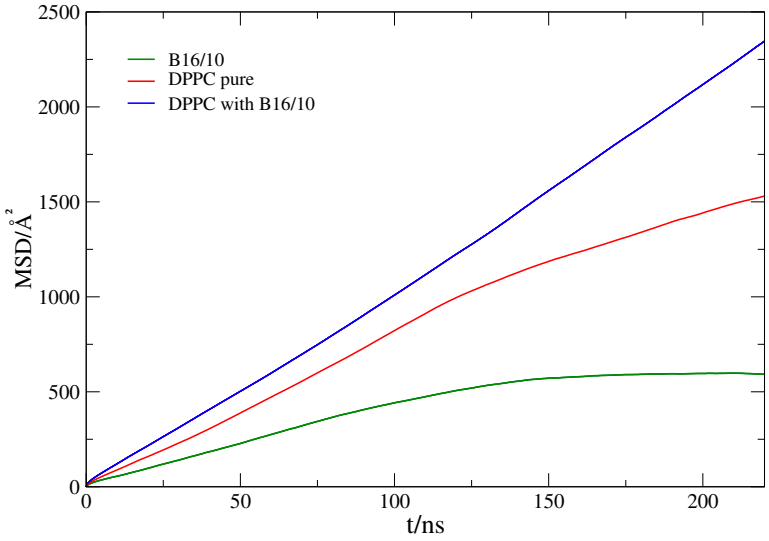

Figure 4. Mean square displacement of lipids in a pure DPPC bilayer (red), the lipids (blue) and B16/10 molecules (green) in the mixed system (lipids/B16/10).

The calculated self-diffusion coefficient of pure DPPC at 335K as presented in Table 1 is in very good agreement with the experimentally determined value of 14.2 $\pm$ 1.2 $\times 10^{-12}$ m^2/s [42]. The diffusion coefficient of B16/10 molecules is slightly lower than the diffusion coefficient of the lipids in a pure bilayer. For the mixed system, we find high diffusivity values for the lipid molecules, which is unexpected.

Table 1. Lateral self-diffusion coefficients (D) at 335 K obtained from MD simulation (MD) and experimental data from literature (exp) [42]. Uncertainties are given as three times the standard deviation.

$D/(10^{-12}$ m^2/s)	Lipids (Pure DPPC)	Lipids (mix)	B16/10 (mix)
MD	13.9 $\pm$ 0.3	24 $\pm$ 0.6	10.7 $\pm$ 0.3
exp	14.2 $\pm$ 1.2		

3.2. B16/10 Radial Distribution Functions

We calculated the pair correlation function, $g(r)$, as the probability of finding a pair of B16/10 molecules at distance r apart, relative to the probability expected for a completely random distribution at the same density [43]. The $g(r)$ of the center of mass for each central phenylene ring of a B16/10 molecule (COR-COR) and of its terminal groups (CH_3 and CF_3) is shown in Figure 5.

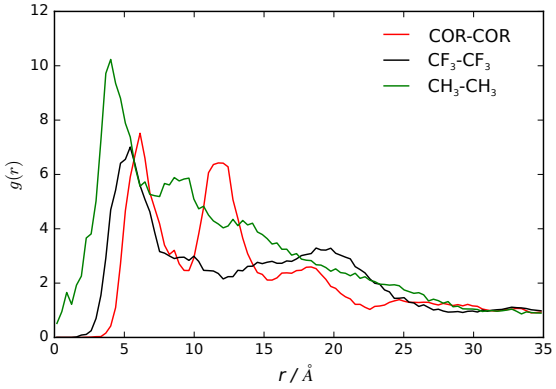

Figure 5. Radial distribution functions of the center of the central phenylene ring (COR), CF_3 and CH_3 terminal groups of B16/10 molecules within the DPPC bilayer.

We observe a clustering effect documented by the two peak nature in the radial distribution function. The first peak at 7 Å distance shows that two B16/10 molecules are directly adjacent to each other, as there is no space for interlaced molecules. Nevertheless the lipid molecules force the B16/10 molecules to tilt a little away from a coplanar orientation and causing this distance of 7 Å. Due to the tilt and high distance, pi–pi stacking does not frequently occur. Nevertheless, the radial distribution function has also non-zero values below 7 Å, which at least can be interpreted as possible pi–pi stacking. As there are only six B16/10 molecules in the system, effects of a big ensemble like in experiment [11,17] cannot be captured and therefore a strong pi–pi stacking behavior cannot be excluded even though it is unfavorable in our simulation. The second peak at 12 Å shows that a third B16/10 molecule is forming a little cluster with the other two. As the second peak is not double of the first one it can be seen that they are not completely aligned but forming a triangle. The clustering can be seen in Figure 6. Comparing Figures 3 and 6, one can see that the molecules inside the cluster are exchanging within the simulation.

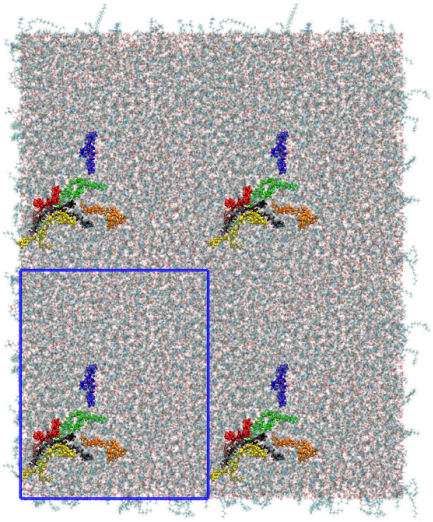

Figure 6. Snapshot of the top view onto the system showing the clustering of the B16/10 molecules. Namely the red, yellow and black colored molecules form a cluster, whereas the green and orange molecules are surrounding the cluster. Compared to Figure 3 (same coloring of the molecules), one can see that the cluster exchanges the molecules within the simulation. The simulation cell dimensions are shown as blue rectangle.

Having this in mind it is even more surprising that the diffusion coefficient discussed in the previous section of $11 \times 10^{-12} \frac{m^2}{s}$ for B16/10 (see Table 1) is rather high. This clustering behavior of x-shaped molecules like the non-perfluorinated B12 molecule was also observed experimentally [11,17]. Therefore it can be assumed that by perfluorinating one side chain, the clustering behavior is maintained. For the terminal groups CH_3 and CF_3 there is only one well defined peak at around 3 Å for CH_3 and at 5 Å for CF_3. Beyond this there is a smooth decay to unity apart from residual structure but with no recognizable pattern. All in all this shows that there is a correlation of the backbones of the B16/10 molecules forming a little cluster whereas there is no correlation of the side chains aside from pairwise orientation.

3.3. B16/10 Backbone Angles Distribution

We use three angels α_1, α_2 and β to characterize the orientation of B16/10 backbone within the bilayer as shown in Figure 7. The distributions of the three angels are displayed in Figure 8.

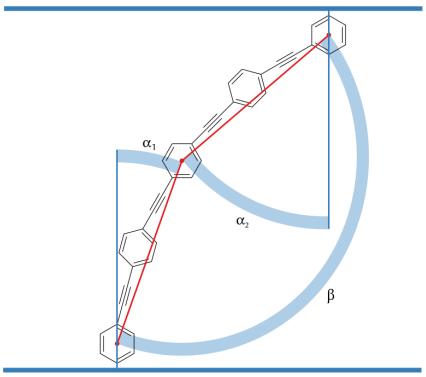

Figure 7. Angels between the bilayer normal and B16/10 backbone (α_1 and α_2) and backbone bending angle β.

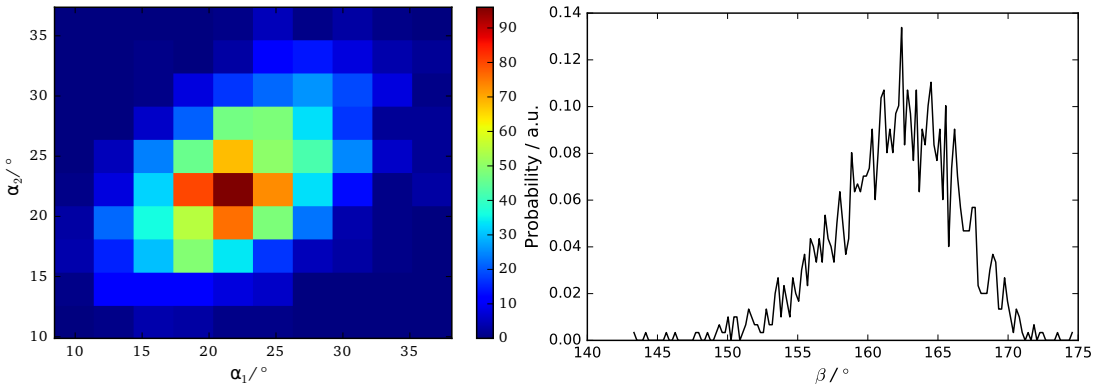

Figure 8. Probability distribution of backbone angles α_1, α_2 and β.

The calculated angular distributions of the B16/10 backbone are in very good agreement with our former results of a single B16/10 molecule inside a DPPC bilayer [35]. The B16/10 molecules are well incorporated into the lipid bilayer, cross the whole bilayer with their well-matched hydrophobic core length and adapting into the bilayer by a slight tilt.

3.4. B16/10 Terminal Group Integration and Side Chain Orientations

In Figure 9 the averaged position distribution of CF_3 and CH_3 terminal groups of B16/10 molecules relative to the center of mass of the system is shown. For avoiding artifacts, the center of mass movement of the whole system has been subtracted. The center of the lipid bilayer is denoted

by $z = 0$ and z is the axis along the normal of the bilayer plane. The bilayer itself has a thickness of approximately 40 ± 2.5 Å. As one can see in Figure 9, both side chains approach the head group region of the bilayer. Nevertheless the CF side chain tends to stay more in the headgroup region than the CH chain. The combination of higher solubility inside the leaflets (which was recently shown by Brehm et al. [3]) and sterical issues force the CF_3 terminal group to stay in the headgroup region as in direct comparison the CF side chain is nearly inflexible whereas the CH side is more flexible and thinner which makes it easier for the CH chain to find its way through the lipid bilayer. Not surprising is, that the CH_3 terminal group has a high occurrence in the middle of the bilayer, as this the most non polar region of the bilayer which has been observed in experiment before for alkanes [2]. Of course sterical issues are more dominant because not every polyphile can arrange like this when incorporated into a cluster and therefore it also stays frequently inside the leaflets. On first sight the occurrence of the CF_3 terminal group in the middle of the bilayer seems astonishing. It is easy explained by attempts to flip the sides of the bilayer. As it is only ninth of the occurrence of the highest peak this rarely happens and is never a stationary state. By closer inspection we found that the flipping of the CF side chain happens on a nanosecond time scale.

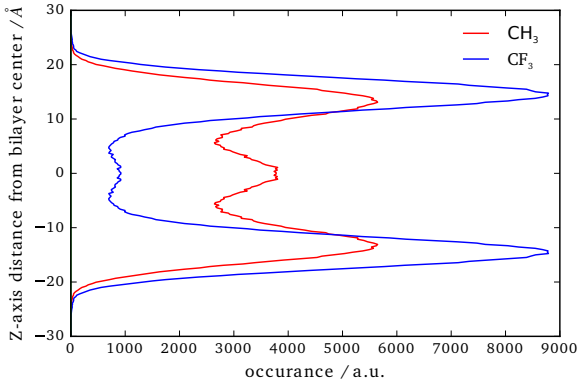

Figure 9. Position of the CF_3 and CH_3 terminal groups along the z-axis relative to the center of mass of the whole system.

The distribution of the side chain angles can be used to confirm these statements as seen in Figure 10. The angles are defined as the angle of the vector from the terminal groups to the center of the phenylene ring in the middle of the backbone and the bilayer normal. Therefore 90° denotes directly aligned between the leaflets in the bilayer plane. The prominent angles around 30° and 150° for the CF_3 terminal group confirms that it mostly stays in head group region of the bilayer. The very slight occurrence around 90° also shows the behavior to flip rather than staying between the leaflets. More or less Figure 9 and 10 resemble each other in appearance and therefore also confirm the statements for CH terminal head group mentioned above.

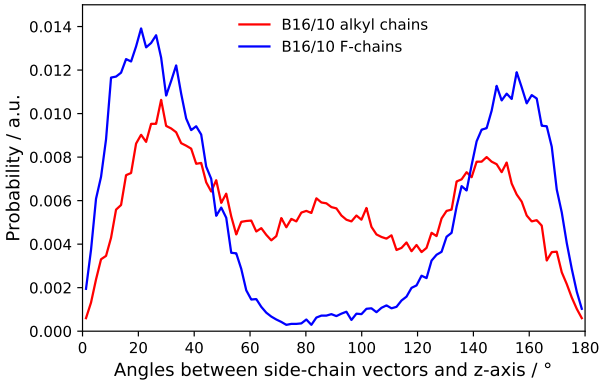

Figure 10. Probability distribution of side chains angles.

4. Conclusions

In this paper, we report a study of six polyphilic molecules embedded in a lipid bilayer/water system. Our results give insights not only into the the conformational preference of the B16/10 molecules inside the DPPC bilayer, but also on the dynamics of the B16/10 molecules in the DPPC bilayer environment. Within 1 ms of simulation the stability of the bilayer maintained upon insertion of the additive B16/10 molecules. The diffusion of the lipid molecules is increased compared to the pure lipid bilayer and B16/10 molecules move only slightly slower than the lipids in the pure bilayer. For the intermolecular structure of the B16/10 molecules a clustering effect can be observed in the RDFs. The difference in the side chain orientation and configuration is also in good agreement with the simulation results we obtained before [35]. In general, the conclusions drawn from simulations are consistent with experimentally observed effects [16,17,42]. We anticipate that these findings will be important for understanding the role of polyphilic molecules in modulating and modifying bilayer properties.

Acknowledgments: This work has been supported by the German Research Foundation (DFG) within the Forschergruppe FOR1145 (grant number Se 1008/9-1). The authors thank the China Scholarship Council (CSC) for providing a scholarship.

Author Contributions: Xiang-Yang Guo, Tobias Watermann and Guido Falk von Rudorff planned and set up the simulation. Xiang-Yang Guo and Christopher Peschel analyzed the data and wrote the manuscript. Daniel Sebastiani supervised this project.

Conflicts of Interest: The authors declare no conflict of interest.

References

1. Ariga, K.; Hill, J.P.; Lee, M.V.; Vinu, A.; Charvet, R.; Acharya, S. Challenges and breakthroughs in recent research on self-assembly. *Sci. Technol. Adv. Mater.* **2008**, *9*, 014109, doi:10.1088/1468-6996/9/1/014109.
2. White, S.H.; King, G.I.; Cain, J.E. Location of hexane in lipid bilayers determined by neutron diffraction. *Nature* **1981**, *290*, 161–163, doi:10.1038/290161a0.
3. Brehm, M.; Saddiq, G.; Watermann, T.; Sebastiani, D. Influence of Small Fluorophilic and Lipophilic Organic Molecules on Dipalmitoylphosphatidylcholine Bilayers. *J. Phys. Chem. B* **2017**, *121*, 8311–8321, doi:10.1021/acs.jpcb.7b06520
4. Bates, M.; Walker, M. Dissipative particle dynamics simulation of T- and X-shaped polyphilic molecules exhibiting honeycomb columnar phases. *Soft Matter* **2009**, *5*, 346–353, doi:10.1039/b813015a.
5. Crane, A.J.; Martínez-Veracoechea, F.J.; Escobedo, F.A.; Müller, E.A. Molecular dynamics simulation of the mesophase behaviour of a model bolaamphiphilic liquid crystal with a lateral flexible chain. *Soft Matter* **2008**, *4*, 1820–1829, doi:10.1039/b802452a.
6. Hill, E.; Stratton, K.; Whitten, D.G.; Evans, D.G. Molecular Dynamics Simulation Study of the Interaction of Cationic Biocides with Lipid Bilayers: Aggregation Effects and Bilayer Damage. *Langmuir* **2012**, *28*, 14849–14854, doi:10.1021/la303158c.

7. Schulz, M.; Olubummo, A.; Binder, W.H. Beyond the lipid-bilayer: Interaction of polymers and nanoparticles with membranes. *Soft Matter* **2012**, *8*, 4849–4864, doi:10.1039/c2sm06999g.
8. Hinks, J.; Wang, Y.; Poh, W.H.; Donose, B.C.; Thomas, A.W.; Wuertz, S.; Loo, S.C.J.; Bazan, G.C.; Kjelleberg, S.; Mu, Y.; et al. Modeling Cell Membrane Perturbation by Molecules Designed for Transmembrane Electron Transfer. *Langmuir* **2014**, *30*, 2429–2440, doi:10.1021/la403409t.
9. James, P.V.; Sudeep, P.K.; Suresh, C.H.; Thomas, K.G. Photophysical and Theoretical Investigations of Oligo(p-phenyleneethynylene)s: Effect of Alkoxy Substitution and Alkyne–Aryl Bond Rotations. *J. Phys. Chem. A* **2006**, *110*, 4329–4337, doi:10.1021/jp055184o.
10. Hill, E.H.; Whitten, D.G.; Evans, D.G. Computational Study of Bacterial Membrane Disruption by Cationic Biocides: Structural Basis for Water Pore Formation. *J. Phys. Chem. B* **2014**, *118*, 9722–9732, doi:10.1021/jp504297s.
11. Lechner, B.-D.; Ebert, H.; Prehm, M.; Werner, S.; Meister, A.; Hause, G.; Beerlink, A.; Saalwächter, K.; Bacia, K.; Tschierske, C.; et al. Temperature-Dependent In-Plane Structure Formation of an X-Shaped Bolapolyphile within Lipid Bilayers. *Langmuir* **2015**, *31*, 2839–2850, doi:10.1021/la504903d.
12. Mukhopadhyay, S.; Maitra, U. Chemistry and biology of bile acids. *Curr. Sci.* **2004**, *87*, 1666–1683.
13. Krafft, M.P. Fluorocarbons and fluorinated amphiphiles in drug delivery and biomedical research. *Adv. Drug Deliv. Rev.* **2001**, *47*, 209–228, doi:10.1016/S0169-409X(01)00107-7.
14. Schwieger, C.; Achilles, A.; Scholz, S.; Rüger, J.; Bacia, K.; Saalwächter, K.; Kressler, J.; Blume, A. Binding of amphiphilic and triphilic block copolymers to lipid model membranes: The role of perfluorinated moieties. *Soft Matter* **2014**, *10*, 6147–6160, doi:10.1039/C4SM00830H.
15. Scholtysek, P.; Achilles, A.; Hoffmann, C.-V.; Lechner, B.-D.; Meister, A.; Tschierske, C.; Saalwächter, K.; Edwards, K.; Blume, A. A T-Shaped Amphiphilic Molecule Forms Closed Vesicles in Water and Bicelles in Mixtures with a Membrane Lipid. *J. Phys. Chem. B* **2012**, *116*, 4871–4878, doi:10.1021/jp207996r.
16. Achilles, A.; Bärenwald, R.; Lechner, B.; Werner, S.; Ebert, H.; Tschierske, C.; Blume, A.; Bacia, K.; Saalwächter, K. Self-Assembly of X-Shaped Bolapolyphiles in Lipid Membranes: Solid-State NMR Investigations. *Langmuir* **2016**, *32*, 673–682, doi:10.1021/acs.langmuir.5b03712.
17. Werner, S.; Ebert, H.; Lechner, B.-D.; Lange, F.; Achilles, A.; Bärenwald, R.; Poppe, S.; Blume, A.; Saalwächter, K.; Tschierske, C.; et al. Dendritic Domains with Hexagonal Symmetry Formed by X-Shaped Bolapolyphiles in Lipid Membranes. *Chem. Eur. J.* **2015**, *21*, 8840–8850, doi:10.1002/chem.201405994.
18. Bärenwald, R.; Achilles, A.; Lange, F.; Mendes, T.F.; Saalwächter, K. Applications of Solid-State NMR Spectroscopy for the Study of Lipid Membranes with Polyphilic Guest (Macro)Molecules. *Polymers* **2016**, *8*, 439, doi:10.3390/polym8120439.
19. Permadi, H.; Lundgren, B.; Andersson, K.; DePierre, J.W. Effects of perfluoro fatty acids on xenobiotic-metabolizing enzymes, enzymes which detoxify reactive forms of oxygen and lipid peroxidation in mouse liver. *Biochem. Pharmacol.* **1992**, *44*, 1183–1191, doi:10.1016/0006-2952(92)90383-T.
20. Heuvel, J.P.V.; Kuslikis, B.I.; Van Rafelghem, M.J.; Peterson, R.E. Tissue distribution, metabolism, and elimination of perfluorooctanoic acid in male and female rats. *J. Biochem. Toxicol.* **1991**, *6*, 83–92, doi:10.1002/jbt.2570060202.
21. Park, K.-H.; Berrier, C.; Lebaupain, F.; Pucci, B.; Popot, J.-L.; Ghazi, A.; Zito, F. Fluorinated and hemifluorinated surfactants as alternatives to detergents for membrane protein cell-free synthesis. *Biochem. J.* **2007**, *403*, 183–187, doi:10.1042/BJ20061473.
22. Brehm, M.; Weber, H.; Thomas, M.; Hollóczki, O.; Kirchner, B. Domain Analysis in Nanostructured Liquids: A Post-Molecular Dynamics Study at the Example of Ionic Liquids. *ChemPhysChem* **2015**, *16*, 3271–3277, doi:10.1002/cphc.201500471.
23. Nagle, J.F.; Tristram-Nagle, S. Structure of lipid bilayers. *Biochim. Biophys. Acta* **2000**, *1469*, 159–195, doi:10.1016/S0304-4157(00)00016-2.
24. Liu, B.; Hoopes, M.I.; Karttunen, M. Molecular Dynamics Simulations of DPPC/CTAB Monolayers at the Air/Water Interface. *J. Phys. Chem. B* **2014**, *118*, 11723–11737, doi:10.1021/jp5050892.
25. Repáková, J.; Holopainen, J.M.; Morrow, M.R.; McDonald, M.C.; Capková, P.; Vattulainen, I. Influence of DPH on the Structure and Dynamics of a DPPC Bilayer. *Biophys. J.* **2005**, *88*, 3398–3410, 10.1529/biophysj.104.055533.
26. Hughes, Z.E.; Mark, A.E.; Mancera, R.L. Molecular Dynamics Simulations of the Interactions of DMSO with DPPC and DOPC Phospholipid Membranes. *J. Phys. Chem. B* **2012**, *116*, 11911–11923, doi:10.1021/jp3035538.

27. Zeng, X.; Kieffer, R.; Glettner, B.; Nürnberger, C.; Liu, F.; Pelz, K.; Prehm, M.; Baumeister, U.; Hahn, H.; Lang, H.; et al. Complex Multicolor Tilings and Critical Phenomena in Tetraphilic Liquid Crystals. *Science* **2011**, *331*, 1302–1306, doi:10.1126/science.1193052.
28. Yoshino, M.; Kikukawa, T.; Takahashi, H.; Takagi, T.; Yokoyama, Y.; Amii, H.; Baba, T.; Kanamori, T.; Sonoyama, M. Physicochemical Studies of Bacteriorhodopsin Reconstituted in Partially Fluorinated Phosphatidylcholine Bilayers. *J. Phys. Chem. B* **2013**, *117*, 5422–5429, doi:10.1021/jp311665z.
29. Bennett, W.F.D.; Tieleman, D.P. Computer simulations of lipid membrane domains. *Biochim. Biophys. Acta* **2013**, *1828*, 1765–1776, doi:10.1016/j.bbamem.2013.03.004.
30. Lehmler, H.-J.; Bummer, P.M. Mixing of perfluorinated carboxylic acids with dipalmitoylphosphatidylcholine. *Biochim. Biophys. Acta* **2004**, *1664*, 141–149, doi:10.1016/j.bbamem.2004.05.002.
31. Korlach, J.; Schwille, P.; Webb, W.W.; Feigenson, G.W. Characterization of lipid bilayer phases by confocal microscopy and fluorescence correlation spectroscopy. *Proc. Natl. Acad. Sci. USA* **1999**, *96*, 8461–8466, doi:10.1073/pnas.96.15.8461.
32. Klauda, J.B.; Venable, R.M.; Freites, J.A.; O'Connor, J.W.; Tobias, D.J.; Mondragon-Ramirez, C.; Vorobyov, I.; MacKerell, A.D.; Pastor, R.W. Update of the CHARMM All-Atom Additive Force Field for Lipids: Validation on Six Lipid Types. *J. Phys. Chem. B* **2010**, *114*, 7830–7843, doi:10.1021/jp101759q.
33. Krafft, M.P. Controlling phospholipid self-assembly and film properties using highly fluorinated components—Fluorinated monolayers, vesicles, emulsions and microbubbles. *Biochimie* **2012**, *10*, 11–25, doi:10.1016/j.biochi.2011.07.027.
34. Feller, S.E.; Venable, R.M.; Pastor, R.W. Computer Simulation of a DPPC Phospholipid Bilayer: Structural Changes as a Function of Molecular Surface Area. *Langmuir* **1997**, *13*, 6555–6561, doi:10.1021/la970746j.
35. Von Rudorff, G.F.; Watermann, T.; Guo, X.Y.; Sebastiani, D. Conformational Space of a Polyphilic Molecule with a Fluorophilic Side Chain Integrated in a DPPC Bilayer. *J. Comput. Chem.* **2017**, *38*, 576–583, doi:10.1002/jcc.24711.
36. Phillips, J.C.; Braun, R.; Wang, W.; Gumbart, J.; Tajkhorshid, E.; Villa, E.; Chipot, C.; Skeel, R.D.; Kalé, L.; Schulten, K. Scalable molecular dynamics with NAMD. *J. Comput. Chem.* **2005**, *26*, 1781–1802, doi:10.1002/jcc.20289.
37. Vanommeslaeghe, K.; Hatcher, E.; Acharya, C.; Kundu, S.; Zhong, S.; Shim, J.; Darian, E.; Guvench, O.; Lopes, P.; Vorobyov, I.; et al. CHARMM General Force Field: A Force Field for Drug-Like Molecules Compatible with the CHARMM All-Atom Additive Biological Force Fields. *J. Comput. Chem.* **2010**, *31*, 671–690, doi:10.1002/jcc.21367.
38. Von Rudorff, G.F.; Watermann, T.; Sebastiani, D, Perfluoroalkane Force Field for Lipid Membrane Environments. *J. Phys. Chem. B.* **2014**, *118*, 12531–12540, doi:10.1021/jp507464m.
39. Humphrey, W.; Dalke, A.; Schulten, K. VMD: Visual molecular dynamics. *J. Mol. Graph.* **1996**, *14*, 33–38, doi:10.1016/0263-7855(96)00018-5.
40. Michaud-Agrawal, N.; Denning, E.J.; Woolf, T.B.; Beckstein, O. MDAnalysis: A toolkit for the analysis of molecular dynamics simulations. *J. Comput. Chem.* **2011**, *32*, 2319–2327, doi:10.1002/jcc.21787.
41. Brehm, M.; Kirchner, B. TRAVIS—A Free Analyzer and Visualizer for Monte Carlo and Molecular Dynamics Trajectories. *J. Chem. Inf. Model.* **2011**, *51*, 2007–2023, doi:10.1021/ci200217w.
42. Junglas, M.; Danner, B.; Bayerl, T.M. Molecular Order Parameter Profiles and Diffusion Coefficients of Cationic Lipid Bilayers on a Solid Support. *Langmuir* **2003**, *19*, 1914–1917, doi:10.1021/la026468s.
43. McQuarrie, D.A. *Statistical Mechanics*; University Science Books: Davis, CA, USA, 1976; p. 641.

Chapter 3

Conclusion

The first project under the scope of this doctoral research concentrates on the liquid dynamics under silica confinement at the nanoscale. Using a simplified planar model based on the structural properties of the MCM-41 pore, DFT based molecular dynamics simulations and first principles of NMR chemical shift calculations are applied as a start. Our calculations show the strong influence of spatial confining on the structure and dynamical properties of water. On the structural level, we see a strong influence on the confined water's ^{1}H chemical shifts. While a 0.5 ppm increased chemical shift is observed in the center of the pore relative to bulk water, the chemical shift slowly decreases when reaching the wall, until it reaches a value of 3 ppm below the comparison of bulk water. It suggests a strengthened hydrogen bonding network for the water at the center, and a severely weakened network near the interface between silica and the water. Distinctive peaks in the density profile can be observed next to the wall, suggesting a restructuring of the water by the wall geometry. By calculating average chemical shifts for fictitious water films in the silanol region, a change from low chemical shifts for thin films towards bulk water like chemical shifts for a film thickness above 4 Å can be found. This is in good agreement with an earlier experimental model on the incremental filling of nanopores. As for the dynamic behavior, we see a decline in the rate of diffusion by a factor of 4 when comparing to bulk water values.

Subsequently, MD simulations using CHARMM Force Field were applied to study a binary (ethanol-water) mixture confined between 2 silanol slabs. The effect of silica confinement on structural, dynamical properties and percolation of confined fluids were investigated and compared with the corresponding properties in bulk. The self-diffusion coefficients of ethanol molecules are significantly reduced in contrast to water molecules. Water molecules percolated in all mixtures and formed stable clusters while ethanol is, in contrast, more flexible and therefore has a higher possibility of hydrogen bonds with a silanol group. This, in return, enhances the water clustering structure. This indicates that a significant restructuring of the hydrogen bond network between water and ethanol occurs as well as changes in the water−water hydrogen bonds due to the presence of the silanol walls. The hydrophobic environment generated by a layer structure of the ethanol alkyl groups further support the stabilization of these water clusters as compared to the unconfined case. The ethanol-water hydrogen bond strength is more than ethanol-ethanol hydrogen bond in bulk mixtures while it is less than its counterpart in the confined system, which is in agreement with segregation tendency in confined systems.

3.1 Polyphile Molecules Constrained in DPPC Bilayer

As a start, classical molecular dynamics simulations were performed in the context of the second project during this doctoral research to determine the transmembrane orientation and in-

tramolecular conformational distribution of a single perfluorinated polyphilic molecule (B16/10) within a DPPC bilayer. Obtained simulation results show clearly that the polyphile molecule lies in aliance with the membrane conformationally. One interesting difference can be found in the orientation preferences between the perfluorinated side chain and the traditional alkane chain. The perflourinated side-chain orients along the lipophilic chains and towards the DPPC molecules' phosphate headgroups, while the alkane side-chain stays mainly in the bilayer's middle. The polyphilic molecule's diffusion constant is declinded by around a factor of 2. It shows that, given its double anchoring at both lipid-water interfaces and additional side chains within the membrane, the polyphile is almost as mobile as a normal lipid.

Consequently, MD simulations of six polyphilic molecules B16/10 as a cluster embedded in a lipid bilayer/water system were performed. The findings provide information not only on the conformational preference of the B16/10 molecules inside the DPPC bilayer but also on the dynamics of the B16/10 molecules in the bilayer context of the DPPC. The stability of the bilayer was preserved within 1 ms of the simulation when the additive B16/10 molecules were inserted. Similar to the pure lipid bilayer, the diffusion of lipid molecules is increased, and the molecules B16/10 travel just slightly slower than the lipids in the pure bilayer. In the RDFs, a clustering effect may be observed for the intermolecular structure of the B16/10 molecules. The variation in orientation and configuration of the side chain is also in good agreement with the results of the simulation obtained above.

Such MD simulations are a first step towards understanding the structure of polyphilic molecules in intramembrane with specifically designed side chains of different philicity. Such molecules have the potential to allow guided modulation of membrane properties, such as permeability of water and ions. In general, the conclusions drawn from simulations are consistent with the[33,34] effects observed experimentally. With confidence, one can predict that these results will be very important in understanding the role of polyphilic molecules in the modulation and alteration of membrane properties.

Bibliography

[1] François Nkinahamira, Tiezhu Su, Yaqiang Xie, Guifeng Ma, Hongtao Wang, and Jun Li. High pressure adsorption of co2 on mcm-41 grafted with quaternary ammonium ionic liquids. *Chemical Engineering Journal*, 326:831 – 838, 2017. 1

[2] Aleksandra Pajzderska, Miguel Gonzalez, J. Mielcarek, and J. Wasicki. Water behavior in mcm-41 as a function of pore filling and temperature studied by nmr and molecular dynamics simulations. *The Journal of Physical Chemistry C*, 118:23701–23710, 10 2014. 1

[3] Antonio Faraone, Kao-Hsiang Liu, Chung-Yuan Mou, Yang Zhang, and Sow-Hsin Chen. Single particle dynamics of water confined in a hydrophobically modified mcm-41-s nanoporous matrix. *The Journal of Chemical Physics*, 130(13):134512, 2009. 1

[4] F. Mansour, R. M. Dimeo, and H. Peemoeller. High-resolution inelastic neutron scattering from water in mesoporous silica. *Phys. Rev. E*, 66:041307, Oct 2002. 1

[5] Claudia Pantalei, Roberto Senesi, Carla Andreani, Piero Sozzani, Angiolina Comotti, Silvia Bracco, Mario Beretta, Paul E. Sokol, and George Reiter. Interaction of single water molecules with silanols in mesoporous silica. *Phys. Chem. Chem. Phys.*, 13:6022–6028, 2011. 1

[6] R. Mancinelli, S. Imberti, A. K. Soper, K. H. Liu, C. Y. Mou, F. Bruni, and M. A. Ricci. Multiscale approach to the structural study of water confined in mcm41. *The Journal of Physical Chemistry B*, 113(50):16169–16177, 2009. PMID: 19928867. 1

[7] Pavel Smirnov, Toshio Yamaguchi, Shigeharu Kittaka, Shuichi Takahara, and Yasushige Kuroda. X-ray diffraction study of water confined in mesoporous mcm-41 materials over a temperature range of 223−298 k. *The Journal of Physical Chemistry B*, 104(23):5498–5504, 2000. 1

[8] Victor Ostroverkhov, Glenn A. Waychunas, and Y. R. Shen. New information on water interfacial structure revealed by phase-sensitive surface spectroscopy. *Phys. Rev. Lett.*, 94:046102, Feb 2005. 1

[9] Vitaly Kocherbitov and Viveka Alfredsson. Hydration of mcm-41 studied by sorption calorimetry. *The Journal of Physical Chemistry C*, 111(35):12906–12913, 2007. 1

[10] Ilja G. Shenderovich, Daniel Mauder, Dilek Akcakayiran, Gerd Buntkowsky, Hans-Heinrich Limbach, and Gerhard H. Findenegg. Nmr provides checklist of generic properties for atomic-scale models of periodic mesoporous silicas. *The Journal of Physical Chemistry B*, 111(42):12088–12096, 2007. PMID: 17915913. 1

[11] X. S. Zhao, G. Q. Lu, A. K. Whittaker, G. J. Millar, and H. Y. Zhu. Comprehensive study of surface chemistry of mcm-41 using 29si cp/mas nmr, ftir, pyridine-tpd, and tga. *The Journal of Physical Chemistry B*, 101(33):6525–6531, 1997. 1

[12] Dennis W. Hwang, Chien-Chih Chu, Anil K. Sinha, and Lian-Pin Hwang. Dynamics of supercooled water in various mesopore sizes. *The Journal of Chemical Physics*, 126(4):044702, 2007. 1

[13] Katsuhiro Shirono and Hirofumi Daiguji. Molecular simulation of the phase behavior of water confined in silica nanopores. *The Journal of Physical Chemistry C*, 111(22):7938–7946, 2007. 1

[14] Silvia Pizzanelli, Shifi Kababya, Veronica Frydman, Miron Landau, and Shimon Vega. Nmr study of the adsorption−desorption kinetics of dissolved tetraalanine in mcm-41 mesoporous material. *The Journal of Physical Chemistry B*, 109(16):8029–8039, 2005. PMID: 16851938. 1

[15] Bob Grünberg, Thomas Emmler, Egbert Gedat, Ilja Shenderovich, Gerhard H. Findenegg, Hans-Heinrich Limbach, and Gerd Buntkowsky. Hydrogen bonding of water confined in mesoporous silica mcm-41 and sba-15 studied by 1h solid-state nmr. *Chemistry – A European Journal*, 10(22):5689–5696, 2004. 1

[16] J. Sung, G. A. Waychunas, and Y. R. Shen. Surface-induced anisotropic orientations of interfacial ethanol molecules at air/ sapphire(1102) and ethanol/sapphire(1102) interfaces. *J. Phys*, 2:1831, 2011. 1

[17] P. Tereshchuk, Da Silva, J. L. F. Ethanol, and Water Adsorption on Close-Packed 3d. 4d, and 5d transition-metal surfaces: A density functional theory investigation with van der waals correction. *J. Phys*, 116:24695, 2012. 1

[18] B. Grünberg, T. Emmler, E. Gedat, I. Shenderovich, G. H. Findenegg, H. Limbach, and G. Buntkowsky. Hydrogen bonding of water confined in mesoporous silica mcm-41 and sba-15 studied by 1h solid-state nmr. *Chem*, 10:5689, 2004. 1

[19] B. Ratajska-Gadomska and W. Gadomski. Influence of confinement on solvation of ethanol in water studied by raman spectroscopy. *J. Chem*, 133:23450, 2010. 1

[20] Katsuhiko Ariga, Jonathan P Hill, Michael V Lee, Ajayan Vinu, Richard Charvet, and Somobrata Acharya. Challenges and breakthroughs in recent research on self-assembly. *Science and Technology of Advanced Materials*, 9(1):014109, 2008. 2

[21] Stephen H. White, Glen I. King, and James E. Cain. Location of hexane in lipid bilayers determined by neutron diffraction. *Nature*, 290(161):161–163, 1981. 2

[22] Martin Brehm, Ghulam Saddiq, Tobias Watermann, and Daniel Sebastiani. Influence of small fluorophilic and lipophilic organic molecules on dipalmitoylphosphatidylcholine bilayers. *J.phys.chem.B*, 121(35):8311–8321, 2017. 2

[23] Martin Bates and Martin Walker. Dissipative particle dynamics simulation of t- and x-shaped polyphilic molecules exhibiting honeycomb columnar phases. *Soft Matter*, 5:346–353, 2009. 2

[24] Andrew J. Crane, Francisco J. Martínez-Veracoechea, Fernando A. Escobedo, and Erich A. Müller. Molecular dynamics simulation of the mesophase behaviour of a model bolaamphiphilic liquid crystal with a lateral flexible chain. *Soft Matter*, 4:1820–1829, 2008. 2

[25] Eric H. Hill, Kelly Stratton, David G. Whitten, and Deborah G. Evans. Molecular dynamics simulation study of the interaction of cationic biocides with lipid bilayers: Aggregation effects and bilayer damage. *Langmuir*, 28(42):14849–14854, 2012. 2, 3

[26] Matthias Schulz, Adekunle Olubummo, and Wolfgang H. Binder. Beyond the lipid-bilayer: interaction of polymers and nanoparticles with membranes. *Soft Matter*, 8:4849–4864, 2012. 2, 3

[27] Jamie Hinks, Yaofeng Wang, Wee Han Poh, Bogdan C. Donose, Alexander W. Thomas, Stefan Wuertz, Say Chye Joachim Loo, Guillermo C. Bazan, Staffan Kjelleberg, Yuguang Mu, and Thomas Seviour. Modeling cell membrane perturbation by molecules designed for transmembrane electron transfer. *Langmuir*, 30(9):2429–2440, 2014. 2, 3

[28] P. V. James, P. K. Sudeep, C. H. Suresh, and K. George Thomas. Photophysical and theoretical investigations of oligo(p-phenyleneethynylene)s: effect of alkoxy substitution and alkyne−aryl bond rotations. *The Journal of Physical Chemistry A*, 110(13):4329–4337, 2006. 2, 3

[29] Eric H. Hill, David G. Whitten, and Deborah G. Evans. Computational study of bacterial membrane disruption by cationic biocides: Structural basis for water pore formation. *The Journal of Physical Chemistry B*, 118(32):9722–9732, 2014. 2, 3

[30] Eric H. Hill, David G. Whitten, and Deborah G. Evans. Computational study of bacterial membrane disruption by cationic biocides: Structural basis for water pore formation. *The Journal of Physical Chemistry B*, 118(32):9722–9732, 2014. 2, 3

[31] Christian Schwieger, Anja Achilles, Sven Scholz, Jan Rüger, Kirsten Bacia, Kay Saalwaechter, Jörg Kressler, and Alfred Blume. Binding of amphiphilic and triphilic block copolymers to lipid model membranes: the role of perfluorinated moieties. *Soft Matter*, 10:6147–6160, 2014. 2, 3

[32] Peggy Scholtysek, Anja Achilles, Claudia-Viktoria Hoffmann, Bob-Dan Lechner, Annette Meister, Carsten Tschierske, Kay Saalwächter, Katarina Edwards, and Alfred Blume. A t-shaped amphiphilic molecule forms closed vesicles in water and bicelles in mixtures with a membrane lipid. *The Journal of Physical Chemistry B*, 116(16):4871–4878, 2012. 2, 3

[33] Anja Achilles, Ruth Bärenwald, Bob-Dan Lechner, Stefan Werner, Helgard Ebert, Carsten Tschierske, Alfred Blume, Kirsten Bacia, and Kay Saalwächter. Self-assembly of x-shaped bolapolyphiles in lipid membranes: Solid-state nmr investigations. *Langmuir*, 32(3):673–682, 2016. 2, 3, 53

[34] Stefan Werner, Helgard Ebert, Bob-Dan Lechner, Frank Lange, Anja Achilles, Ruth Bärenwald, Silvio Poppe, Alfred Blume, Kay Saalwächter, Carsten Tschierske, and Kirsten Bacia. Dendritic domains with hexagonal symmetry formed by x-shaped bolapolyphiles in lipid membranes. *Chemistry – A European Journal*, 21(24):8840–8850, 2015. 2, 53

[35] Ruth Bärenwald, Anja Achilles, Frank Lange, Tiago Ferreira, and Kay Saalwächter. Applications of solid-state nmr spectroscopy for the study of lipid membranes with polyphilic guest (macro)molecules. *Polymers*, 8(12):439, Dec 2016. 2

[36] Harnowo Permadi, Bo Lundgren, Karin Andersson, and Joseph W. DePierre. Effects of perfluoro fatty acids on xenobiotic-metabolizing enzymes, enzymes which detoxify reactive forms of oxygen and lipid peroxidation in mouse liver. *Biochemical Pharmacology*, 44(6):1183 – 1191, 1992. 2

[37] John P. Vanden Heuvel, Benedict I. Kuslikis, Marc J. Van Rafelghem, and Richard E. Peterson. Tissue distribution, metabolism, and elimination of perfluorooctanoic acid in male and female rats. *Journal of Biochemical Toxicology*, 6(2):83–92, 1991. 2

[38] Kyu-Ho Park, Catherine Berrier, Florence Lebaupain, Bernard Pucci, Jean-Luc Popot, Alexandre Ghazi, and Francesca Zito. Fluorinated and hemifluorinated surfactants as alternatives to detergents for membrane protein cell-free synthesis. *Biochemical Journal*, 403(1):183–187, 2007. 2

[39] John F. Nagle and Stephanie Tristram-Nagle. Structure of lipid bilayers. *Biochimica et Biophysica Acta (BBA) - Reviews on Biomembranes*, 1469(3):159 – 195, 2000. 3

[40] Bin Liu, Matthew I. Hoopes, and Mikko Karttunen. Molecular dynamics simulations of dppc/ctab monolayers at the air/water interface. *The Journal of Physical Chemistry B*, 118(40):11723–11737, 2014. 3

[41] Masaru Yoshino, Takashi Kikukawa, Hiroshi Takahashi, Toshiyuki Takagi, Yasunori Yokoyama, Hideki Amii, Teruhiko Baba, Toshiyuki Kanamori, and Masashi Sonoyama. Physicochemical studies of bacteriorhodopsin reconstituted in partially fluorinated phosphatidylcholine bilayers. *The Journal of Physical Chemistry B*, 117(18):5422–5429, 2013. PMID: 23611734. 3

[42] Xie, W.; Kania-Korwel, I.; Bummer, P. M.; and Lehmler, H. J. Effect of potassium perfluorooetanesulfonate, perfluorooctanoate and octanesulfonate on the phase transition of dipalmitoylphosphatidylcholine (DPPC) bilayers. *Biochim. et Biophys. Acta-Biomembr.*, 1768(5):1299–1308, 2007. 3

[43] Jyoti, A.; Prokop, R. M.; Li, J.; Vollhardt, D.; Kwok, D. Y.; Miller, R.; Mohwald, H.; and Neumann, A. W. An investigation of the compression rate dependence on the surface pressure-surface area isotherm for a dipalmitoyl phosphatidylcholine monolayer at the air/water interface. *Colloids and Surfaces A-Physicochemical and Engineering Aspects*, 116(1-2):173–180, 1996. 3

[44] Klopfer, K. J.; and Vanderlick, T. K. Isotherms of dipalmitoylphosphatidylcholine (DPPC) monolayers: Features revealed and features obscured. *J. Colloid and Interface Sci.*, 182(1):220–229, 1996. 3

[45] Eeman, M.; and Deleu, M. From biological membranes to biomimetic model membranes. *Biotechnologie Agronomie Societe et Environnement*, 14(4):719–736, 2010. 3

[46] Repáková J, Holopainen JM, Morrow MR, McDonald MC, Capková P, and Vattulainen I. Influence of dph on the structure and dynamics of a dppc bilayer. *Biophysical Journal*, 88(5):3398 – 3410, 2005. 4

[47] Zak E. Hughes, Alan E. Mark, and Ricardo L. Mancera. Molecular dynamics simulations of the interactions of dmso with dppc and dopc phospholipid membranes. *The Journal of Physical Chemistry B*, 116(39):11911–11923, 2012. 4

[48] Marie Pierre Krafft. Controlling phospholipid self-assembly and film properties using highly fluorinated components – fluorinated monolayers, vesicles, emulsions and microbubbles. *Biochimie*, 94(1):11 – 25, 2012. Lipids in all their states. 4

[49] Tuckerman, M. *Statistical Mechanics: Theory and Molecular Simulation.* (Oxford University Press, 2010). 6, 9

[50] Swope, W. C.; Andersen, H. C.; Berens, P. H.; and Wilson, K. R. A computer simulation method for the calculation of equilibrium constants for formation of physical molecules application to small water clusters. *J. Chem. Phys.*, 76(1):637–649, 1982. 6, 7

[51] Allen, M. P.; and Tildesley, D. J. *Computer Simulation of Liquids.* Oxford university press, (1987). 6, 8

[52] Ryckaert, J. P.; Ciccotti, G.; and Berendsen, H. J. C. numerical integration of cartesian equations of motion of a system with constraints molecular dynamics of n-alkanes. *J. Computat. Phys.*, 23(3):327–341, 1977. 6, 8

[53] Celine, A.; Alex, H. V.; Hans-Dieter, H.; Peter T. D.; and Siewert-Jan, M. Methodological issues in lipid bilayer simulations. *J. Phys. Chem. B.*, 107(35):9424–9433, 2003. 6

[54] Jorgensen, W. L.; Chandrasekhar, J.; Madura, J. D.; Impey, R. W.; and Klein, M. L. Comparison of simple potential functions for simulating liquid Water. *J. Chem. Phys.*, 79(2):926–935, 1983. 6

[55] Neria, E.; Fischer, S.; and Karplus, M. Simulation of activation free energies in molecular systems. *J. Chem. Phys.*, 105(5):1902–1921, 1996. 6, 10

[56] Torby, B. J. *Advanced Dynamics For Engineers.* Holt Rinehart & Winston, 1984. 6

[57] Rapaport, D. C. *The Art of Molecular Dynamics Simulation.* Cambridge University Press, 1995. 6

[58] Haile, J. M. *Molecular Dynamics Simulation.* John Wiley and Sons., (1997). 6

[59] Verlet, L. Computer experiments on classical fluids.I. Thermodynamical properties of lennard-jones molecules. *Phys. Rev.*, 159(1):98, 1967. 7

[60] Findcham, D.; and Heyes, D. M. Ccp5 quarterly. 6:4–10, (1982). 7

[61] Heyes, D. M.; and Singer, K. Ccp5 quarterly. 6:11–23, 1982. 7

[62] Andersen, H. C. Rattle - A velocity version of the shake algorithm for molecular dynamics calculations. *J. Computat. Phys.*, 52(1):24–34, 1983. 8

[63] Robert I McLachlan, Klas Modin, Olivier Verdier, and Matt Wilkins. Geometric generalisations of shake and rattle. *Foundations of Computational Mathematics*, 14(2):339–370, Jun 2013. 8

[64] William G. Hoover. Canonical dynamics: Equilibrium phase-space distributions. *Phys. Rev. A*, 31:1695–1697, 1985. 9, 10

[65] D. J. Evans and B. L. Holian . The nose–hoover thermostat. *J. Chem. Phys.*, 83, 1985. 9

[66] Glenn J. Martyna, Michael L. Klein, and Mark Tuckerman. Nosé–hoover chains: The canonical ensemble via continuous dynamics. *The Journal of Chemical Physics*, 97(4):2635–2643, 1992. 9, 10

[67] M. E Tuckerman, C. J Mundy, and G. J Martyna. On the classical statistical mechanics of non-hamiltonian systems. *Europhysics Letters (EPL)*, 45(2):149–155, 1999. 9

[68] Pullman, B. In intermolecular forces. 14:331, 1981. 10

[69] Berweger, C. D.; Vangunsteren, W. F.; and Mullerplathe, F. Force field parameterization by weak coupling reengineering SPS water force-field. *Chem. Phys. Lett.*, 232(5-6):429–436, 1995. 10

[70] Berendsen, H. J. C.; Grigera, J. R.; and Straatsma, T. P. The missing term in effective pair potentials. *J. Phys. Chem.*, 91(24):6269–6271, 1987. 10, 11

[71] Vanommeslaeghe, K.; Hatcher, E.; Acharya, C.; Kundu, S.; Zhong, S.; Shim, J.; Darian, E.; Guvench, O.; Lopes, P.; Vorobyov, I.; and MacKerell, Jr. A. D. CHARMM General force field: a force field for drug like molecules compatible with the charmm all-atom additive biological force fields. *J. Computat. Chem.*, 31(4):671–690, 2010. 11

[72] MacKerell, A. D.; Banavali, N.; and Foloppe, N. Development and current status of the CHARMM force field for nucleic acids. *Biopolymers*, 56(4):257–265, 2001. 11

[73] Wang, J. M.; Wolf, R. M.; Caldwell, J. W.; Kollman, P. A.; and Case, D. A. Development and testing of a general amber force field. *J. Computat. Chem.*, 25(9):1157–1174, 2004. 11

[74] William, L. J.; and Julian, T. R. The opls [optimized potentials for liquid simulations] potential functions for proteins, energy minimizations for crystals of cyclic peptides and crambin. *J. Am. Chem. Soc.*, 110(6):1657–1666, 1988. 11

[75] Matsuoka, O.; Clementi, E.; and Yoshimine, M. CL study of water dimer potential surface. *J. Chem. Phys.*, 64(4):1351–1361, 1976. 11

[76] Watanabe, K.; and Klein, M. L. Effective pair potentials and the properties of water. *Chem. Phys.*, 131(2-3):157–167, 1989. 11

[77] Mayne, C. G.; Saam, J.; Schulten, K.; Tajkhorshid, E.; and Gumbart, J. C. Rapid parameterization of small molecules using the force field toolkit. *J. Computat. Chem.*, 34(32):2757–2770, 2013. 11

[78] Borodin, O.; Smith, G. D.; and Bedrov, D. A quantum chemistry based force field for perfluoroalkanes and poly(tetrafluoroethylene). *J. Phys. Chem. B*, 106(38):9912–9922, 2002. 11

[79] Scott, E. F.; Richard, W. P.; Atipat, R.; Stephen, B.; and Bernard, R. B. Effect of electrostatic force truncation on interfacial and transport properties of water. *J. Phys. Chem.*, 100(42):17011–17020, 1996. 11

List of Figures

List of Abbreviations

MD	Molecular Dynamics
DFT	Density functional theory
FF	Force Field
EtOH	Ethanol
MCM-41	Mobil Composition of Matter No. 41
PFCs	Perfluorinated Compounds
DPPC	Dipalmitoylphosphatidylcholine
B16/10	A X-shaped Bolapolyphile molecule with 16 -(CH2) and 10 -(CF2) segments
ns	Nanosecond
CHARMM	Chemistry at HARvard Macromolecular Mechanics
OPLS	Optimized Potential for Liquid Simulations
AMBER	Assisted Model Building and Energy Refinement
NAMD	Nanoscale Molecular Dynamics , formerly Not Another Molecular Dynamics
UB	Urey-Bradley
LJ	Lennard-Jones
NPT	Number, Pressure and Temperature
NVT	Number, Volumn and Temperature
NVE	Number, Volumn and Energy
GROMACS	Groningen Machine for Chemical Simulations
PME	Particle Mesh Ewald
TCL	Tool Command Language
TIP3P	Transferable intermolecular potential 3P
BP	Bolapolyphile
MSD	Mean Square Displacement
RDF	Radial Distribution Function

Curriculum Vitae

XIANGYANG GUO

Working Experience

06.2019 - Present
System Analyst
HSBC Germany

09.2017 - 06.2019
Junior Data Warehouse Consultant
Smartify IT Solutions

03.2017 - 08.2017
Intern IT Consultant
EITCO

10.2016 - 03.2017
Intern
ITmops

Education

03.2013 - 08.2016
AG Sebastiani, Theoretische Chemie, Uni Halle
Research Topics:
MD simulations of binary (ethanol-water) mixture under nanoscale silica confinement
MD simulations of x-shaped polyphilic molecules solvated in a DPPC bilayer

06.2011 - 02.2013
AG Sebastiani, Theoretische Physik, FU Berlin
Research Topic:
Ab initio MD simulations of water under silica confinement

09.2008 - 01.2011
Nanjing University of Science & Technology, China
M.Eng. in Physical Electronics
Study of Quantum efficiency of NEA GaN photocathode.

09.2004 - 06.2008
Nanjing University of Science & Technology, China
B.Eng. in Electronic Science & Technology
microelectronics & optoelectronics